# The Shape of an Elastic Boundary Deformed by Transmural Pressure

A thesis submitted to the School of Mathematics at the University of East Anglia in partial fulfilment of the requirements for the degree of Master of Philosophy

Danny Hoskin

Student Number: 3401758

June 2018

University of East Anglia

# Signed Statement

This work contains no material which has been accepted for the award of any other degree or diploma in any university or other tertiary institution and, to the best of my knowledge and belief, contains no material previously published or written by another person, except where due reference has been made in the text.

I consent to this copy of my thesis, when deposited in the University Library, being available for loan and photocopying.

Signed:  Date: 29th June 2018

# Abstract

This thesis is an exploration of some problems involving flexible boundaries subjected to transmural pressure differences. During the thesis, we explore a few example problems with the common theme of finding the shape profile of these flexible boundaries. We begin with the problem of a cross section of an elastic tube that is subjected to a pressure difference between the inside and outside pressures. This chapter is based on Flaherty et al. [10], but is essential to the thesis as a whole as we use the structure here to define the governing equations for the flexible boundary that we will refer to throughout the rest of the chapters. We then look at these circular cross sections as a fluid annulus where we have fluid contained between two of these flexible boundaries, and this fluid flow causes the pressure differences. The thesis then takes the governing elastic equations (again with the transmural pressure differences) but instead of an enclosed ring, we have a setup where the boundary is fixed at two points. Interestingly here we discover the existence of non-symmetric solutions that have not been found before. The setup of the elastic boundary that is fixed is then extended by passing a flow across the elastic boundary to create the pressure differences, firstly as a weak flow perturbation analysis and then via numerical computation.

# Contents

# List of Figures

# Acknowledgements

Firstly, a thank you to Mark and Emilian for your time and knowledge, but most importantly your patience. There have been trying times but you have been supportive throughout.

A big thank you to all my family and friends who have been beside me. I have always been blessed with good people around me and I appreciate all of you.

And the last acknowledgment is reserved for my Grandad, Brian. You have always been a supportive and inspiring influence and I am grateful for you being there for me.

# 1

# Introduction

The central theme of this thesis is about finding the shape profiles of elastic boundaries that are deformed due to pressure difference either side of them. These pressure differences can be simply because the elastic boundary is a closed loop that contains a certain pressure and differing pressure outside, or these elastic boundaries can be deformed by pressure as a result of fluid passing over or around it. The elastic boundaries throughout this thesis will be assumed to be inextensible, and rather than elastic in the sense of changing length they will be regarded as elastic in the sense that they are free to deform and change shape. Korobkin et al. [14] provides an introduction to problems related to hydroelasticity. Their paper outlines a number of different situations related to these elastic deformations. The fluid flows in this thesis will be assumed to be inviscid, irrotational and incompressible and so a velocity potential can be formed which satisfies Laplaces equation (see Bachelor [3] for example). Additionally, we will solve focusing on two dimensional problems, for example taking a cross-section of the three dimensional physical situation.

In 1972 Flaherty at al. [10] presented a paper on the buckling behaviour of elastic tubes. In this paper they take a cross section of the elastic tube and consider it as a two dimensional problem of an enclosed elastic ring with differing inside and outside pressures. This paper is not only important due to the specific problem that we will be concerned with, but also because it includes the main governing equations that dictate the elastic profile. Flaherty at al. cover not only the shape as the pressure changes, but also have a discussion into contact points, i.e. when two sides come into contact. They introduce a model that allows them to carry on after contact has been made, and they analyse after this contact point as the contact point then becomes a section of each elastic side that are then in contact. The authors allude to a flow around this elastic membrane causing deformations, but this is extended significantly in more detail by Blyth & Parau [4] where the authors consider examples of a uniform stream for flow, and then circulatory flow with a point vortex in the centre of the elastic shell. As a

slightly different take on this problem Blyth & Pozrikidis [6] and Pozrikidis [18] examine the problem of these cells deforming into various different shapes when they are filled with the fluid and resting on horizontal and then inclined planes.

One key way to analyse these free boundary problems where the shape of the boundary must come as part of the solution is to follow a conformal mapping procedure to map the profile into the complex plane, and then solve this system numerically in the fixed geometry. This solution method is described in Keller & Vanden-Broeck [13] in the case of bubbles inside a uniform flow. In this thesis we follow this procedure. It is possible to check that the numerical procedure is being applied well by comparing to Ozugurlu & Vanden-Broeck [17], this time looking at the distortion of a bubble that is in a corner flow.

In addition to enclosed elastic rings, this thesis also takes a look at situations where we have an elastic boundary with a uniform flow over the top of it. The flow creates a pressure difference along the boundary and it is this that causes it to deform. Blyth et al. [5] and Blyth & Vanden-Broeck [7] investigated similar problems, and consider the wave-like solutions due to fluid flow. Interestingly they present symmetric and antisymmetric solutions to the problems. A large portion of the discussion goes to explaining how, given specific pressure (and flow speed) ranges, solutions bifurcate and it is possible to have multiple solutions. The ideas of these bifurcations are examined more closely in more detail by Pozrikidis & Blyth [19].

There are many other interesting papers that study the problems of elastic boundaries that are not explicitly referenced in the coming research in this thesis but do provide excellent additional background reading. An example is Crowdy [9] where the author presents solutions on an annulus surrounded by an irrotational flow. During this thesis we are concerned with the shape of the profiles possible in the situations, and also looking at the stability of the solutions found. Toland [21] gives a good insight into a situation that is somewhat different to the elastic problems presented in this thesis and very bespoke to a specific application.

The structure of the thesis that follows is such: firstly, we define the main set of equations that define the shape profiles we seek. These governing equations come from the internal and external forces for the elastic cell that are created by the various pressure situations. We validate the work we do by comparing to Flaherty et al. [10] and recreating their results

whilst explaining in detail how we got there; secondly, we continue in the enclosed elastic loop theme, but consider a fluid annulus. This was studied by Blyth & Vanden-Broeck [7] where forces on the boundaries were surface tension, rather than elastic; we then move on the setup of the elastic arch problem. Here we effectively hold the elastic in two places to fix these points, and then see how the elastic between these two points behaves. We discover some antisymmetric solutions, which could be expected from previous work, but not presented previously in this particular context. The elastic arch is then investigated for the rest of the thesis, with the deformation due to the fluid flow over the top to the system.

# 2

# Profiles for a Buckling Elastic Tube under Pressure

To begin with we shall follow the work of Flaherty et al. [10]. This is concerned with finding the effects of pressure differences on a closed but flexible boundary. This can be imagined as an elastic ring with the surrounding pressure either being increased or decreased. The problem formulation in [10] forms the basis of much of the work in the following chapters and so we will provide its derivation in full.

## 2.1 Deriving The Governing Equations

We will look at deriving governing equations for a closed elastic tube that encloses some pressure, $p_i$, and is exposed to some pressure on the outside, $p_o$. To derive our equations consider the elastic ring to be made of a continuous string of very small sections of length $ds$, where $ds << 1$. This idea is pictured in Figure 2.1, notice also the defined unit vectors we will look at to measure forces in the normal, $\mathbf{n}$, and tangential, $\mathbf{t}$, directions as we travel along the elastic surface.

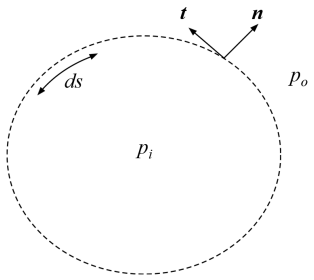


Figure 2.1: Enclosed elastic ring subjected to pressure differences. In practice the ring is a complete ring, the sections in the figure is just for illustration only. We will measure forces in the tangential ($\mathbf{t}$) and normal ($\mathbf{n}$) directions.

We will define the internal forces of the elastic parts by $\mathbf{f} = q\mathbf{n} + \tau\mathbf{t}$. $q(s)$ is the force on the tube wall acting in the outward normal direction, $\tau(s)$ is the force on the tube wall in the

tangential direction and $p$ is the difference in pressures between the inside and outside of the elastic ring. If we choose the right end of the section in Figure 2.2 as point $s$, then we can consider forces as shown by the arrows on each small section of the ring. Remember $ds << 1$ so that we can in effect think of the forces acting on a point rather than a line section.

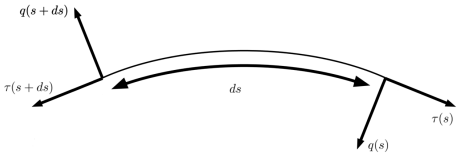


Figure 2.2: Forces acting upon a small section of elastic. $q$ and $\tau$ are internal forces in the $\mathbf{n}$ and $\mathbf{t}$ directions respectively.

Defining $p = p_o - p_i$, then balancing the forces acting on our small element is given by,

$$\begin{aligned} \mathbf{f}(s) &= \mathbf{f}(s+ds) - ds(p_o - p_i)\mathbf{n} \\ \Rightarrow \mathbf{f}(s+ds) - ds(p_o - p_i)\mathbf{n} - \mathbf{f}(s) &= \mathbf{0}. \end{aligned} \tag{2.1}$$

Note the negative sign in equation (2.1) for pressure. This is because pressure is acting in towards the enclosed elastic ring, and in the opposite direction to $\mathbf{n}$ in Figure 2.1. If we perform a Taylor expansion on $\mathbf{f}(s+ds)$ then divide through by $ds$ and take take the limit $ds \to 0$, then (2.1) becomes,

$$\frac{d\mathbf{f}}{ds} - p\mathbf{n} = \mathbf{0}. \tag{2.2}$$

From $\mathbf{f} = q\mathbf{n} + \tau\mathbf{t}$, we can obtain,

$$\frac{d\mathbf{f}}{ds} = \frac{d}{ds}\left(q\mathbf{n} + \tau\mathbf{t}\right) = q'\mathbf{n} + q\mathbf{n}' + \tau'\mathbf{t} + \tau\mathbf{t}'. \tag{2.3}$$

Using some standard results (see *Casey* [8] for example) on the vectors $\mathbf{n}$ and $\mathbf{t}$,

$$\mathbf{n}' = \kappa\mathbf{t} \quad \text{and} \quad \mathbf{t}' = \kappa\mathbf{n},$$

where $\kappa(s)$ is the curvature of the elastic tube at a given point $s$. (2.3) then becomes,

$$\frac{d\mathbf{f}}{ds} = q'\mathbf{n} + q(\kappa\mathbf{t}) + \tau'\mathbf{t} - \tau(\kappa\mathbf{n}),$$

and so (2.2) becomes,

$$\left(q' - \kappa\tau\right)\mathbf{n} + \left(\tau' + \kappa q\right)\mathbf{t} - p\mathbf{n} = \mathbf{0}.$$

Hence the governing equations defined by the forces on the elastic are,

$$q' - \kappa\tau - p = 0, \quad \tau' + \kappa q = 0.$$

The bending moment (the internal stress when external forces are applied) is assumed to be $m = \epsilon_B \kappa$ (as suggested by Blyth et al. [5]) where $\kappa$ is the curvature of the elastic and $\epsilon_B$ is the bending modulus which can be assumed constant as discussed in Blyth et al. [6]. From *Figure 2.2* we have a moment balance of $q = m'$. Hence, we have $q = \epsilon_B \kappa'$. There is more explination of what bending moments are located in *Appendix D*.

## 2.2 Multiple Mode Solutions

Working from our governing equations for the elastic ring,

$$q' - \kappa\tau - p = 0, \quad \tau' + \kappa q = 0, \quad \epsilon_B \kappa' = q \ , \tag{2.4}$$

we can substitute the last two equations of (2.4) to eliminate $q$ and using integration by parts we obtain,

$$\tau = -\epsilon_B \frac{\kappa^2}{2} + c, \tag{2.5}$$

where $c$ is a constant of integration. From (2.4) we note that $q' = \epsilon_B \kappa''$, so using this along with (2.5) we can write (2.4a) in terms of $\kappa$ as,

$$\epsilon_B \kappa'' + \epsilon_B \frac{\kappa^3}{2} - c\kappa - p = 0. \tag{2.6}$$

To make the mathematics simpler we can non-dimensionalise using $s = L\hat{s}$, where $L$ is the cell length. The definition of curvature gives $\kappa = \theta'(s)$ where $\theta$ is the angle between the horizontal and the tangent of a curve at a point, and so $\kappa = \frac{1}{L}\hat{\kappa}$. We can also redefine the constant $c = \frac{\epsilon_B}{L^2}\hat{c}$ so (2.6) becomes,

$$\hat{\kappa}'' + \frac{\hat{\kappa}^3}{2} - \hat{c}\hat{\kappa} - \hat{p} = 0, \tag{2.7}$$

where we have completed our non-dimensionalising with $\hat{p} = \frac{L^3}{\epsilon_B} p$. We can then work in a non-dimensional form of the equation. It is important to note that the equation (2.7) is equivalent to non-dimensional form of (2.4). It will be easier to look at the stability of the problem using the non-dimensional formulation. If the curvature is constant in our problem (say $\kappa = 1$) then we have a circular solution for our elastic ring, i.e. forces on the curve are the same at all points. If this is the case then (2.7) reduces to,

$$\frac{1}{2} - \hat{c} - \hat{p} = 0 \Rightarrow \hat{c} = \frac{1}{2} - \hat{p}.$$

To investigate the stability of our circular solution we shall assume the solution of the form,

$$\hat{\kappa} = 1 + \epsilon\gamma(\hat{s}),$$

where $\epsilon\gamma(\hat{s})$ is a small perturbation. If we substitute our perturbed solution into (2.7) and perform a Taylor expansion on the $\hat{\kappa}^3$ term we obtain,

$$\epsilon\left[\gamma'' + \frac{3}{2}\gamma - \hat{c}\gamma\right] + \left(\frac{1}{2} - \hat{c} - \hat{p}\right) + O\left(\epsilon^2\right) = 0.$$

Recall that we already have $\hat{c} = \frac{1}{2} - \hat{p}$ for the circular solution and so to leading order we have,

$$\gamma'' + (\hat{p} + 1)\,\gamma = 0. \tag{2.8}$$

A general solution to (2.8) is given by,

$$\gamma = A\cos(\mu\hat{s}) + B\sin(\mu\hat{s}),$$

where $\mu = (\hat{p} + 1)^{\frac{1}{2}}$ and $\hat{s} \in [0, 2\pi]$. We require our solution to be periodic (since the elastic loop is a closed loop) and since the elastic cell is inextensible we must have the same perimeter as the circle and so $\mu \in [1, 2, 3, 4, ...]$. This tells us that we have multiple solutions when the condition $(\hat{p} + 1)^{\frac{1}{2}} = n$, where $n$ is a natural number, is satisfied. Alternatively, we could say that additional solutions appear when,

$$\hat{p} = n^2 - 1. \tag{2.9}$$

For example, when $n = 2$ and then $\hat{p} = 3$ we expect to have a Mode 2 solution which has a period that is half of our circular solution, i.e. $0 \leq \hat{s} \leq \pi$. Then for a Mode 3 solution we have a solution that has a third of the period of the circular solution and so $0 \leq \hat{s} \leq \frac{2\pi}{3}$ , and so on. Up to a value of $\hat{p} = 3$ we have only our circular solution, then up to $\hat{p} = 8$ we have a circular solution and also a Mode 2 solution, then up to $\hat{p} = 15$ we also then have a Mode 3 solution, and so on.

At the value $n = 1$, this gives $\hat{p} = 0$. This relates to the solution when there is no pressure difference between the inside and and outside of the elastic ring and then we have a solution $\tau = q = 0$.

## 2.3 Elastic Ring with Pressure Difference

In addition to the equations for an elastic ring in 2D space given by (2.4), we also have,

$$\kappa(s) = \theta'(s), \tag{2.10}$$

from the definition of curvature, where $\theta$ is the angle between the horizontal and the tangent of the elastic tube at a point and (if $s$ is a distance of measure around the elastic tube). If the length of the elastic ring is given by $L$ then we can solve the setup shown in Figure 2.3 (using an example of a buckled solution of Mode 2) as there will be a symmetric solution of this type that Flaherty et al. [10] notes for $\hat{p} < 5.247$, where $\hat{p}$ is a non-dimensional form of $p$.

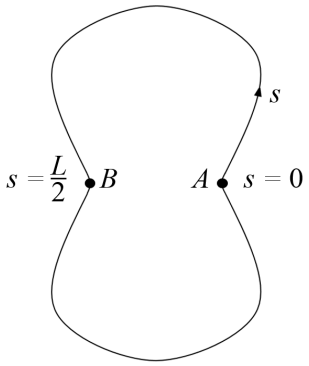


Figure 2.3: Final solution for Elastic Ring for $\hat{p} < 5.247$ See [10]. There will be two lines of symmetry, one vertically bisecting $AB$ and the other horizontally through $AB$. Here $L$ is the length of the loop. $s = 0$ is at $A$ and increases in an anti-clockwise direction. In the dimensional form we have $0 \leq s \leq L$, and in the non-dimensional form where $s = \frac{L\hat{s}}{2\pi}$ we have $0 \leq \hat{s} \leq 2\pi$, for a complete loop.

The equations for the elastic ring (2.4), in their non-dimensional form (where $s = L\hat{s}$) and (2.10) can be written as a first order system as,

$$\frac{d}{d\hat{s}} \begin{pmatrix} \hat{q} \\ \hat{\tau} \\ \hat{\kappa} \\ \theta \end{pmatrix} = \begin{pmatrix} \hat{p} + \hat{\kappa}\hat{\tau} \\ -\hat{\kappa}\hat{q} \\ \hat{q} \\ \hat{\kappa} \end{pmatrix}. \tag{2.11}$$

We solve numerically this system of equations, subject to the conditions that,

$$\hat{q}(0) = 0, \quad \hat{q}(\tfrac{\pi}{n}) = 0, \quad \hat{\tau}(0) = \hat{\tau}(\tfrac{\pi}{n}), \quad |\theta\left(\tfrac{\pi}{n}\right) - \theta(0)| = \tfrac{\pi}{n}.$$

These conditions arise as there are two lines of symmetry in the problem in the example in Figure 2.3 (one vertical and one horizontal). There would be 3 lines of symmetry for $n = 3$ and then so on. Then we are no longer looking at the solution $0 \leq \hat{s} \leq 2\pi$ but instead $0 \leq \hat{s} \leq \frac{\pi}{n}$. We can assume for our numerical scheme that our final value for $\hat{q}$ is still zero from symmetry, i.e. $\hat{q}(\frac{\pi}{n}) = 0$. However, we no longer have a similar condition for $\hat{\tau}$. We do have information about $\theta$. By definition it should be equal to $\frac{\pi}{2}$ (in the example in Figure 2.3 at point $A$ and at the end of our domain it should have turned through $\frac{\pi}{2}$, i.e. $\theta(0) = \frac{\pi}{2}$ and $|\theta(\frac{\pi}{2}) - \theta(0)| = \frac{\pi}{2}$ in the specific case of $n = 2$ and then $\theta(0) = \frac{\pi}{n}$ and $|\theta(\frac{\pi}{n}) - \theta(0)| = \frac{\pi}{n}$ in general.

Setting $\hat{q}(0) = 0$ and $\theta(0) = \frac{\pi}{n}$ we can solve the system (2.11) numerically [1] to find $\hat{\tau}(0)$ and $\hat{\kappa}(0)$ whilst enforcing $\hat{q}(\frac{\pi}{n}) = 0$ and $|\theta(\frac{\pi}{n}) - \theta(0)| - \frac{\pi}{n} = 0$.

Note that we will also include in numerical computation $x' = \cos(\theta)$ and $y' = \sin(\theta)$ to draw out the shape of the curve. The initial conditions of $x$, $y$, and $\theta$ are arbitrary as it does not matter where we place the elastic ring in space. It may be worth noting in a bit more detail where we have obtained $x' = \cos(\theta)$ and $y' = \sin(\theta)$ from. Figure 2.4 shows a sketch linking $\theta$ and $\alpha$, where $\alpha$ is the angle between the tangent to the curve at a point and the horizontal axis on the inside of the curve. From the triangle we can see,

$$\tfrac{dx}{ds} = -\cos\alpha \quad \tfrac{dy}{ds} = \sin\alpha,$$

but since $\alpha = \pi - \theta$ we have,

$$\frac{dx}{ds} = \cos\theta,$$
$$\frac{dy}{ds} = \sin\theta.$$

From (2.9), the relation of $\hat{p}$ and $n$, mode 2 (i.e $n = 2$) solutions exist when $\hat{p} \geq 3$. The initial conditions and forcing condition for the numerical scheme more explicitly become $\hat{q}(0) = 0$, $\theta(0) = \frac{\pi}{2}$, $\hat{q}(\frac{\pi}{2}) = 0$ and $|\theta(\frac{\pi}{2}) - \theta(0)| - \frac{\pi}{2} = 0$ respectively. We solve this numerically to obtain a solution as shown in Figure 2.5.

If we use subscripted notation to denote numerically computed values from 1 (as the initial condition) over $N$ numerical steps then our final $x$ and $y$ values will be given by $x_{N+1}$ and $y_{N+1}$ respectively. It is easy to see that we can create the whole top half of the picture (such

[1] Appendix A includes a discussion to the general numerical scheme we will be deploying.

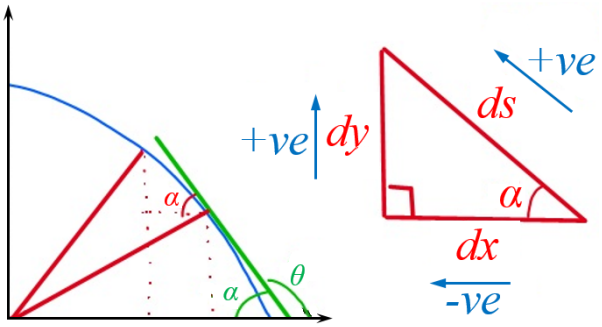


Figure 2.4: Sketch to show the relations $x' = cos(\theta)$ and $y' = sin(\theta)$. Here $\alpha$ is the angle between the curve and a tangent at a point, and the arrows are showing the direction of increasing $s$, traveling around the curve.

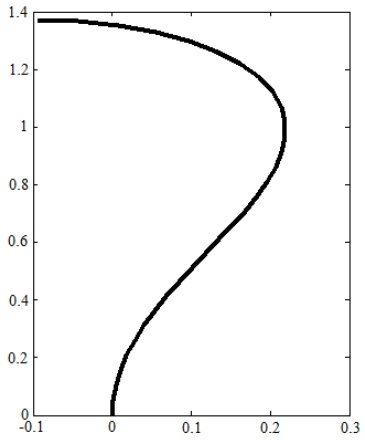


Figure 2.5: Numerically computed solution curve for $n = 2$ when $\hat{p} = 4.75$. Solution of (2.11), the equations an the elastic profile subjected to pressure. Here we have a solution for $0 \leq \hat{s} \leq \frac{\pi}{2}$. This is a quarter solution for a loop of length $L = 2\pi$.

as in Figure 2.3) by translating our coordinates by moving the whole image right by $x_{N+1}$ units, and reflecting the image in the $y - axis$. We can then create the entire image by rotating the upper solution 180°. This process is shown in Figure 2.6.

## 2.4 Mode 3, and Higher Mode Solutions (i.e. $n \geq 3$)

From (2.9) we achieve mode 3 solutions when $\hat{p} \geq 8$. We can take a similar approach to find a mode 3 solution as a mode 2 solution changing $n = 2$ to $n = 3$ and solving where $0 \leq \hat{s} \leq \frac{\pi}{3}$.

The more complicated aspect for a mode 3 solution compared to a mode 2 solution is considering our initial translation of our computed solution so that we are then able to reflect and

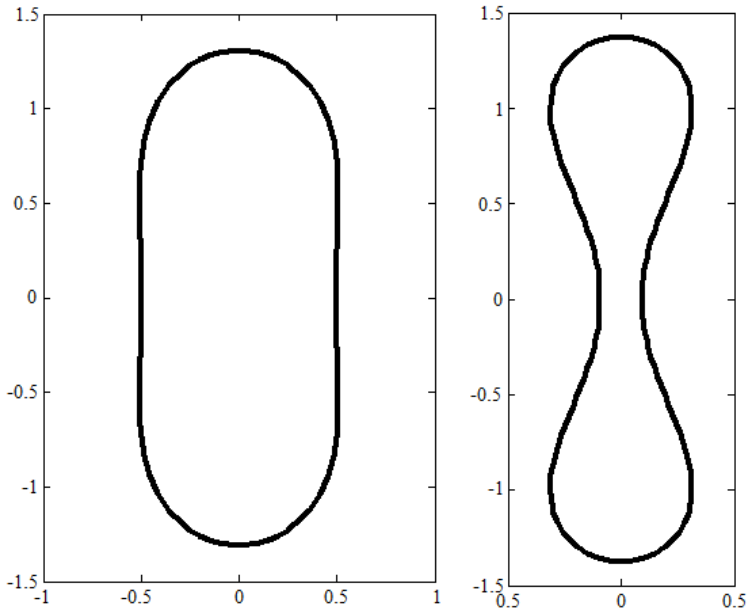


Figure 2.6: Complete solutions for $n = 2$. The first when $\hat{p} = 3.5$ and the second when $\hat{p} = 4.75$. The quarter solution shown in Figure 2.5 is transformed to create the whole ring for the length $L = 2\pi$.

rotated to complete the entire picture. If we define the matrix of our computed points as,

$$\begin{bmatrix} x_1 & x_2 & \cdots & x_{N+1} \\ y_1 & y_2 & \cdots & y_{N+1} \end{bmatrix},$$

we can then use matrix transformations to create our picture. In Figure 2.7 we can see the lines of reflection (centered at the origin) showing the solid lines that cross over our solution and dashed lines as lines of symmetry not over the shape. The curves line joining the lines $y = \frac{1}{\sqrt{3}}x$ and $y = -\frac{1}{\sqrt{3}}x$. Note that these are the lines of symmetry as these create a $30°$ angle between the lines and the $x - axis$ which in turn creates $120°$ between the solid lines of reflection in Figure 2.7.

As our computed solution has a start position at the origin, our translation vector will be given by $\begin{bmatrix} c \\ d \end{bmatrix}$. We have computed the size of our initial curve and so $a - c = x_{N+1} - x_1$ and $b - d = y_{N+1} - y_1$, which implies $a = x_{N+1} - x_1 + c$ and $b = x_{N+1} - x_1 + d$. As we also know from our lines of symmetry $b = \frac{a}{\sqrt{3}}$, and so,

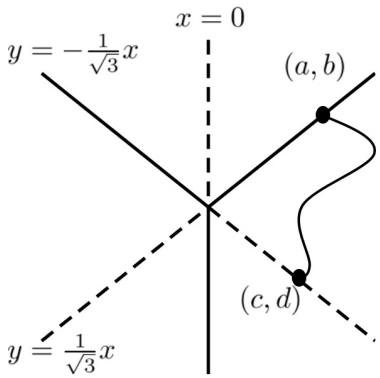


Figure 2.7: Lines of symmetry for the Mode 3 solution. The curve from $(a, b)$ to $(c, d)$ will be a translated solution curve.

$$x_{N+1} - x_1 + d = \frac{x_{N+1} - x_1 + c}{\sqrt{3}}.$$

We can solve the equation above as a simultaneous equation using our 3rd line of symmetry,

$$d = -\frac{c}{\sqrt{3}}.$$

This will need to be done numerically on the computer with the computed values of $x$ and $y$.

Once we have then translated our original curve we then multiply our matrix of (translated) points by a reflection matrix and then rotation matrices to complete the picture. Reflection and rotation matrices are given respectively by,

$$\begin{bmatrix} \cos(2\lambda) & \sin(2\lambda) \\ \sin(2\lambda) & -\cos(2\lambda) \end{bmatrix}, \begin{bmatrix} \cos(\lambda) & \sin(\lambda) \\ -\sin(\lambda) & \cos(\lambda) \end{bmatrix},$$

where $\lambda$ can be either the angles between the line of symmetry in the case of reflection, or the degrees of rotation in the case of rotation. Hence we reflect using the matrix,

$$\begin{bmatrix} \frac{1}{2} & \frac{\sqrt{3}}{2} \\ \frac{\sqrt{3}}{2} & -\frac{1}{2} \end{bmatrix},$$

and then rotating both of these images (original and reflected) 120° in anti-clockwise and clockwise using the matrices,

$$\begin{bmatrix} \cos(\frac{2\pi}{3}) & \sin(\frac{2\pi}{3}) \\ -\sin(\frac{2\pi}{3}) & \cos(\frac{2\pi}{3}) \end{bmatrix}, \begin{bmatrix} \cos(\frac{2\pi}{3}) & -\sin(\frac{2\pi}{3}) \\ \sin(\frac{2\pi}{3}) & \cos(\frac{2\pi}{3}) \end{bmatrix}.$$

Figure 2.8 shows the result of these reflections and transformations to complete a full solution for mode 3.

Once we understand the computation of mode 2 and the translation, reflection and rotation nature of mode 3, as we increase $n$ we continue in the same way adjusting only our initial conditions and then our transformation matrices. Some results demonstrated in Figure 2.9.

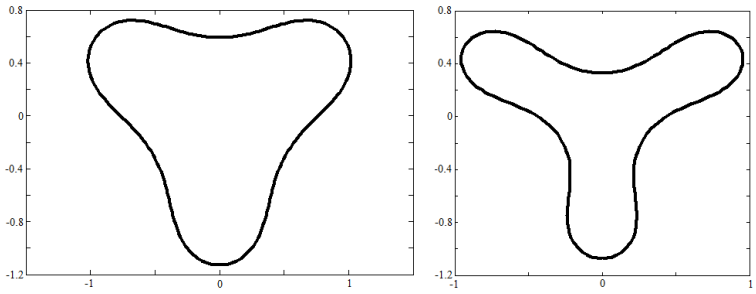

Figure 2.8: Complete solutions for $n = 3$. The first when $\hat{p} = 10$ and the second when $\hat{p} = 13.5$. Plot obtained by solving (2.11), the equations an the elastic profile subjected to pressure, with $n = 3$.

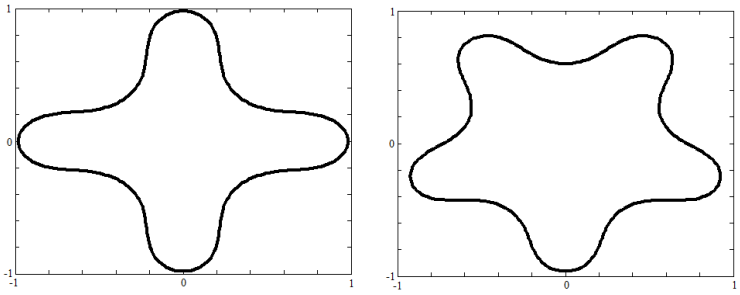

Figure 2.9: Complete solutions for $n = 4$ when $\hat{p} = 24$ and $n = 5$ when $\hat{p} = 34.5$. Plots obtained by solving (2.11), the equations an the elastic profile subjected to pressure numerically. The solutions here are results from the plotting procedure as described, but in Appendix G an alternative plotting method is briefly described.

## 2.5 Contact Pressure

It should be noted that there exists an upper bound for pressure in order to obtain valid solutions. As the elastic ring buckles more and more under an increasing pressure difference

there will come a point where the sides will come into contact. This we will term the 'point of contact'. Once this condition is reached a different approach to a solution is required (and discussed in Flaherty et al. [10]). Some points of contact are shown in Figure 2.10. These contact points were calculated in [10], they can be found relativity easily by running the numerical scheme to solve the problem and checking to see when we have overlapping $(x, y)$ coordinates for a given position in $s$.

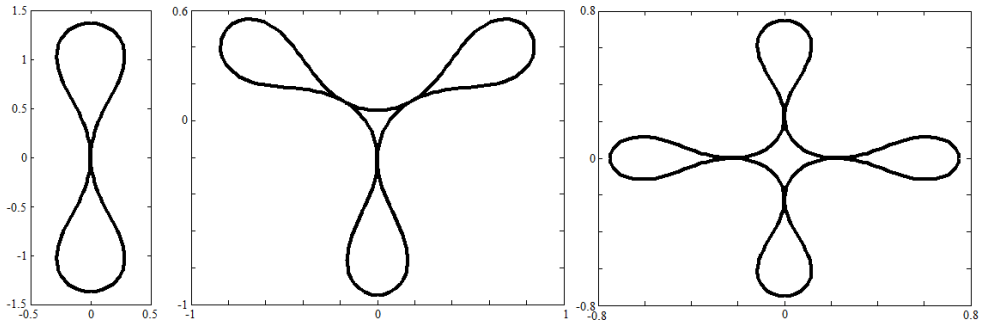


Figure 2.10: Points of contact for $n = 2, 3, 4$ with corresponding pressures $p = 5.247$, $p = 21.65$ and $p = 51.84$.

# 3

# Profiles of Boundaries for a Fluid Annulus

In the coming section we are concerned with the problem of a cross section that creates an annular fluid sheet contained between two boundaries as shown in Figure 3.1. In Figure 3.1 we have a natural resting state of circular boundaries and are interested to find the profiles of these boundaries under certain conditions, namely the fluid between the boundaries moving in a steady state as if rotating around a point vortex in the centre of the sheet. The problem has been studied by Blyth and Vanden-Broeck [7] for the situation where surface tension creates each boundary. We begin the section by following the work of [7], and then explain how to extend this for the case where each boundary is elastic. The flow is assumed to be inviscid, incompressible and irrotational.

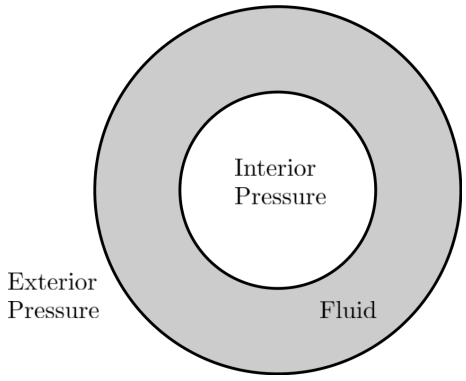


Figure 3.1: The setup to the fluid annulus problem. We have fluid bound between two rings. There is an interior pressure caused by the inner boundary that is free to be different to the exterior pressure.

## 3.1 Profiles of Boundaries held by Surface Tension

As discussed in the introduction for Chapter 3, we are considering the situation where a fluid is contained between two surfaces that are held with surface tension. The setup of

this configuration is shown in more detail in Figure 3.2, where we have also fixed standard cartesian and polar axes as shown. We have also labelled the outer boundary as $A$ and the inner as $B$, and sub-scripting show which boundary is being discussed, for example we have denoted the surface on $A$ as $S_A$, and on $B$ as $S_B$. The pressure inside the fluid is $p$, while the constant internal and external pressures are $p_i$ and $p_e$ respectively.

We will make the assumptions that the fluid contained between $S_A$ and $S_B$ is inviscid and

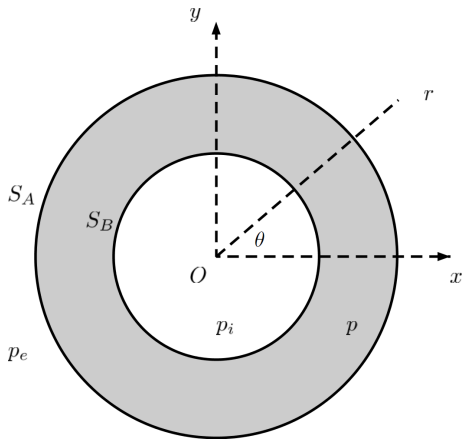


Figure 3.2: Defining key parts of the fluid annulus. $S_A$ and $S_B$ are the outer and inner surfaces respectively. There are three pressures: inside the inner cell; in the fluid; and exterior to the system, these are $p_i$, $p$ and $p_e$ respectively. The coordinate axes are setup ut wit the origin i the centre of the circles.

incompressible. We will assume the flow to be moving as a result of a point vortex at the origin in Figure 3.2, which would be the centre of the circles before any deformation due to the flow. To model the flow we will introduce a complex potential, $w$, (see Acheson [1] for example) in the form $w(z) = \phi + i\psi$, where $\phi$ and $\psi$ are the potential and streamfunction respectively for the fluid flow, and $z = x + iy$. Hence $\phi$ is the velocity potential, $w$ is the complex potential, and $\psi$ is the streamfunction, all of which are functions of both $x$ and $y$. The basic anticlockwise flow for a fluid with circular boundaries is known and is be given by,

$$w = -i\frac{\Gamma}{2\pi}\log z, \tag{3.1}$$

where $\Gamma$ is a circulation constant, and so a measure the flow strength. More explanations of the form of $w$ can be found in [1]. Substituting $w$ and $z$ in to (3.1) we have,

$$\phi + i\psi = -i\frac{\Gamma}{2\pi}\log(x + iy),$$

$$\Rightarrow \quad x = e^{-\frac{2\pi}{\Gamma}\psi}\cos\left(\tfrac{2\pi}{\Gamma}\phi\right) \quad , \quad y = e^{-\frac{2\pi}{\Gamma}\psi}\sin\left(\tfrac{2\pi}{\Gamma}\phi\right), \tag{3.2}$$

$$\Rightarrow x^2 + y^2 = e^{-\frac{4\pi}{\Gamma}\psi},$$

and so plotting streamlines in the $(x, y)$ plane would yield a series of circles with the radius defined by the value of the stream function and the strength of the flow.

If we subscript the fluid pressure, $p$ in Figure 3.2, to be $p_A$ and $p_B$ at the surfaces $S_A$ and $S_B$ respectively then a simple force balance along the boundaries tell us that the pressure difference across the boundary must be equal and opposite to the stress due to surface tension. This gives us,

$$p_B - p_i = \gamma_B \kappa_B,$$

$$p_A - p_e = -\gamma_A \kappa_A,$$

where we have defined $\kappa$ as the curvature of the surface. By definition we will have negative curvature for a circle. $\gamma_A$ and $\gamma_B$ are the constants for surface tension along the boundaries. Writing $U_A$ and $U_B$ as the magnitude for the velocities on the two boundaries, the Bernoulli's equations (see Acheson [1]) gives,

$$\frac{1}{2}U_A^2 - \frac{\gamma_A \kappa_A}{\rho} = c_1, \tag{3.3}$$

$$\frac{1}{2}U_B^2 + \frac{\gamma_B \kappa_B}{\rho} = c_2, \tag{3.4}$$

on each boundary, where $\rho$ is the fluid density. Here $c_1$ and $c_2$ are generally different constants due to the fact that the internal and external pressure may differ.

The solutions can be characterised by the dimensionless parameters,

$$\alpha = \left(\tfrac{2\pi}{\Gamma}\right)^2 \tfrac{\gamma_A r_A}{\rho} \quad , \quad \lambda = \tfrac{r_B}{r_A} \quad , \quad \beta = \tfrac{\gamma_B}{\gamma_A} \ , \tag{3.5}$$

where $r$ is the radius of an unperturbed surface, $S$, which would be a circular solution. The definitions of $\alpha$, $\lambda$ and $\beta$ arise naturally from analysis presented in the next section. We will later find a numerical solution to (3.3) and (3.4), but to get an understanding of the characteristics of the solution we will first look at a linearised solution.

### 3.1.1 Linear Analysis

As previously stated, the equation (3.1) gives a solution for a circular flow. Given the setup of the problem as set up in Figure 3.2 it makes sense to seek a linear solution to the Bernoulli

equations (3.4) and (3.4) as a perturbation of a circular solution. We will work in plane polar coordinates $(r, \theta)$ and have $\beta = 1$, and hence $\gamma = \gamma_A = \gamma_B$ representing the same surface tension on each surface $S_A$ and $S_B$, and the radius of the circular solution is given by $r_A$ and $r_B$ respectively. From (3.2) for circular flow and $x = r\cos\theta$ and $y = r\sin\theta$ we have,

$$\frac{y}{x} = \tan\theta = \tan\left(\frac{2\pi}{\Gamma}\phi\right) \Rightarrow \phi = \frac{\Gamma}{2\pi}\theta.$$

Hence we seek a solution in the form of,

$$r = r_A + \epsilon f_A(\theta) \quad \text{on} \quad S_A,$$

$$r = r_B + \epsilon f_B(\theta) \quad \text{on} \quad S_B,$$

$$\phi = \frac{\Gamma}{2\pi}\theta + \epsilon f_\phi(r, \theta),$$

where $\epsilon$ is a small dimensionless parameter and $f_A$, $f_B$ and $f_\phi$ are functions to be defined. We could continue with the general $f_A$, $f_B$ and $f_\phi$ functions, but using Blyth and Vanden-Broeck [7] we will continue with,

$$r = r_A + \epsilon d\cos k\theta \quad \text{on} \quad S_A, \tag{3.6}$$

$$r = r_B + \epsilon\cos k\theta \quad \text{on} \quad S_B, \tag{3.7}$$

$$\phi = \frac{\Gamma}{2\pi}\theta + \epsilon F(r)\sin k\theta, \tag{3.8}$$

where $d$ and $k$ are dimensionless constants. From the definition of the potential we have $\nabla\phi = (u, v) = \left(\frac{d\phi}{dr}, \frac{1}{r}\frac{d\phi}{d\theta}\right)$ and $U^2 = |\nabla\phi|^2$, and then using (3.8),

$$\Rightarrow U^2 = |\nabla\phi|^2 = \frac{1}{r^2}\left(\frac{\Gamma^2}{4\pi^2} + \frac{\epsilon k\Gamma}{\pi}F\cos k\theta\right) + O\left(\epsilon^2\right). \tag{3.9}$$

Working from (3.6) on $S_A$,

$$\frac{1}{r^2} = \frac{1}{r_A^2}\left(1 - \frac{2\epsilon d}{r_A}\cos k\theta + O(\epsilon^2)\right),$$

and so from (3.9) on $S_A$ we have,

$$U_A^2 = \frac{1}{r_A^2}\left(\frac{\Gamma^2}{4\pi^2} + \frac{\epsilon k\Gamma}{\pi}F\cos k\theta - \frac{\epsilon d\Gamma^2}{2\pi^2 r_A}\cos k\theta\right) + O(\epsilon^2). \tag{3.10}$$

In addition to $U_A$ we also need to find an expression for the curvature to solve (3.3). The general expression for curvature in polar coordinates is given by (see Casey [8] for example),

$$\kappa(\theta) = \frac{|r^2 + 2r'^2 - rr''|}{(r^2 + r'^2)^{\frac{3}{2}}}.$$

From (3.6) we can substitute into the curvature formula to give,

$$\kappa_A = \frac{1}{r_A^3}|r_A^2 + 2r_A\epsilon d\cos k\theta + \epsilon r_A k^2 d\cos k\theta|\left(1 - \frac{3\epsilon d}{r_A}\cos k\theta + O\left(\epsilon^2\right)\right).$$

From Figure 3.2 and the definition of curvature, $\kappa = \nabla \cdot \mathbf{n}$, we have negative curvature since $\mathbf{n}$ is pointing towards the origin. The expression for curvature in our problem becomes,

$$\kappa_A = -\frac{1}{r_A^2}\left(r_A - \epsilon d\cos k\theta + \epsilon k^2 d\cos k\theta\right) + O\left(\epsilon^2\right). \tag{3.11}$$

Using (3.10) and (3.11), to leading order the Bernoulli equation on $S_A$ (3.3) becomes,

$$\frac{\Gamma^2}{8r_A^2\pi^2} + \frac{\gamma}{\rho r_A} = c_1,$$

and to $O(\epsilon)$ we have,

$$\left(\frac{\Gamma}{2\pi}\right)\left[kF(r_A) - \frac{\Gamma d}{2\pi r_A}\right] - \frac{d\gamma}{\rho}\left(1 - k^2\right) = 0. \tag{3.12}$$

Following the same process through as above using (3.7) instead of (3.6), we find that the Bernoulli equation on $S_B$ given by (3.4) yields,

$$\left(\frac{\Gamma}{2\pi}\right)\left[kF(r_B) - \frac{\Gamma}{2\pi r_B}\right] + \frac{\gamma}{\rho}\left(1 - k^2\right) = 0. \tag{3.13}$$

The fluid flow between the two surfaces $S_A$ and $S_B$ needs to satisfy the kinematic condition (see Acheson [1]), which essentially states that fluid particles at the boundary will remain at the boundary. Mathematically this means $\nabla\phi \cdot \mathbf{n} = 0$. Using standard coordinate geometry results in polar coordinates (see MacIlwaine [15] for example) and (3.6), the normal is calculated by,

$$\mathbf{n} = \nabla\Big(r - (r_A + \epsilon d\cos k\theta)\Big) = \left(1, \frac{1}{r}\epsilon dk\sin k\theta\right),$$

and so using (3.8) with $\nabla\phi \cdot \mathbf{n} = 0$ the kinematic condition becomes,

$$\left(\epsilon F'\sin k\theta, \frac{1}{r}\left(\frac{\Gamma}{2\pi} + k\epsilon F\cos k\theta\right)\right) \cdot \left(1, \frac{1}{r}\epsilon dk\sin k\theta\right) = 0 \Rightarrow F' + \frac{\Gamma dk}{2\pi r^2} = 0,$$

where the prime denotes differentiation with respect to $r$, and evaluated at $r = r_A$. To leading order, the kinematic condition on the surface $S_A$ is given by,

$$F'(r_A) = -\frac{\Gamma dk}{2\pi r_A^2}. \tag{3.14}$$

Following the same process by using (3.7) in place of (3.6), the kinematic condition on the surface $S_B$ is given by,

$$F'(r_B) = -\frac{\Gamma k}{2\pi r_B^2}. \tag{3.15}$$

In the introduction we stated we were looking at an annulus where the fluid contained is incompressible and irrotational. Therefore the fluid flow must satisfy Laplace's equation (see Acheson [1]) at all points throughout the fluid. This is given by,

$$\nabla^2\phi = \phi_{rr} + \frac{\phi_r}{r} + \frac{\phi_{\theta\theta}}{r^2} = 0.$$

Seeking a solution to Laplace's equation of the form $\phi = F(r)\sin k\theta$ as is suggested by (3.8) gives,

$$F'' + \frac{F'}{r} + k\frac{F}{r^2} = 0.$$

Therefore a general solution is given by $F(r) = a_1 r^k + a_2 r^{-k}$.

As a quick summary, we have six parameters that we can fix and will define the physical setup of the situation. The physical parameters are: the circulation strength $\Gamma$; the natural radius of the circular flow with no distortion, $r_A$ and $r_B$; the wave number $k$; the fluid density $\rho$; and, the surface tension on the surfaces $\gamma$. These physical parameters are combined in the dimensionless parameters $\alpha$, $\beta$ and $\lambda$. We have three unknown constants for the linear analysis that we need to find, these are $a_1$, $a_2$ and $d$. We have four equations we can use to find these constants, these come from the two Bernoulli equations (3.12) and (3.13) and the two kinematic conditions (3.14) and (3.15). This means we can use three of the equations to find the three constants in terms of the parameters, and then the fourth will give us a set of values for the parameters that will give us a solution for any specified wave number, $k$. As an example[1], and to find agreement with Blyth and Vanden-Broeck [7], below is the equation that needs to be satisfied when $k = 2$,

$$3\lambda(\lambda-1)(\lambda^2+1)\alpha^2 + (\lambda^4+2\lambda^3-2\lambda^2+2\lambda+1)\alpha + (\lambda-1)(\lambda^2+1) = 0, \tag{3.16}$$

where $\alpha$ and $\lambda$ are given by (3.5) with $\beta = 1$ .

We can now also sketch out an example solution. Given its definition in (3.5) we have $\lambda \in \mathbb{R}$

[1]The procedure for finding the constants $a_1$, $a_2$ and $d$ and then substituting into the fourth equation by hand is a rather laborious task but can be easily achieved with a package such as Maple.

and $\lambda \leq 1$, we can take $\lambda = \frac{1}{2}$ for example, and if we want $k = 2$, from (3.16) we have,

$$-\frac{15}{16}\alpha^2 + \frac{29}{16}\alpha - \frac{5}{8} = 0 \Rightarrow \alpha = \frac{29 \pm \sqrt{241}}{30} \approx 0.449, 1.484.$$

To achieve $\lambda = \frac{1}{2}$ we simply need an appropriate ratio such as $r_A = 2$ and $r_B = 1$. Then all that remains to be done is choose $\Gamma$, $\rho$ and $\gamma$ appropriately such that $\alpha$ satisfies one of the values above from the definition in (3.5), e.g.

$$\frac{8\pi^2\gamma_A}{\Gamma^2\rho} = \frac{29 - \sqrt{241}}{30}.$$

An example, appropriate values for water would be, surface tension $\gamma = 0.05$ and density $\rho = 1$, this then gives $\Gamma \approx 8.789$. Substituting these values into our expression for $d$, we can then use (3.6) and (3.7) with a small value for $\epsilon$ to produce an example sketch, as we have done in Figure 3.3.

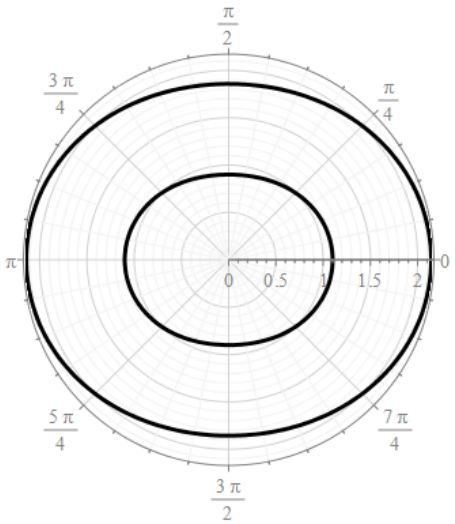


Figure 3.3: Example solution of the fluid annulus problem. Example values were $r_A = 2$, $r_B = 1$, $\gamma = 0.05$, $\rho = 1$, $\Gamma \approx 8.789$, $\epsilon = 0.1$

### 3.1.2 Numerical Computations

If we introduce $u$ and $v$ to be horizontal and vertical velocity components respectively, then we can introduce $\tau(\phi, \psi)$ and $\theta(\phi, \psi)$ such that,

$$u - iv = e^{\tau - i\theta} = e^{\tau}\left(\cos(\theta) - i\sin(\theta)\right). \tag{3.17}$$

Then in general from (3.17) we have,

$$U^2 = u^2 + v^2 = (u - iv)(u + iv) = e^{2\tau}\left(\cos(\theta) - i\sin(\theta)\right)\left(\cos(\theta) + i\sin(\theta)\right) = e^{2\tau}. \tag{3.18}$$

and the curvature can be written as,

$$\kappa = -e^{\tau}\frac{\partial\theta}{\partial\phi}. \tag{3.19}$$

Taking $r_A$ as the radius of the circular boundary for a non-perturbed profile as the characteristic length, and $\frac{\Gamma}{2\pi r_A}$ as the characteristic speed to non-dimensionalise (3.3) and (3.4) we obtain,

$$\frac{1}{2}\tilde{U_A^2}\left[\frac{\Gamma}{2\pi r_A}\right]^2 - \left[\frac{1}{r_A}\right]\frac{\gamma_A\tilde{\kappa_A}}{\rho} = c_1 \Rightarrow \frac{1}{2}\tilde{U_A^2} - \alpha\tilde{\kappa_A} = B_1, \tag{3.20}$$

$$\frac{1}{2}\tilde{U_B^2}\left[\frac{\Gamma}{2\pi r_A}\right]^2 + \left[\frac{1}{r_A}\right]\frac{\gamma_B\tilde{\kappa_B}}{\rho} = c_2 \Rightarrow \frac{1}{2}\tilde{U_B^2} + \alpha\beta\tilde{\kappa_B} = B_2, \tag{3.21}$$

where $\tilde{}$ denotes non-dimensional variables and,

$$\alpha = \left[\tfrac{2\pi}{\Gamma}\right]^2\frac{r_A\gamma_A}{\rho} \quad \text{and} \quad \beta = \tfrac{\gamma_B}{\gamma_A}.$$

From (3.18) we can replace $\tilde{U_A^2}$ and $\tilde{U_B^2}$ in (3.20) and (3.21) with $e^{2\tau}$ noting that $\tau$ will be different on each of the surfaces (also we make explicitly clear that $\tau$ is a measure of flow velocity and will not be constant along the boundary). Also using (3.19) we find that (3.20) and (3.21) become,

$$\frac{1}{2}e^{2\tau} + \alpha e^{\tau}\frac{\partial\theta}{\partial\phi} = B_1, \tag{3.22}$$

$$\frac{1}{2}e^{2\tau} - \alpha\beta e^{\tau}\frac{\partial\theta}{\partial\phi} = B_2, \tag{3.23}$$

on the surfaces $A$ and $B$ respectively, and $B_1$ and $B_2$ are generally different Bernoulli constants. We seek solutions that are periodic in $\phi$ (since we physically require a closed loop), then we can introduce,

$$t = e^{2i\pi f} \quad \text{where} \quad f = \phi + i\psi, \tag{3.24}$$

and express the solution, $\zeta$, as a series in the form,

$$\zeta = \tau - i\theta = \log\left(\frac{1}{2\pi}\right) - i\left(2\pi f + \frac{\pi}{2}\right) + \sum_{n=1}^{\infty} a_n t^n + \sum_{n=1}^{\infty} b_n t^{-n}. \tag{3.25}$$

The first two terms on the right hand side of (3.25) are suggested by Blyth and Vanden-Broeck [7] and come from the point vortex at the origin. The unknown constants $a_n$ and $b_n$ are calculated numerically as part of the solution. We can choose the value of the stream-function along one surface, and so we will have $\psi = 0$ along $S_A$, and for now we will denote the value for the stream-function on $S_B$ as $\psi = Q$.

In order to solve numerically we truncate (3.25) at $N-1$ terms and introduce $2N$ collocation points for $\phi_i^A$ and $\phi_i^B$ along $S_A$ and $S_B$ respectively where,

$$\phi_i^A = \phi_i^B = \tfrac{1}{N}(i-1), \quad i = 1, \ \ldots \ , N. \tag{3.26}$$

We can fix the value of $\beta$, and so applying (3.26) with (3.25) on (3.22) and (3.23), we have $2N$ nonlinear equations, along with $2N+1$ unknowns $(a_1, \ \ldots \ , a_{N-1}, b_1, \ \ldots \ , b_{N-1}, B_1, B_2, \alpha)$ and can solve this numerically. In this thesis we choose Newton's method to solve this system of equations. Once we have a solution we then need to find $(x, y)$ coordinates in order to plot the wave profiles. From (3.18) we have,

$$u + iv = \frac{U^2}{u - iv},$$

but since we have non-dimesionalised such that $U \equiv 1$, when we also use (3.17) we have,

$$u + iv = \frac{1}{u - iv} = e^{-\tau + i\theta}.$$

The definition of the complex potential then gives us,

$$\frac{\partial x}{\partial \phi} = e^{-\tau}\cos\theta \quad \text{and} \quad \frac{\partial y}{\partial \phi} = e^{-\tau}\sin\theta.$$

We can numerically compute our wave profiles with,

$$x_i = x_{i-1} + e^{-\tau_i}\,(\phi_i - \phi_{i-1})\cos\theta_i,$$

$$y_i = y_{i-1} + e^{-\tau_i}\,(\phi_i - \phi_{i-1})\sin\theta_i,$$

on each surface $A$ and $B$, where $i = 1, \ \ldots \ , N$ and we only need to specify $x_0$ and $y_0$. In a sense these values are arbitrary so it is convenient to solve the system and the transpose such that the surfaces have a common focal point.

As a numerical approach Blyth and Vanden-Broeck [7] suggest fixing the value of $a_1$ to give $2N$ unknowns. Figure 3.4 is provided as an example numerical solution.

## 3.2 Profiles of Elastic Boundaries

Here we give a brief outline of an extension to Blyth and Vanden-Broeck [7] by looking at the profiles of boundaries in Figure 3.1 when we have elastic boundaries at the surfaces $A$ and $B$,

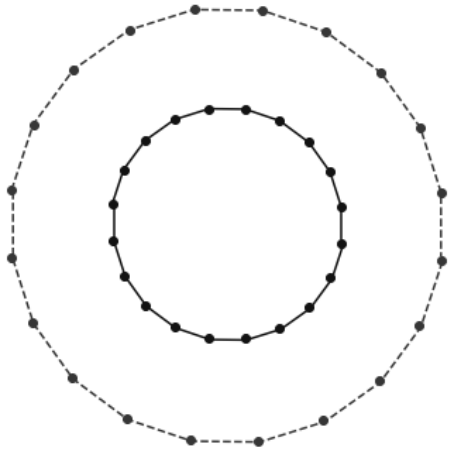

Figure 3.4: Example numerical solution for the profiles of elastic boundaries for the fluid annulus.

rather than surface tension. In Section 2.1 we derived the elastic surface equations resulting in (2.6) which was,

$$\epsilon_B \kappa'' + \epsilon_B \frac{\kappa^3}{2} - c\kappa - p = 0,$$

where $\epsilon_B$ was the bending modulus of the elastic, $\kappa$ was the curvature of the surface, and $p$ is the normal pressure difference across the surface, and $c$ is a constant to be determined. Hence, using,

$$p = \epsilon_B \kappa'' + \epsilon_B \frac{\kappa^3}{2} - c\kappa,$$

we can replace the Bernoulli equations (3.3) and (3.4) with,

$$\frac{1}{2}\rho U_A^2 - \left(\epsilon_A \kappa_A'' + \epsilon_A \frac{\kappa_A^3}{2} - c_A \kappa_A\right) = C_1, \tag{3.27}$$

$$\frac{1}{2}\rho U_B^2 + \left(\epsilon_B \kappa_B'' + \epsilon_B \frac{\kappa_B^3}{2} - c_B \kappa_B\right) = C_2, \tag{3.28}$$

where we have sub-scripted $A$ and $B$ to denote which surface the equation applies to, $\rho$ is the fluid density, and $C_1$ and $C_2$ are Bernoulli constants. The numerical process is then essentially the same as in the previous section, but we will also include numerical finite difference methods to include $\kappa''$.

# 4

# Profiles of an Elastic Arch Subjected to Pressure

In this chapter we are looking at a curved piece of elastic membrane that is fixed at two points to a fixed surface. The membrane encloses a given pressure and the elastic is subjected to a different pressure on the outside. We are looking to find solutions of the shape of the elastic as the pressure difference changes. The physical setup of the problem is analogous to that as presented in chapter 2 but holding in place two points on the non-stretchable elastic.

## 4.1 Problem Formulation

Our problem is shown in Figure 4.1. We have an elastic membrane that is attached at the fixed points $A$ and $B$. We will fix standard $xy$-plane such that $(0,0)$ is centered at $A$. The surface we are attached to will be assumed to be solid and perfectly straight laying along the $x-axis$. $p_i$ and $p_o$ are the inside and outside pressure respectively. $\theta(s)$ is the angle between the tangent to the elastic at point $s$ which is a measure of how far along the elastic we are such that $s=0$ at $A$ and $s=L$ at $B$ where $L$ is the total length of the elastic material. If we have two fixed points then we can define the coordinates at $A$ as $(0,0)$ and at $B$ as $(X,0)$, where we are free to choose the distance of $|X|$. It is worth noting that using this setup $X$ will be a negative number.

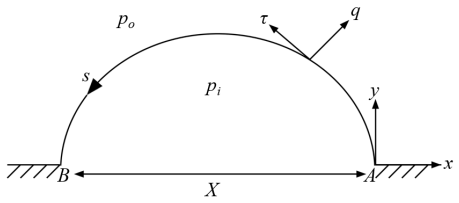


Figure 4.1: Elastic membrane attached at the points $A$ and $B$. There is a pressure difference across the boundary with a fixed inside pressure, $p_i$, and outside pressure, $p_o$.

We will assume the values of $\theta$ at both $A$ and $B$, and define them as $\theta_A$ and $\theta_B$. This would

depend on how the elastic is fixed to our surface below. We have already derived the equation of an elastic boundary subjected to pressure in chapter 2. These equations are again stated in (4.1a) - (4.1f) for easy references. Here $q$, $\tau$, $\kappa$, $\theta$, $x$ and $y$ are all functions of $s$. The forces of the elastic membrane are $q$ and $\tau$ in the respective normal and tangential directions. $\kappa$ is a measure of the curvature, and $p = p_o - p_i$

$$q' = p + \kappa\tau, \tag{4.1a}$$

$$\tau' = -\kappa q, \tag{4.1b}$$

$$\kappa' = q, \tag{4.1c}$$

$$\theta' = \kappa, \tag{4.1d}$$

$$x' = \cos\theta, \tag{4.1e}$$

$$y' = \sin\theta, \tag{4.1f}$$

subject to the conditions that,

$$x(0) = 0, \quad y(0) = 0, \quad x(L) = X, \quad y(L) = 0, \quad \theta(0) = \theta_A, \quad \theta(L) = \theta_B. \tag{4.2}$$

We will solve this system numerically using the numerical scheme detailed in Appendix A by setting $\theta(0) = \theta_A$, $x(0) = 0$ and $y(0) = 0$ and then finding $q(0)$, $\tau(0)$ and $k(0)$ subject to the forcing conditions $x(L) - x = 0$, $y(L) = 0$ and $\theta(L) - \theta_B = 0$.

## 4.2 Symmetric Solutions

Working from our initial formulation equation (2.2), the force balance, we can integrate over the length of the membrane,

$$[\tau\mathbf{t} + q\mathbf{n}]_0^L - p\int_0^L \mathbf{n}\, ds = 0. \tag{4.3}$$

Note that when integrating around the whole enclosed shape, along the membrane and the solid base we have,

$$\oint_C \mathbf{n}\, ds = \int_0^L \mathbf{n}\, ds - \int_L^{L-X} \mathbf{j}\, ds, \tag{4.4}$$

since along the horizontal wall the normal is always pointing downwards in Figure 4.1. Note the upper limit of $L - X$. It is possibly not immediately obvious that the minus sign must be included. This is because the total length of the membrane and the lower boundary wall have

a total length of $|L| + |X|$, and whilst $L$ is a positive constant in our setup $X$ is a negative constant, hence $|L| + |X| = L - X$. We can apply the divergence theorem (see Schey [20] for example) in the form,

$$\int_C \phi \mathbf{n}\, ds = \int\int_A \nabla\phi\, dA.$$

The Divergence theorem in general says that the outward flux of a vector field though a closed surface is equal to the volume over the region inside the surface, i.e. all in and out flow is equal to the internal volume. As long as there in no flow in and out then this holds for any value of $\phi$, and so (choosing a value of $\phi = 1$ for example) we must have,

$$\int_C \mathbf{n}\, ds = 0.$$

Using this along with (4.4) we find,

$$\int_0^L \mathbf{n}\, ds = \int_L^{L-X} \mathbf{j}\, ds = -X\mathbf{j},$$

and then (4.3) becomes,

$$\tau(L)\mathbf{t} + q(L)\mathbf{n} - \tau(0)\mathbf{t} - q(0)\mathbf{n} + pX\mathbf{j} = 0. \tag{4.5}$$

Using the $\mathbf{i}$ and $\mathbf{j}$ direction vectors in the horizontal and vertical directions, from Figure 4.1 and using trigonometric identities we can show that $\mathbf{t} = \cos(\theta)\mathbf{i} + \sin(\theta)\mathbf{j}$ and $\mathbf{n} = \sin(\theta)\mathbf{i} - \cos(\theta)\mathbf{j}$. Then after substituting $\mathbf{t}$ and $\mathbf{n}$ into (4.5) and taking the dot product with $\mathbf{i}$ and then $\mathbf{j}$, respectively, we obtain,

$$\tau(L)\cos(\theta_B) + q(L)\sin(\theta_B) - \tau(0)\cos(\theta_A) - q(0)\sin(\theta_A) = 0, \tag{4.6}$$

$$\tau(L)\sin(\theta_B) - q(L)\cos(\theta_B) - \tau(0)\sin(\theta_A) + q(0)\cos(\theta_A) + pX = 0. \tag{4.7}$$

The conditions (4.6) and (4.7) hold for any solution of our problem, symmetric or not. However, with a symmetric solution we have $\tau(0) = \tau(L)$ and $q(0) = -q(L)$ and so (4.6) and (4.7) become,

$$\tau(0)\left[\cos(\theta_B) - \cos(\theta_A)\right] - q(0)\left[\sin(\theta_B) + \sin(\theta_A)\right] = 0, \tag{4.8}$$

$$\tau(0)\left[\sin(\theta_B) - \sin(\theta_A)\right] + q(0)\left[\cos(\theta_B) + \cos(\theta_A)\right] + pX = 0. \tag{4.9}$$

In addition, with a symmetric solution $\theta_B = 2\pi - \theta_A$ and so $\sin(\theta_B) = -\sin(\theta_A)$ and $\cos(\theta_B) = \cos(\theta_A)$. This means (4.8) is automatically satisfied but (4.9) becomes,

$$\tau(0)\sin(\theta_A) - q(0)\cos(\theta_A) = \frac{pX}{2}. \tag{4.10}$$

In our problem $\theta_A$, $p$ and $X$ are defined constants and so (4.10) gives us a relationship between $\tau(0)$ and $q(0)$. There are some interesting conditions that come about from (4.10), namely when we have the membrane attached perpendicularly ($\theta_A = \pi/2$) and tangentially ($\theta_A = \pi$) to the horizontal base. These cases give us conditions $\tau(0) = \frac{pX}{2}$ and $q(0) = \frac{pX}{2}$ respectively.

## 4.3 Perturbed Solution

As we will see, a semi-circular solution is always possible if the elastic length and initial angles for the geometry of the shape allow this. For here we are concerned with finding bifurcations from the semi-circular solution. We will start from our original set of equations taken from (4.1a) - (4.1f). For a setup where a semi-circular solution is possible we have a clear link between $X$ and $L$ namely that $|2L| = |\pi X|$. With the benefit of hindsight we will conveniently scale the problem such that the radius of the semi-circle is of length 1 and so $L = \pi$. We will proceed using the hat notation to make it clear when working in this particular scale.

For the semi-circular solution we have $\hat{q} = 0$, $\hat{\kappa} = 1$, and $\hat{\tau} = -\hat{p}$. We also have $\theta = \pi/2$, $x = 0$, $y = 0$ at $\hat{s} = 0$. Using (4.1d) we then have,

$$\theta' = \hat{\kappa} \Rightarrow \theta = \hat{\kappa}\hat{s} + constant \Rightarrow \theta = \hat{s} + \frac{\pi}{2}, \tag{4.11}$$

which we can then substitute into (4.1e) and (4.1f) to obtain,

$$x' = \cos\left(\hat{s} + \frac{\pi}{2}\right) = -\sin(\hat{s}) \Rightarrow x = \cos(\hat{s}) - 1 = x_0(\hat{s}), \tag{4.12}$$

$$y' = \sin\left(\hat{s} + \frac{\pi}{2}\right) = \cos(\hat{s}) \Rightarrow y = \sin(\hat{s}) = y_0(\hat{s}). \tag{4.13}$$

We can look to find bifurcation points for additional solutions by perturbing the semi-circular solution and finding when solutions exist for the perturbation. We will seek solutions of the

form,

$$\hat{q} = 0 + \epsilon\bar{q} \tag{4.14a}$$

$$\hat{\tau} = -\hat{p} + \epsilon\bar{\tau} \tag{4.14b}$$

$$\hat{\kappa} = 1 + \epsilon\bar{\kappa} \tag{4.14c}$$

$$\theta = \hat{s} + \frac{\pi}{2} + \epsilon\bar{\theta} \tag{4.14d}$$

$$x = x_0(\hat{s}) + \epsilon\bar{x} \tag{4.14e}$$

$$y = y_0(\hat{s}) + \epsilon\bar{y}, \tag{4.14f}$$

where $\epsilon << 1$ and $\bar{q}$, $\bar{\tau}$, $\bar{\kappa}$, $\bar{\theta}$, $\bar{x}$ and $\bar{y}$ are all functions of $\hat{s}$. Substituting (4.14a)-(4.14d) into (4.1a)-(4.1d) and taking leading order terms in $\epsilon$ we obtain,

$$\epsilon\bar{q}' = \hat{p} + (1 + \epsilon\bar{\kappa})(-\hat{p} + \epsilon\bar{\tau}) \Rightarrow \bar{q}' = \bar{\tau} - \hat{p}\bar{\kappa},$$

$$\epsilon\bar{\tau}' = -\epsilon\bar{q}(1 + \epsilon\bar{\kappa}) \Rightarrow \bar{\tau}' = -\bar{q},$$

$$\epsilon\bar{\kappa}' = \epsilon\bar{q} \Rightarrow \bar{\kappa}' = \bar{q},$$

$$1 + \epsilon\bar{\theta} = 1 + \epsilon\bar{\kappa} \Rightarrow \bar{\theta} = \bar{\kappa}.$$

Using (4.14e) and (4.11) together with (4.1e), and noting that $x_0' = \cos\left(\hat{s} + \frac{\pi}{2}\right)$ from (4.12) we obtain,

$$\bar{x}' = -\bar{\theta}\sin\left(\hat{s} + \frac{\pi}{2}\right) = -\bar{\theta}\cos(\hat{s}).$$

Using (4.14f) and (4.11) together with (4.1f), and noting that $y_0' = \sin\left(\hat{s} + \frac{\pi}{2}\right)$ from(4.13) we obtain,

$$\bar{y}' = \bar{\theta}\cos\left(\hat{s} + \frac{\pi}{2}\right) = -\bar{\theta}\sin(\hat{s}).$$

From our boundary conditions, $\bar{x}(0) = \bar{y}(0) = \bar{\theta}(0) = 0$, on a semi-circle and (4.14d)-(4.14f) we require a solution that satisfies the system of equations,

$$\bar{q}' = \bar{\tau} - \hat{p}\bar{\kappa}, \tag{4.15a}$$

$$\bar{\tau}' = -\bar{q}, \tag{4.15b}$$

$$\bar{\kappa}' = \bar{q}, \tag{4.15c}$$

$$\bar{\theta}' = \bar{\kappa}, \tag{4.15d}$$

$$\bar{x}' = -\bar{\theta}\cos(\hat{s}), \tag{4.15e}$$

$$\bar{y}' = -\bar{\theta}\sin(\hat{s}). \tag{4.15f}$$

Differentiating (4.15a) and substituting in (4.15b) and (4.15c) gives,

$$\bar{q}'' = -\bar{q} - \hat{p}\bar{q} \Rightarrow \bar{q}'' + (1+\hat{p})\bar{q} = 0, \tag{4.16}$$

which has a general solution $\bar{q} = Am^2\cos(m\hat{s}) + Bm^2\sin(m\hat{s})$ where $m^2 = (1+\hat{p})$, and $A$ and $B$ are constants to be found. It then follows from (4.15c) and (4.15d) that,

$$\bar{\kappa} = Am\sin(m\hat{s}) - Bm\cos(m\hat{s}) + C,$$

$$\bar{\theta} = -A\cos(m\hat{s}) - B\sin(m\hat{s}) + C\hat{s} + D,$$

where $C$ and $D$ are constants of integration. We can use one of the boundary conditions here, namely $\bar{\theta}(0) = 0$ to yield $A = D$, and so,

$$\bar{\theta} = -A\cos(m\hat{s}) - B\sin(m\hat{s}) + C\hat{s} + A. \tag{4.17}$$

Substituting (4.17) into (4.15e) and (4.15f) we obtain,

$$\bar{x}' = A\cos(m\hat{s})\cos(\hat{s}) + B\sin(m\hat{s})\cos(\hat{s}) - C\hat{s}\cos(\hat{s}) - A\cos(\hat{s}), \tag{4.18a}$$

$$\bar{y}' = A\cos(m\hat{s})\sin(\hat{s}) + B\sin(m\hat{s})\sin(\hat{s}) - C\hat{s}\sin(\hat{s}) - A\sin(\hat{s}). \tag{4.18b}$$

After using trigonometric identities and then integrating (4.17) and (4.18), we can evaluate the new constants of integration using the conditions $\bar{x}(0) = \bar{y}(0) = 0$. Then factorising for $A$, $B$ and $C$ gives the system of equations,

$$\bar{\theta} = A\bigg(1 - \cos(m\hat{s})\bigg) - B\sin(m\hat{s}) + C\hat{s}, \tag{4.19}$$

$$\begin{aligned}\bar{x} = A\bigg(\frac{m\sin(m\hat{s})\cos(\hat{s}) - \cos(m\hat{s})\sin(\hat{s})}{m^2-1} - \sin(\hat{s})\bigg) \\ + B\bigg(\frac{m - m\cos(m\hat{s})\cos(\hat{s}) - \sin(m\hat{s})\sin(\hat{s})}{m^2-1}\bigg) + C\bigg(1 - \hat{s}\sin(\hat{s}) - \cos(\hat{s})\bigg).\end{aligned} \tag{4.20}$$

$$\begin{aligned}\bar{y} = A\bigg(\frac{m\sin(m\hat{s})\sin(\hat{s}) + \cos(m\hat{s})\cos(\hat{s}) - 1}{m^2-1} + \cos(\hat{s}) - 1\bigg) \\ + B\bigg(\frac{\sin(m\hat{s})\cos(\hat{s}) - m\cos(m\hat{s})\sin(\hat{s})}{m^2-1}\bigg) + C\bigg(\hat{s}\cos(\hat{s}) - \sin(\hat{s})\bigg).\end{aligned} \tag{4.21}$$

If we then denote matrix elements $M_{ij}$ (and matrix $\mathbf{M}$) where $i = \{\bar{\theta}, \bar{x}, \bar{y}\}$ and $j = \{A, B, C\}$ are the coefficient terms from the equations above then (since we have $\bar{x}(\pi) = \bar{y}(\pi) = \bar{\theta}(\pi) = 0$ by symmetry when $\hat{s} = \pi$),

$$\begin{bmatrix} M_{\bar{\theta}A} & M_{\bar{\theta}B} & M_{\bar{\theta}C} \\ M_{\bar{x}A} & M_{\bar{x}B} & M_{\bar{x}C} \\ M_{\bar{y}A} & M_{\bar{y}B} & M_{\bar{y}C} \end{bmatrix} \begin{bmatrix} A \\ B \\ C \end{bmatrix} = \begin{bmatrix} 0 \\ 0 \\ 0 \end{bmatrix}. \tag{4.22}$$

From this matrix system, one possible way to locate multiple solutions to our problem (and bifurcation points) would be to have [1],

$$det \begin{bmatrix} M_{\bar{\theta}A} & M_{\bar{\theta}B} & M_{\bar{\theta}C} \\ M_{\bar{x}A} & M_{\bar{x}B} & M_{\bar{x}C} \\ M_{\bar{y}A} & M_{\bar{y}B} & M_{\bar{y}C} \end{bmatrix}, = 0$$

hence,

$$M_{\bar{\theta}A}\left(M_{\bar{x}B}M_{\bar{y}C} - M_{\bar{x}C}M_{\bar{y}B}\right) - M_{\bar{\theta}B}\left(M_{\bar{x}A}M_{\bar{y}C} - M_{\bar{x}C}M_{\bar{y}A}\right) + M_{\bar{\theta}C}\left(M_{\bar{x}A}M_{\bar{y}B} - M_{\bar{x}B}M_{\bar{y}A}\right) = 0. \tag{4.23}$$

Before we substitute in our values for the matrix elements we can simplify (4.19), (4.20) and (4.21) since $\hat{s} = \pi$. This substitution gives,

$$\bar{\theta} = A\Big(1 - \cos(m\pi)\Big) - B\sin(m\pi) + C\pi \tag{4.24a}$$

$$\bar{x} = -A\left(\frac{m\sin(m\pi)}{m^2-1}\right) + B\left(\frac{m + m\cos(m\pi)}{m^2-1}\right) + 2C \tag{4.24b}$$

$$\bar{y} = -A\left(\frac{\cos(m\pi)+1}{m^2-1} + 2\right) - B\left(\frac{\sin(m\pi)}{m^2-1}\right) - C\pi. \tag{4.24c}$$

Substituting (4.24) into (4.23) simplifies to the equation,

$$\frac{m^2}{(m^2-1)^2}\left(2m^2\sin(m\pi) + m\pi + m\pi\cos(m\pi) - 2\sin(m\pi)\right) = 0. \tag{4.25}$$

Clearly $\frac{1}{(m^2-1)^2}$ cannot equal zero, and also we have $m \neq \pm 1$, and so we have solutions at $m = 0$ and when,

$$G(m) = 0,$$

[1] See Anton [2] for example.

where,

$$G(m) = 2m^2 \sin(m\pi) + m\pi + m\pi \cos(m\pi) - 2\sin(m\pi). \tag{4.26}$$

Note that $G(m) = 0$ is also satisfied when $m = 0$ and so it will be sufficient to look at roots of the function (4.26) only to find bifurcation points. Also note that due to the properties of sine and cosine all odd integers of $m$ will also be roots of (4.26).

We can see from Figure 4.2 that there are other solutions for $m$ when $G(m) = 0$, in addition

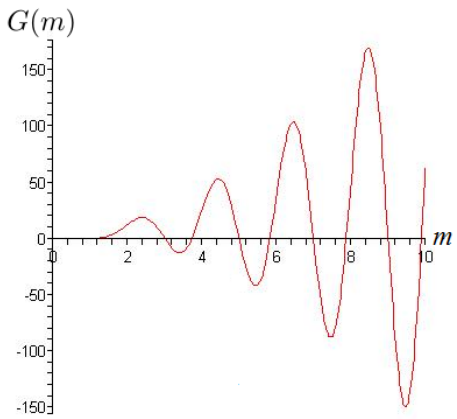


Figure 4.2: Graph of $G(m) = 2m^2 \sin(m\pi) + m\pi + m\pi \cos(m\pi) - 2\sin(m\pi)$. All solutions of (4.26) appear where the curve crosses the $m$-axis. $G(m) = 0$ relates to bifurcation points from when $det(\mathbf{M}) = 0$ from the system (4.22).

to the odd integers of $m$. (It is also worth noting at this stage that $G(m)$ has rotational symmetry of 180° about the origin since $G(-m) = -G(m)$, and so the negative roots of (4.26) for $m$ are of the same magnitude as the positive values). Using our graphical image it is relatively straight forward to have reasonable estimates to solve (4.26) numerically using Newton's Method. Clearly there would be an infinite number of solutions but Table 4.1 lists some of these, and also uses our earlier formula $m^2 = (1 + \hat{p})$.

Notice from Table 4.1 that $m = 0$ and $m = 1$ have been identified as points where we do not have bifurcation even though they are roots of (4.26). To arrive at (4.26) from (4.25) we have already seen that for our problem $m \neq \pm 1$ as the mathematics breaks down at this point. To see about $m = 0$ we need to go back to (4.16) where we first define $m$. This leads to $\bar{q} = A\hat{s} + B$, which gives $\bar{\kappa} = \frac{A}{2}\hat{s}^2 + B\hat{s} + C$ from(4.15c). Equations (4.15d), (4.15e) and (4.15f) then give us,

| $m$ | $\hat{p}$ | Possible Bifurcation Point |
|---|---|---|
| 0 | -1 | × |
| 1 | 0 | × |
| 3 | 8 | ✓ |
| 3.72873 | 12.90343 | ✓ |
| 5 | 24 | ✓ |
| 5.82754 | 32.96022 | ✓ |

Table 4.1: Some solution values for $G(m) = 0$ in (4.26), given to 5 decimal places. Values for $m$ correspond to the axis intersections in Figure 4.2

$$\bar{\theta} = \frac{A}{6}\hat{s}^3 + \frac{B}{2}\hat{s}^2 + C\hat{s} + D,$$

$$\bar{x} = -\frac{A}{6}\Big(\hat{s}^3\sin(\hat{s}) + 3\hat{s}^2\cos(\hat{s}) - 6\cos(\hat{s}) - 6\hat{s}\sin(\hat{s})\Big) - \frac{B}{2}\Big(\hat{s}^2\sin(\hat{s}) - 2\sin(\hat{s}) + 2\hat{s}\cos(\hat{s})\Big) - C\Big(\cos(\hat{s}) + \hat{s}\sin(\hat{s})\Big) - D\sin(\hat{s}) + E,$$

$$\bar{y} = -\frac{A}{6}\Big(-\hat{s}^3\cos(\hat{s}) + 3\hat{s}^2\sin(\hat{s}) - 6\sin(\hat{s}) + 6\hat{s}\cos(\hat{s})\Big) - \frac{B}{2}\Big(-\hat{s}^2\cos(\hat{s}) + 2\cos(\hat{s}) + 2\hat{s}\sin(\hat{s})\Big) - C\Big(\sin(\hat{s}) - \hat{s}\cos(\hat{s})\Big) + D\cos(\hat{s}) + F,$$

respectively, where $A, B, C, D, E, F$ are all constants to be found. Recall that our initial boundary conditions were $\bar{x}(0) = \bar{y}(0) = \bar{\theta}(0) = 0$. This immediately gives us $D = 0$, $E = C - A$, and $F = B$. If we then apply the conditions $\bar{x}(\pi) = \bar{y}(\pi) = \bar{\theta}(\pi) = 0$, we then also find that $A = B = C = 0$. This then gives us a zero solution for all of our perturbed variables, hence there is no bifurcation at this point.

## 4.4 The Shape of Solutions

We will be looking at more detail in the matrix system (4.22). This is a system of equations in the form,

$$\mathbf{Mx} = \mathbf{0}.$$

In order to have a non-trivial solution we must have that $\mathbf{M}$ has no inverse we are looking for the condition $det(\mathbf{M}) = \mathbf{0}$. If we then substitute in the values of $m$ that we found in (4.26) and solve the system of equations we will find we have a vector for $[A\ B\ C]^T$ but there will be a linear dependence included in the vector. As long as we choose values of $A$, $B$ and $C$ in this format we will obtain a solution of (4.22) which we can then use, along with equations (4.19) - (4.21), to plot the shape of the perturbation from our semi-circular solution. Note that this vector is an eigenvector of $\mathbf{M}$ (with the corresponding eigenvalue of zero).

If we substitutive in the value of $m = 3$ (or any odd integer) and $\hat{s} = \pi$ into (4.22) then we obtain $\mathbf{M}$ as,

$$\begin{bmatrix} 2 & 0 & \pi \\ 0 & 0 & 2 \\ 2 & 0 & -\pi \end{bmatrix}, \tag{4.27}$$

the corresponding and relevant eigenvector of (4.27) is,

$$\begin{bmatrix} 0 \\ t \\ 0. \end{bmatrix}. \tag{4.28}$$

Using these values for $A$, $B$ and $C$ along with (4.20), (4.21), (4.12) and (4.13) substituted into (4.14e) and (4.14f), the equations that give $x$ and $y$, with a suitable value for $t$ and $\epsilon$ on the domain $0 \leq \hat{s} \leq \pi$ we can plot a basic shape we would expect for the curved elastic at this bifurcation point. A point to note is that "suitable" values for $t$ and $\epsilon$ are the same as having a single suitable value for $\epsilon t$ since the linear dependence from our eigenvector, along with our approximation of (4.14a) - (4.14f). This is shown in Figure 4.3.

For the non-odd integer solutions for $m$ we can only substitute in the approximated values into (4.22) to obtain $\mathbf{M}$ and find the corresponding eigenvector. For $m = 3.72873$ we obtain,

$$\begin{bmatrix} 0.45392t \\ t \\ -0.28898t \end{bmatrix}, \tag{4.29}$$

which we can plot in the same way we did for $m = 3$. This is shown in Figure 4.4. The eigenvector for $m = 5.82754$ is,

$$\begin{bmatrix} 0.27773t \\ t \\ -0.17681t \end{bmatrix}, \tag{4.30}$$

and the corresponding shape is shown in Figure 4.5.

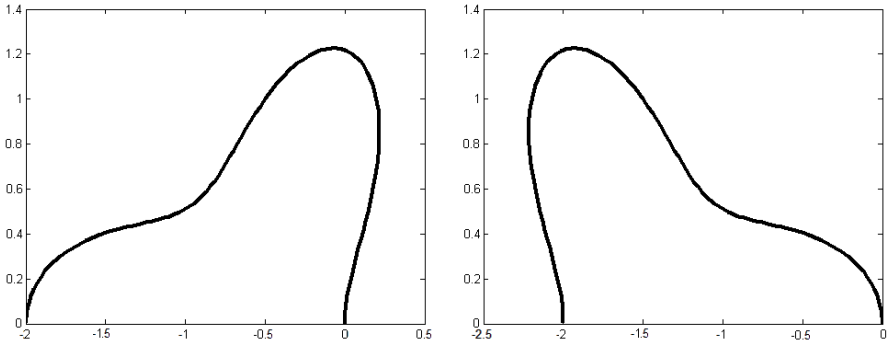


Figure 4.3: Shape of the curved elastic deviation from the semi-circular solution from bifrication point at $m = 3$ ($p = 8$). The left using values $\epsilon t = 1$ and the right using $\epsilon t = -1$. This shape is a consequence of the vector (4.28). It is important to note the shapes here are for illustrative purposes because in reality $\epsilon t \ll 1$.

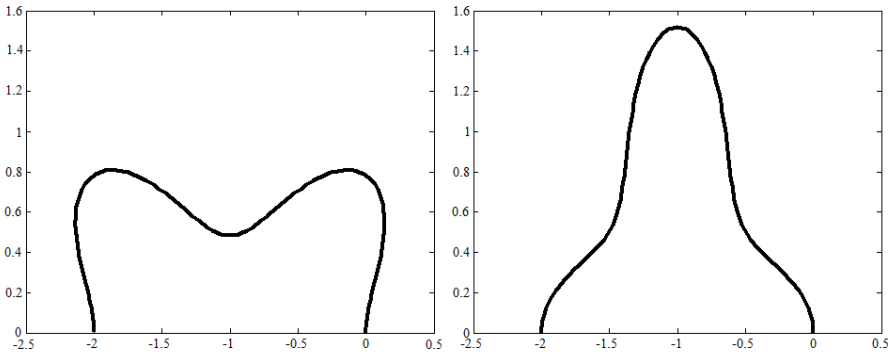


Figure 4.4: Shape of the curved elastic deviation from the semi-circular solution from bifrication point at $m = 3.72873$ ($p = 12.90343$). The left using values $\epsilon t = 1$ and the right using $\epsilon t = -1$. This shape is a consequence of the vector (4.29). It is important to note the shapes here are for illustrative purposes because in reality $\epsilon t \ll 1$.

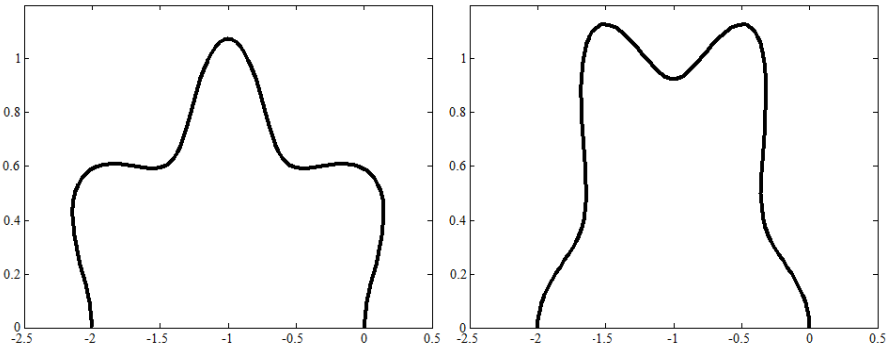


Figure 4.5: Shape of the curved elastic deviation from the semi-circular solution from bifrication point at $m = 5.82754$ ($\hat{p} = 32.96022$). The left using values $\epsilon t = 1$ and the right using $\epsilon t = -1$. This shape is a consequence of the vector (4.30). It is important to note the shapes here are for illustrative purposes because in reality $\epsilon t \ll 1$.

## 4.5 Symmetric Solution Shapes

To simplify we shall define $m_{odd}$ to be the set of all odd integer bifurcation points shown in Table 4.1 calculated from (4.26), i.e. all odd integers except $m = 1$. Notice that as $m$ becomes large the dominating term of (4.26) reduces this equation to $2m^2 \sin(m\pi) = 0$, and so the other solutions to (4.26) tend toward the even integers. Even though the other bifurcation points are not exactly the even integers it will be simpler to define the set $m_{even}$ as the other bifurcation points, i.e. $\{3.72873, 5.82754, ...\}$.

Looking at the shapes from Figure 4.4 and Figure 4.5 it appears as if they are symmetric solutions. If this is indeed the case then we should have that $x$ is an odd function and $y$ is an even function (as visually demonstrated in Figure 4.6) and so $\bar{x}(\hat{s}) = -\bar{x}(\pi - \hat{s})$ and $\bar{y}(\hat{s}) = \bar{y}(\pi - \hat{s})$.

To look only at our bifurcation solutions we can enforce a condition on $m$ from (4.26) such

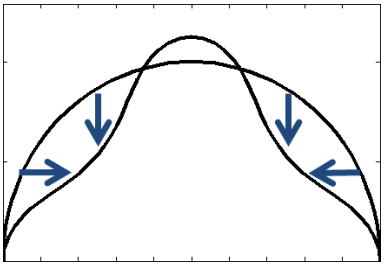

Figure 4.6: Visual aid to show for symmetric solutions we have $x$ as an odd function and $y$ is an even function.

that we substitute,

$$\cos(m\pi) = \frac{2\sin(m\pi) - 2m^2\sin(m\pi) - m\pi}{m\pi},$$

into (4.24) to solve (4.22). However this will include $m_{odd}$ solutions as well as $m_{even}$ solutions, but we can separate these solutions away looking at the vectors we found as (4.28), (4.29) and (4.30). Whilst $A = 0$ for $m_{odd}$, this is not the case for $m_{even}$. As we know we have linear dependence in our system we could choose our constant term (in effect our $t$ when we calculated the eigenvectors) such that $A \neq 0$, e.g. $A = 1$.

## 4.6 Solution Curves

We are now in a position where we have an understanding of the shape of our solutions and where they occur and bifurcate. We can now solve the system numerically for many values of $\hat{p}$ to plot solution curves. Figure 4.7 shows initial values for solutions of the problem of the curved elastic as a function of pressure.

Not all the intersections show bifurcation points. The value $E$ has been introduced as a measure of the energy of the curve, as a deviation from the perfect semi circle. This has the formula,

$$E = \int_0^{\pi} (\hat{\kappa} - 1)^2 \, d\hat{s}.$$

All the lines that grow from the pressure-axis (when $E = 0$) are the bifurcation points from the semi-circle solution. An interesting issue that arises is that the numerical solutions suggest additional bifurcation points. These additional bifurcation points appear to come at the other points where our solution curves cross over the line $\hat{\kappa}(0) = 1$. For example, for the crossover close to $\hat{p} = 20$ the solution that we can track from the blue curve becomes identical to that for the red curve at a given point. We can look at out numerical output for approximations for the location of these points. These are $\hat{p} = 3.3$, $\hat{p} = 9.8$, and $\hat{p} = 19.9$. These points did not show themselves in our earlier analysis since we were looking for bifurcations from the semi-circle solutions, and these are bifurcations from non-semi-circle solutions.

To see all of the bifurcation points a little more clearly we plotted $\hat{\tau}(0)$, $\hat{q}(0)$ and $\hat{\kappa}(0)$ in 3D. This is possible because of the properties linking $\hat{\tau}$ and $\hat{p}$. In the plot all the intersections are bifurcation points. The colours in Figure 4.8 are the same colours that correspond to the

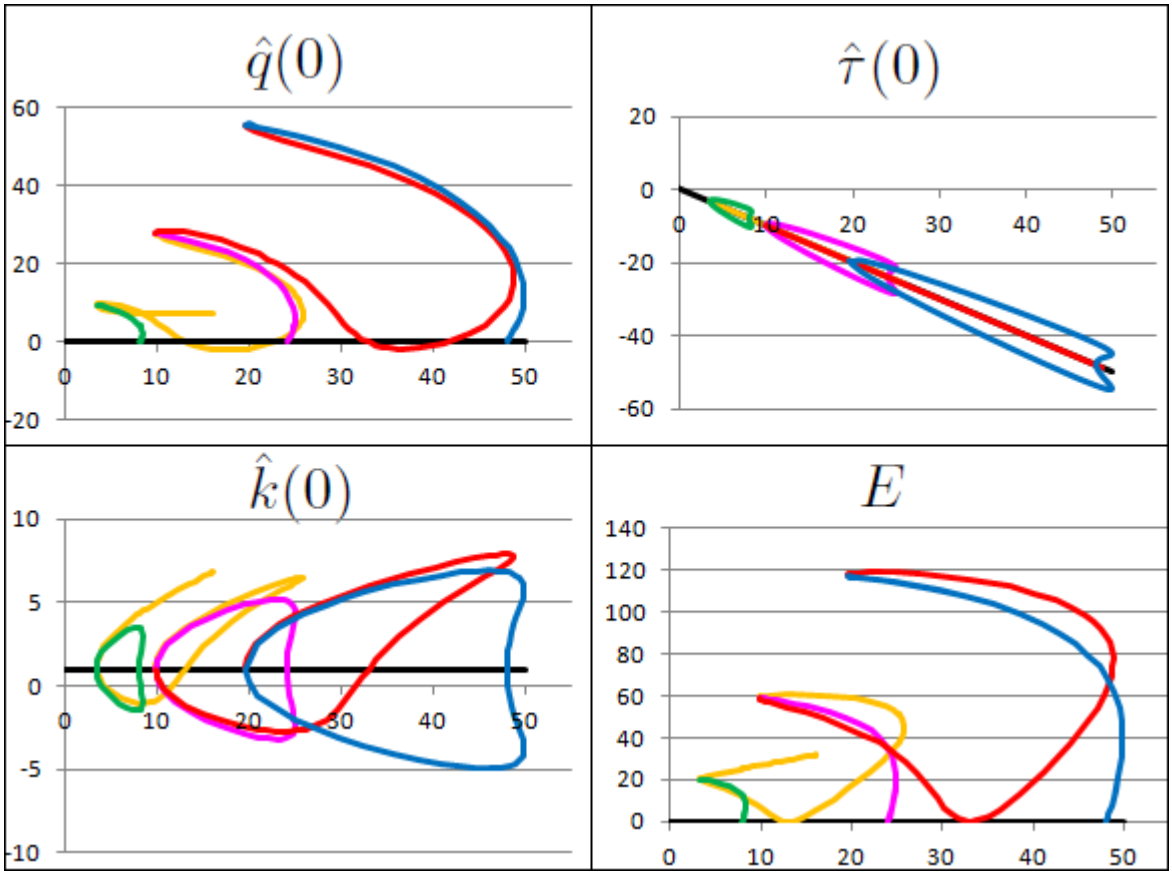


Figure 4.7: Initial values for the curved elastic at different pressures. The green curves comes from the bifurcation point (from the semi-circle solution - shown in black) at $\hat{p} = 8$, orange at $\hat{p} = 12.90$, pink at $\hat{p} = 24$, red at $\hat{p} = 32.96$, and blue at $\hat{p} = 48$. These are solutions of (4.1).

lines in Figure 4.7.

Since it is a little difficult to see the bifurcations that occur away from the black semi-circular solution line I have enlarged one of these bifurcations. This is shown in Figure 4.9.

With a little numerical work we can find the solution shapes at the different bifurcation points. The details of finding sensible initial estimates to use for the numerical scheme are not very rigorous and have been moved to Appendix A. However the results of the different solutions curves are shown in Figure 4.10.

The shapes that we have so far plotted have all been created using certain parameters that

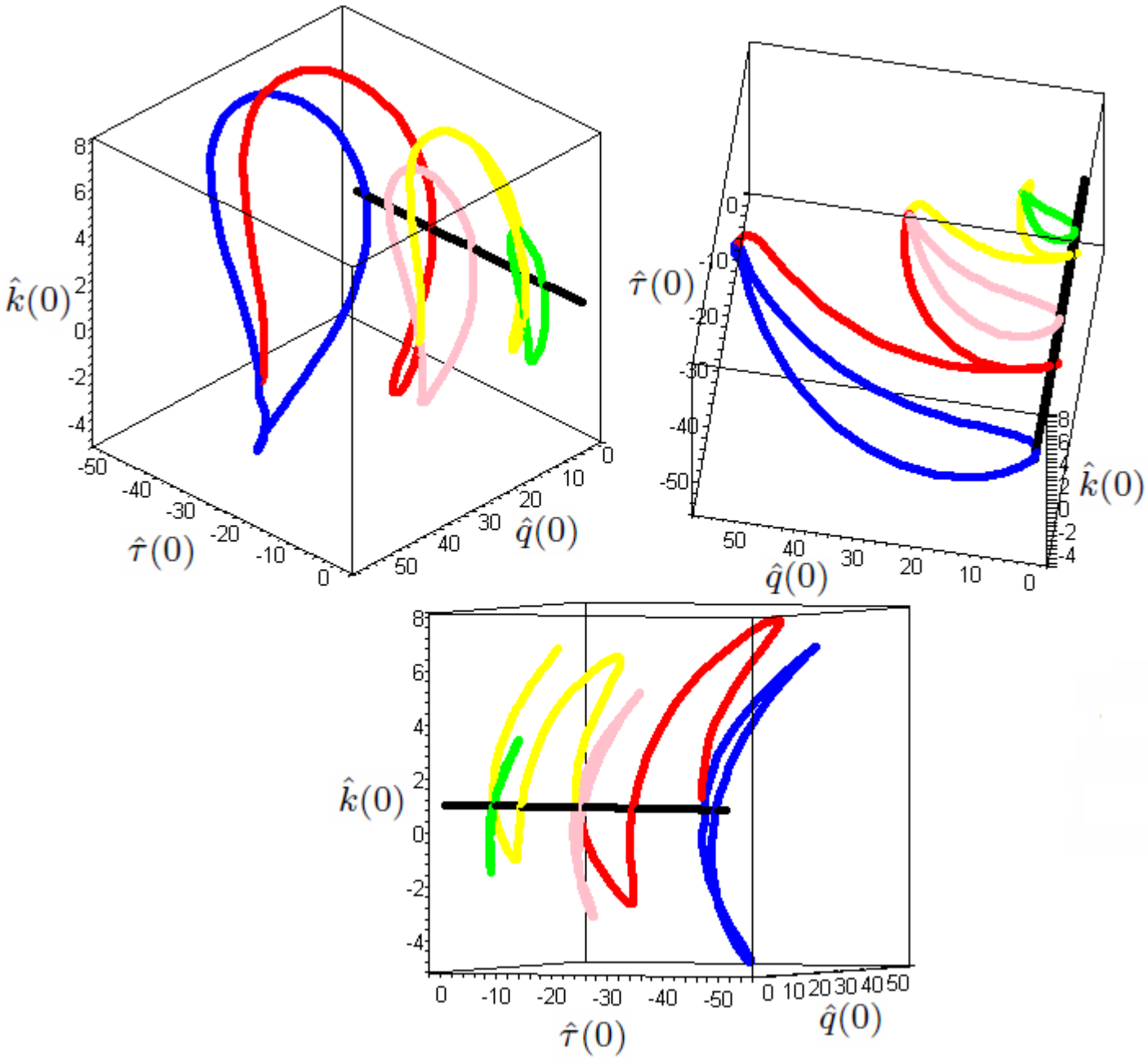


Figure 4.8: Views from a 3D plot of the initial conditions for $\hat{\tau}(0)$, $\hat{q}(0)$ and $\hat{\kappa}(0)$ for solutions of the curved elastic problem. All 3D intersections are bifurcation points. These curves are solutions of (4.1a) - (4.1f).

Figure 4.9: Enlargement of one of the bifurcation points from Figure 4.8.

make it possible to achieve the conditions of a semi-circular solution. It is still achievable to solve the system and find solution curves when conditions are forces so that a semi-circular solution is not possible. Figure 4.11 and Figure 4.12 show situations where a perfect semi-circular solution cannot exist due the changing of the length of the elastic (which would be the same mathematically as changing the gap between where each end of the elastic was fixed) and also when changing the angle at which the elastic is connected to the horizontal wall. We can gain a greater insight into the bifurcation points if we adjust the length of the elastic boundary slightly so that it is no longer possible to have a perfect semi-circle. These bifurcation points then break as shown in Figure 4.13.

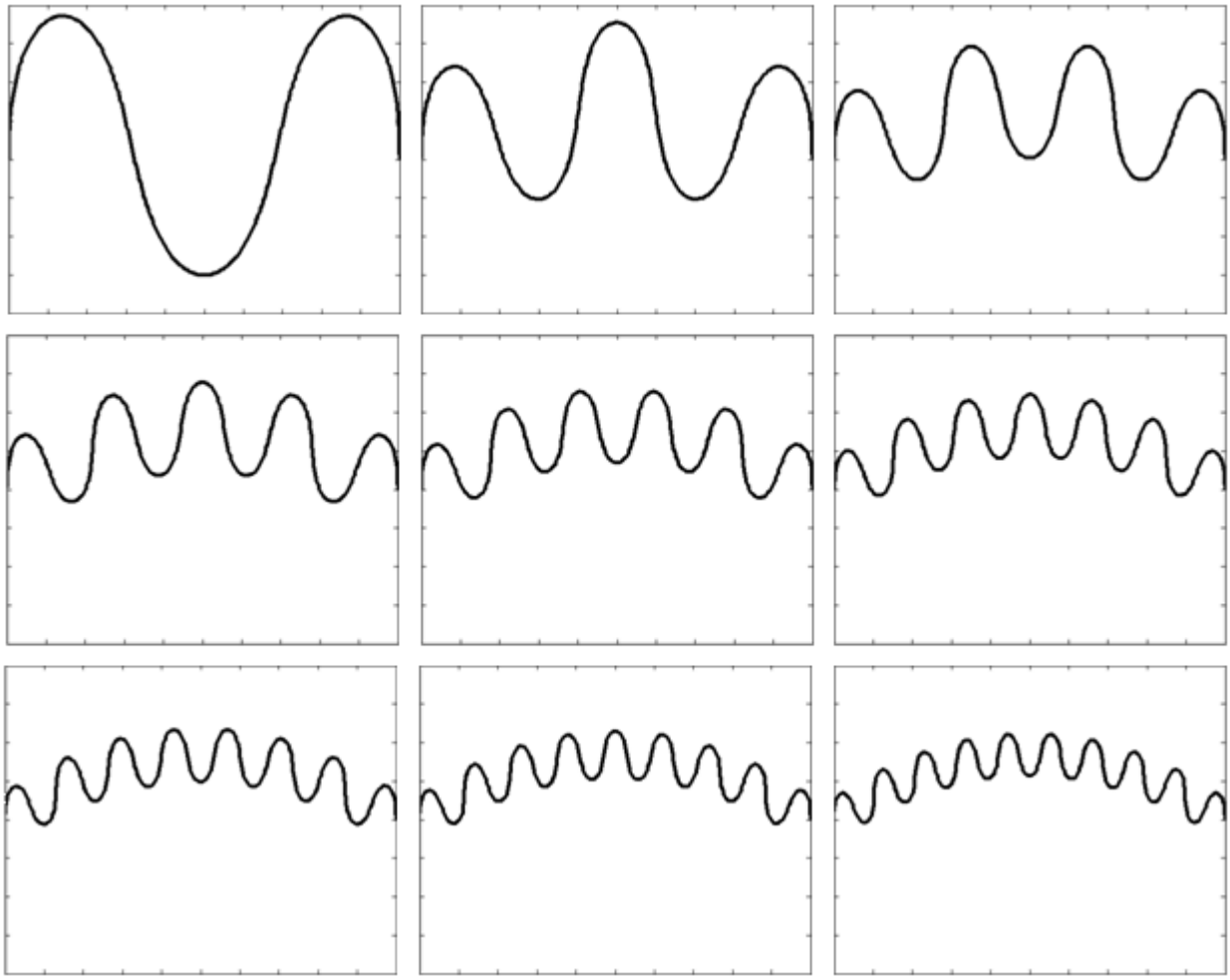

Figure 4.10: The shapes of the elastic at the bifurcation points for $m_{even}$. We start at $\hat{p} = 12.90343$, then $\hat{p} = 32.96022$, and then obtain the further values of $\hat{p}$ by numerically solving 4.26 and applying $m^2\,(1+\hat{p})$.

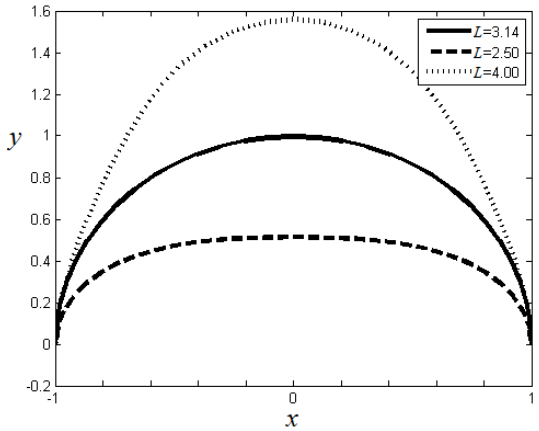


Figure 4.11: Solution curves shown for different lengths of the elastic boundary for the problem shown in Figure 4.1. These were obtained by numerically solving (4.1) with $L = 2.5,\ \pi,\ 4$. A value of $p = 5$ was assigned for each solution.

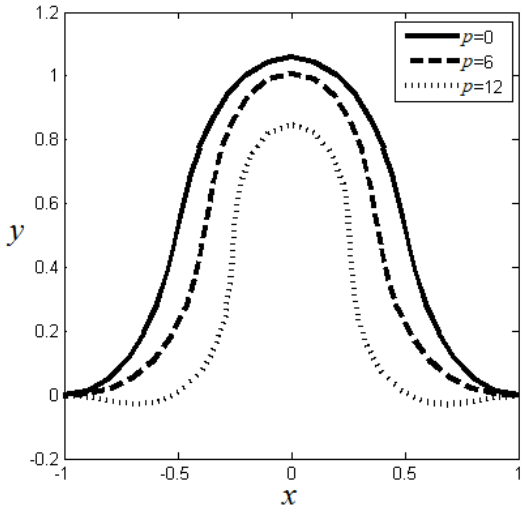


Figure 4.12: Solution curves when $L = \pi$ and $\theta_A = \theta_B = \pi$ for the problem shown in Figure 4.1. These were obtained by numerically solving (4.1).

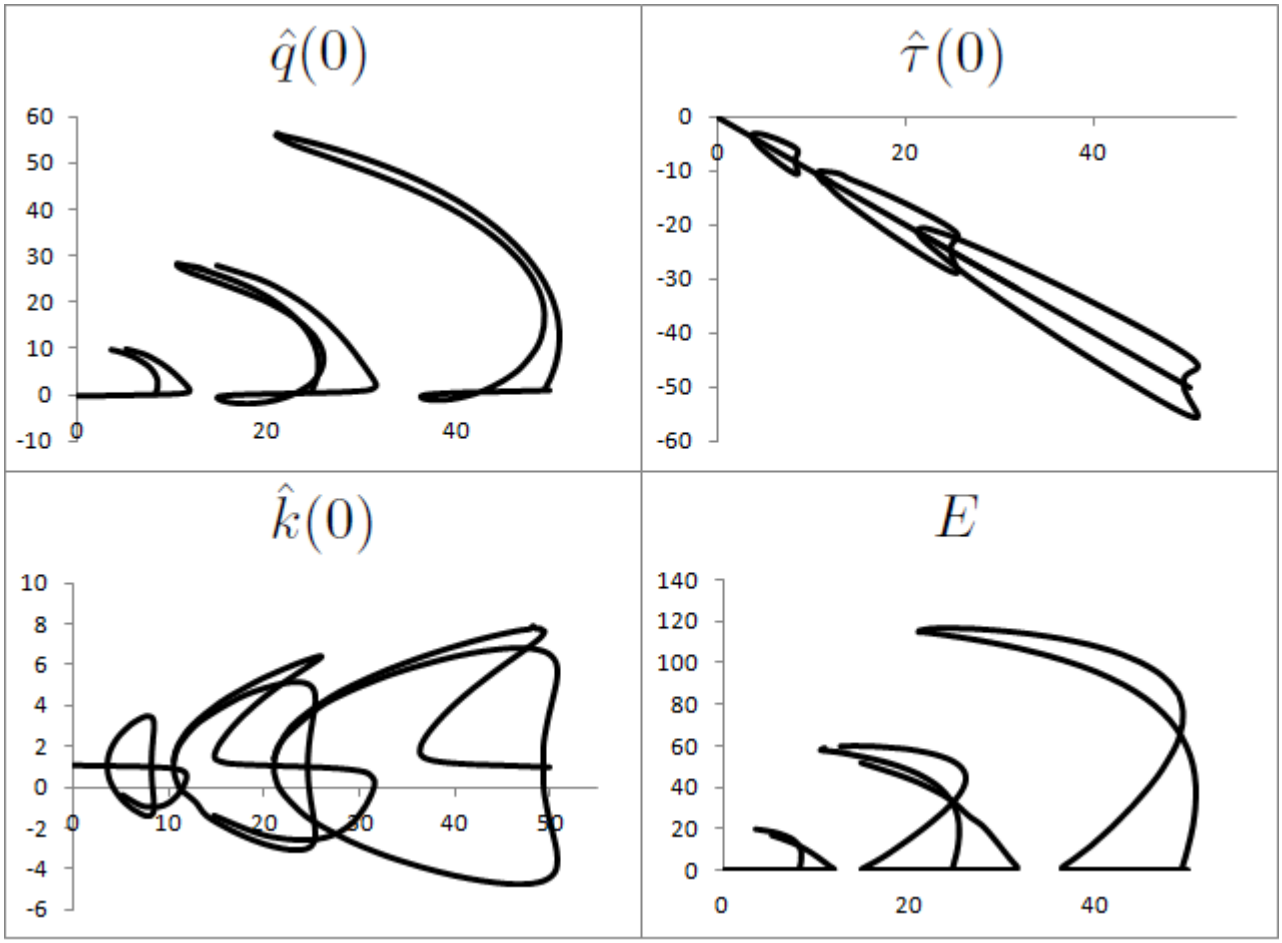


Figure 4.13: The break-down of bifurcation points when the semi-circular solution is no longer possible. To create these solutions we have adjusted the length of the elastic to be 3.14 instead of $\pi$. This can be compared to Figure 4.7 to see where bifurcations were when we did have an elastic length of $\pi$. Note that we can still have solutions in a physical sense where the solution previously bifurcated, but we would lose the smooth transition between one solution to the next.

# 5

# Profiles of an Elastic Arch Under Weak Flow

In this section we are looking at the problem of a curved boundary attached to a horizontal base with a neutral position of a semi-circle when pressure under and over the elastic boundary are equal. We then pass a flow over the boundary, which affects the external pressure exerted on the boundary, and look to see the resulting shape. This setup is shown in Figure 5.1.

The elastic boundary will still follow the same set of equations we had for a curved elastic connected to a surface with no flow. The equations were from (4.1a) to (4.1f). We will also assume no gravity to simplify the problem for this chapter, and then pick up the idea of gravity later in the thesis.

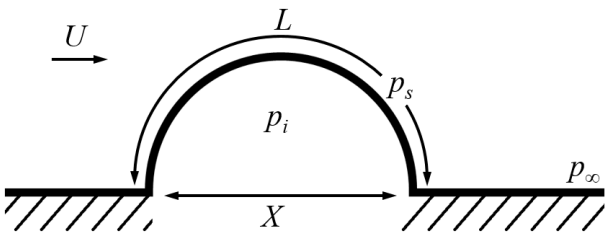


Figure 5.1: Elastic membrane attached at the points at the end of the semi-circle with a flow at steady speed $U$ traveling across it. The three pressures are: inside the elastic ($p_i$); on the surface ($p_s$); and, at a distance a long way from the elastic ($p_\infty$).

When we had no flow the pressure $p$ is defined as the difference between $p_i$ and $p_\infty$ since $p_\infty = p_s$ and is assumed to be constant over the boundary. If we introduce a flow then the pressure on the surface, $p_s$, will vary over the elastic and not be constant. We need to know the pressure on the surface due to the flow.

## 5.1 Flow around the circle

We will take a brief digression to look at the flow around the circle shown in Figure 5.2.

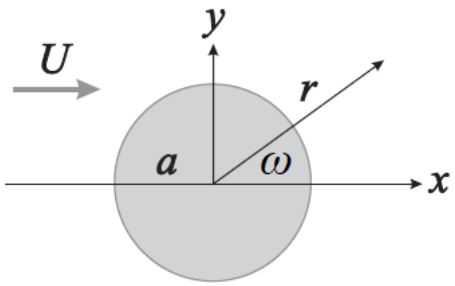


Figure 5.2: Flow around a circle of radius length $a$, using polar coordinates. Here $r$ is the distance from the origin and $\omega$ is the polar angle. For the purpose of this analysis we will assume the flow is uniform and at a steady speed of $U$ parallel to the $x$-axis.

We will try to find an equation for the flow around the circle in the form $\mathbf{u} = \nabla\phi = \left(\phi_r, \frac{\phi_\omega}{r}\right)$. We will look for a solution of Laplace's equation, $\nabla^2\phi = 0$, for an inviscid and irrotational flow.

For one boundary condition we require no normal flow (in and out of the circle) so $u_r = 0$ on $r = a$. This is equivalent to $\phi_r = 0$ on $r = a$.

In Cartesian coordinates the second boundary condition is $\nabla\phi \to U\mathbf{i}$ as $r \to \infty$. If we integrate we obtain the condition, $\phi \to Ux$ as $r \to \infty$. But transforming between polar and Cartesian coordinates we have $x = r\cos\omega$ and so the condition becomes $\phi \to Ur\cos\omega$ as $r \to \infty$.

In polar coordinates Laplace's equation is given by,

$$\frac{1}{r}\frac{\partial}{\partial r}\left(r\frac{\partial\phi}{\partial r}\right) + \frac{1}{r^2}\frac{\partial^2\phi}{\partial\omega} = 0. \tag{5.1}$$

Looking for a solution of the form $\phi = \cos\omega f(r)$ and substituting this into (5.1) we obtain,

$$f_{rr} + \frac{f_r}{r} - \frac{f}{r^2} = 0.$$

If we try to find a solution of the form $f = r^\alpha$ and substitute this in we find $\alpha = \pm 1$. Hence

$f = Ar + \frac{B}{r}$, and so $\phi = \cos\omega\left(Ar + \frac{B}{r}\right)$. Applying the boundary conditions we obtain,

$$\phi = U\left(r + \frac{a^2}{r}\right)\cos\omega. \tag{5.2}$$

Now, we want to find the pressure on the surface of the circle. Bernoulli's equation (see Acheson [1]) with a steady flow and no gravity is given by,

$$\frac{1}{2}|\mathbf{u}|^2 + \frac{p}{\rho} = \text{Constant}, \tag{5.3}$$

which will need to be satisfied through the fluid flow. At a point far from our circle we have $p = p_\infty$ and $|\mathbf{u}| = U$ and so (5.3) becomes,

$$\frac{1}{2}|\mathbf{u}|^2 + \frac{p}{\rho} = \frac{1}{2}U^2 + \frac{p_\infty}{\rho}, \tag{5.4}$$

throughout the fluid flow. From (5.2) and evaluating on $r = a$ we then have $\phi_r = 0$ and $\frac{\phi_\omega}{r} = -2U\sin\omega$. This is useful to us since $|\mathbf{u}|^2 = |\nabla\phi|^2 = (\phi_r)^2 + \left(\frac{\phi_\omega}{r}\right)^2 = 4U^2\sin^2\omega$. Then on the surface of the circle from (5.4)

$$p_s(\omega) = p_\infty + \frac{1}{2}\rho U^2\left(1 - 4\sin^2\omega\right). \tag{5.5}$$

This gives us an expression for the pressure on the surface of the curved elastic boundary. An issue arises in that this is a function of $\omega$, and our problem is defined as a functions of $s$, the distance along the arc. Figure 5.3 is an illustration of how we can link together the quantities of $\omega$ and $s$.

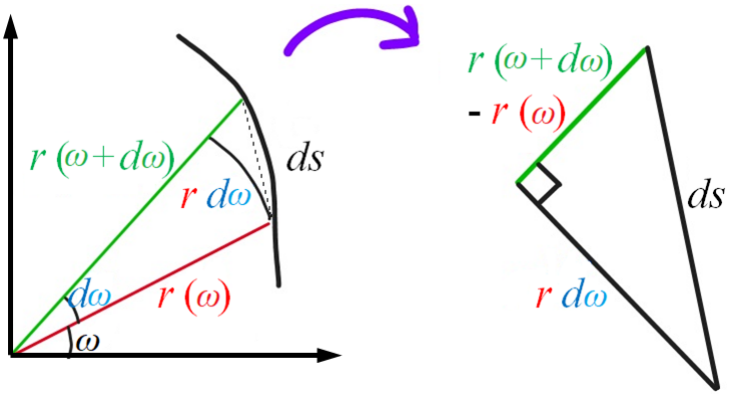


Figure 5.3: Finding the link between $\omega$ and $s$ using small increases in both $\omega$ and $s$ denoted by $d\omega$ and $ds$. As these are small, the small segment can be approximated by a right-angled triangle and hence satisfy Pythagoras theorem.

Using a Taylor expansion on $r(\omega + d\omega)$ we have,

$$r(\omega + d\omega) = r(\omega) + \frac{dr}{d\omega}d\omega + O((d\omega(^2) \Rightarrow r(\omega + d\omega) - r(\omega) = \frac{dr}{d\omega}d\omega + O((d\omega)^2).$$

Using Pythagoras theorem on the triangle in Figure 5.3,

$$(ds)^2 = r^2(d\omega)^2 + \left(\frac{dr}{d\omega}\right)^2 (d\omega)^2 + O((d\omega)^4) \Rightarrow \frac{ds}{d\omega} \approx \sqrt{r^2 + \left(\frac{dr}{d\omega}\right)^2}.$$

Substituting in $r = a\,(1 + \delta f(\omega))$, where $\delta f(\omega)$ represents a small deformation from a circular shape, we have,

$$\frac{ds}{d\omega} = a\Big(1 + 2\delta f + O(\delta^2)\Big)^{\frac{1}{2}} \approx a\Big((1 + \delta f)^2\Big)^{\frac{1}{2}} = a(1 + \delta f) = r, \tag{5.6}$$

since $\delta$ is small. Therefore,

$$s = \int_0^\omega r d\omega = a\int_0^\omega \Big(1 + \delta f(\omega)\Big)d\omega = a\omega + a\delta \int_0^\omega \Big(f(\omega)\Big)d\omega.$$

To make manipulation easier we shall temporarily denote $\omega = \frac{s}{a} - \delta A(s)$ which we can substitute into the expression above and introduce the dummy variable $x$ and simplify to obtain,

$$0 = -a\delta A(s) + a\delta \int_0^{\frac{s}{a}-\delta A(s)} \Big(f(x)\Big)dx.$$

Approximating by taking out $O\left(\delta^2\right)$ terms,

$$A(s) = \int_0^{\frac{s}{a}} \Big(f(x)\Big)dx,$$

$$\therefore \omega = \frac{s}{a} - \delta \int_0^{\frac{s}{a}} \Big(f(x)\Big)dx. \tag{5.7}$$

## 5.2 Introducing a Weak Flow and Seeking a Deformed Semi-circular Solution

As we introduce a flow to our situation, the shape of the elastic boundary will deform and will not be a perfect semi-circle. However, it would seem reasonable for a very small flow that we could seek a solution as a perturbation of the solution for the flow around a semi-circle. If we have a shape that is a very slightly deformed circle then we can model the boundary as $r = a + a\delta f(\omega)$ where $r$ is the radius of the circle and $\delta << 1$ and will be a measure of the flow speed that will be chosen explicitly and conveniently in due course. Note that we have $a\delta f(\omega)$ as opposed to $\delta f(\omega)$ to be consistent with the dimensions for $r$ because $\delta$ and $f(\omega)$

are dimensionless.The setup is again shown in the Figure 5.4 and the basic equations for the elastic are given by (5.8a)-(5.8d).

$$q' = p + \kappa\tau, \tag{5.8a}$$

$$\tau' = -\kappa q, \tag{5.8b}$$

$$m' = \epsilon_B \kappa' = q, \tag{5.8c}$$

$$m = \epsilon_B \kappa, \tag{5.8d}$$

where $p = p_s - p_i$ in Figure 5.4. In sections 2 and 4 we had $p = p_\infty - p_i$ since $p_s = p_\infty$ and was constant around the boundary when there was no flow. Also note that from (5.5) and (5.7) we have that $p = p(s)$.

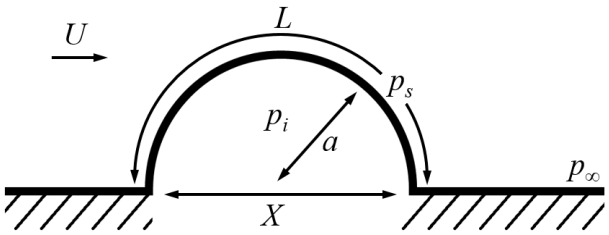


Figure 5.4: Elastic membrane attached at the points at then end of the semi-circle with a flow at steady speed $U$ traveling across it. The three pressures are inside the elastic ($p_i$), on the surface ($p_s$) and at a distance a long way from the elastic ($p_\infty$).

Substituting (5.8c) into (5.8b) we obtain,

$$\tau' = -\epsilon_B \kappa \kappa', \tag{5.9}$$

$$\Rightarrow \tau = -\epsilon_B \frac{\kappa^2}{2} + c,$$

where $c$ is a constant of integration. From (5.8c) we have $q' = \epsilon_B \kappa''$ and so also using the result above we can write (5.8a) as,

$$\kappa'' + \frac{\kappa^3}{2} - c\frac{\kappa}{\epsilon_B} = \frac{p}{\epsilon_B}.$$

Equation (5.5) suggests it is sensible to write the pressure for our situation in the form $p_s(s) = p_\infty + \frac{1}{2}\rho U^2 P(s)$ and we can set $p_i = 0$ since $p = p_s - p_i$. Non-dimensionalizing by

letting $s = L\hat{s}$, and so $r = L\hat{r}$, $\frac{d}{ds} = \frac{1}{L}\frac{d}{d\hat{s}}$, and $\kappa = \frac{d\theta}{ds} = \frac{\hat{\kappa}}{L}$ gives,

$$\hat{\kappa}_{\hat{s}\hat{s}} + \frac{1}{2}\hat{\kappa}^3 - \hat{c}\hat{\kappa} = \frac{p_\infty L^3}{\epsilon_B} + \frac{1}{2}\frac{\rho U^2 L^3}{\epsilon_B}P,$$

after also introducing $\hat{c} = \frac{cL^2}{\epsilon_B}$. To simplify we will introduce $E = \frac{p_\infty L^3}{\epsilon_B}$. Also, since we have a small flow, $U$ is a small value we will introduce the small parameter $\delta = \frac{1}{2}\frac{\rho U^2 L^3}{\epsilon_B}$. When we introduce small perturbations we will do these in terms of $\delta$ and so this will give a sense of the effect of the flow compare to a semi-circle solution with no flow. When $U = 0$, we then have $\delta = 0$ and the problem is identical to the no-flow problem, but as we gradually increase $U$ we also increase $\delta$ and so $\delta$ is a measure of how strong the flow is. It is worth remembering here that due to the series expansion in the analysis this model will only be valid for small flow, and hence $\delta << 1$. Hence we have,

$$\hat{\kappa}_{\hat{s}\hat{s}} + \frac{1}{2}\hat{\kappa}^3 - \hat{c}\hat{\kappa} = E + \delta P(\hat{s}). \tag{5.10}$$

It is worth noting here that when the flow is (in effect) turned off and we have $\delta = 0$, (5.10) is identical to (2.7), with the non-dimensional $E$ in (5.10) being identical to the non-dimensional $\hat{p}$ in (2.7). The problem is then reduced to that of the tube and curved arch problems with no-flow that we have already looked at.

On the semi-circle solution we have that the curvature is equal to 1 and so in our non-dimensional form we have that $\hat{\kappa} = \frac{1}{\lambda}$, we also have $r = a$ where we introduce the non-dimensional quantity $\lambda = \frac{a}{L} = \frac{1}{\pi}$. We can seek perturbed (from the semi-circle solution) solutions in the form,

$$\hat{\kappa} = \tfrac{1}{\lambda} + \delta\kappa_1(\hat{s}), \quad P = P_0(\hat{s}) + \delta P_1(\hat{s}) + ..., \quad \hat{r} = \lambda + \lambda\delta F(\hat{s}), \quad \hat{c} = c_0 + \delta c_1, \tag{5.11}$$

where the $\frac{1}{\lambda}$, $P_0(\hat{s})$, $\lambda$ and $c_0$ terms are solutions to the no-flow problem when we have a semi-circular shape, and the terms multiplied by $\delta$ are as a direct result of the introduced flow. Recall that $\delta$ is a measure of the strength of the flow. Also $f$ and $F$ are equivalent functions such that $f(\omega) = F(\hat{s})$, i.e. $f$ defined by $\omega$ gives the same values at the same points as $F$ defined by the distance around the arc length. Matching up (5.5) with $p_s(s) = p_\infty + \frac{1}{2}\rho U^2 P(s)$ , and using $P(\hat{s}) = P_0(\hat{s}) + \delta P_1(\hat{s}) + ...$ we can see that,

$$P_0(\hat{s}) = 1 - 4\sin^2\left(\frac{\hat{s}}{\lambda}\right),$$

gives an explicit formula for $P_0(\hat{s})$. Note that $\frac{\hat{s}}{\lambda}$ is a result of (5.7) and $s = L\hat{s}$

It may be an intuitive approach to perturb $\kappa$, $P$ and $r$, but it may not be immediately obvious why we are perturbing $\hat{c}$ since this is essentially a constant of integration[1]. To see this is if we look at Flaherty et. al.[10], the paper here is concerned with the shape of an elastic boundary (with no flow) subject to changing the parameter $p$ which is the pressure, $\hat{p}$ as we have defined it. They solve a similar equation to that of (5.10) that is,

$$\kappa_{ss} + \frac{1}{2}\kappa^3 - c\kappa = p, \tag{5.12}$$

derived from the same set of equations we started with. Since $c$ is a constant and (5.12) will hold for all values of $s$ and $p$, we can take the case of when $p = 0$ and $s = 0$ to obtain,

$$c = \frac{\kappa_{ss}(0)}{\kappa(0)} + \frac{1}{2}\kappa^2(0).$$

Using the non-dimensional forms of (5.8c) and then (5.8a) at $s = 0$ and $p = 0$ we have,

$$\kappa_{ss}(0) = q_s(0) = \kappa(0)\tau(0) \Rightarrow \frac{\kappa_{ss}(0)}{\kappa(0)} = \tau(0),$$

and so,

$$c = \tau(0) + \frac{1}{2}\kappa^2(0).$$

The point here is that $c$ depends on $\tau(0)$ and $\kappa(0)$, which will be different for different shapes of the elastic boundary, even after bifurcations where we can have different shapes at the same pressure values.

From $\hat{\kappa} = \frac{1}{\lambda} + \delta\kappa_1$, we have $\hat{\kappa}^3 = \frac{1}{\lambda^3} + \frac{3}{\lambda^2}\delta\kappa_1 + O\left(\delta^2\right)$. Substituting this and (5.11) into (5.10) to leading order we obtain an explicit value for our integration constant $c_0$. Since $E$ is a (non-dimensional) constant we have,

$$c_0 = \frac{1}{2\lambda^2} - \lambda E.$$

To $O(\delta)$ we have,

$$\kappa_1'' + \frac{3}{2\lambda^2}\kappa_1 - c_0\kappa_1 - \frac{c_1}{\lambda} = P_0(s). \tag{5.13}$$

[1]In Appendix C we are concerned with finding an expression for the perturbation of the pressure for semi-circular elastic under weak flow, i.e. $P_1(\hat{s})$. This is done and obtained at the end of Appendix C, but the algebra has since shown that this is not a necessary function for the analysis. However, this may come in useful when continuing work so it is included here.

Using standard polar coordinates with $\omega$ as our polar angle and $\omega = \frac{s}{\lambda} + O(\delta)$, then general equation for curvature[2] is given by,

$$\hat{\kappa}(\omega) = \frac{\hat{r}^2 + 2\hat{r}_\omega^2 - \hat{r}\hat{r}_{\omega\omega}}{(\hat{r}^2 + \hat{r}_\omega^2)^{\frac{3}{2}}}$$

Since $\hat{r} = \lambda + \lambda\delta f(\omega)$ we then have,

$$\hat{\kappa}(\omega) = \frac{1}{\lambda}\left(1 - \delta(f + f_{\omega\omega})\right) + O(\delta^2). \tag{5.14}$$

Here we have an equation in terms of $\omega$, however, (5.13) is defined in terms of $\hat{s}$, so we need to find (5.14) defined in terms of $\hat{s}$. The non-dimensional version of (5.6) gives,

$$\frac{d\hat{s}}{d\omega} = \lambda(1 + \delta f) + O(\delta^2). \tag{5.15}$$

We then have,

$$\frac{df}{d\omega} = \frac{df}{d\hat{s}}\frac{d\hat{s}}{d\omega} = \lambda F_{\hat{s}}\left(1 + \delta F\right). \tag{5.16}$$

Differentiating again this becomes,

$$\begin{aligned}\frac{d^2 f}{d\omega^2} &= \frac{df}{d\hat{s}}\lambda\delta\frac{df}{d\omega} + \left(\lambda(1+\delta f)\right)^2\frac{d^2 f}{d\hat{s}^2} + O\left(\delta^2\right),\\ \Rightarrow \frac{d^2 f}{d\omega^2} &= \lambda^2\delta\left(F_{\hat{s}}\right)^2 + \lambda^2\left(1 + 2\delta F\right)F_{\hat{s}\hat{s}} + O\left(\delta^2\right).\end{aligned} \tag{5.17}$$

Substituting (5.17) into (5.14) we have,

$$\kappa(\hat{s}) = \frac{1}{\lambda} + \delta\left(-\frac{F}{\lambda} - \lambda F_{\hat{s}\hat{s}}\right) + O(\delta^2),$$

and so matching up with (5.11) we have,

$$\kappa_1(\hat{s}) = -\frac{F}{\lambda} - \lambda F_{\hat{s}\hat{s}}.$$

Using this with (5.13) we have,

$$\lambda F_{\hat{s}\hat{s}\hat{s}\hat{s}} + \left(\frac{5}{2\lambda} - c_0\lambda\right)F_{\hat{s}\hat{s}} + \left(\frac{3}{2\lambda^3} - \frac{c_0}{\lambda}\right)F = -P_0(\hat{s}) - \frac{c_1}{\lambda}.$$

Substituting in $P_0 = 1 - 4\sin^2\left(\frac{\hat{s}}{\lambda}\right)$ and using standard trigonometric identities this becomes,

$$F_{\hat{s}\hat{s}\hat{s}\hat{s}} + \left(\frac{5}{2\lambda^2} - c_0\right)F_{\hat{s}\hat{s}} + \left(\frac{3}{2\lambda^4} - \frac{c_0}{\lambda^2}\right)F = \frac{1}{\lambda} - \frac{2}{\lambda}\cos\left(\frac{2\hat{s}}{\lambda}\right) - \frac{c_1}{\lambda^2}. \tag{5.18}$$

[2]See Casey [8] for example.

Since this is a fourth order equation we require four boundary conditions to find a solution. The elastic membrane is fixed at the two ends and so this length has got to be equal to the radius of the semi-circle. Since $\hat{r} = \lambda + \delta F(\hat{s})$, we must have $F(0) = F(1) = 0$.

We have boundary conditions arising from the angle at which the elastic is attached to the horizontal wall, i.e. at right angles. The gradient of the curve at that point is given by,

$$\frac{dy}{dx} = \frac{\frac{d\hat{r}}{d\omega}\sin\omega + \hat{r}\cos\omega}{\frac{d\hat{r}}{d\omega}\cos\omega - \hat{r}\sin\omega},$$

where $\omega$ is the polar angle. This expression will be infinite at $\omega = 0, \pi$ (which is $\hat{s} = 0, 1$). At these points we have $\sin(\omega) = 0$ and $\cos(\omega) = \pm 1$. The condition then becomes,

$$\frac{d\hat{r}}{d\omega}\cos(\omega) - \hat{r}\sin(\omega) = 0 \Rightarrow \frac{d\hat{r}}{d\omega} = 0.$$

This immediately gives the boundary condition in terms of $\omega$, i.e. $f_\omega(0) = f_\omega(\pi) = 0$. We require these in terms of $F(\hat{s})$.

$$\frac{d\hat{r}}{d\omega} = \frac{d}{d\omega}(\lambda + \lambda\delta f) = \lambda\delta\frac{df}{d\omega},$$

which we can substitute in (5.16) to give,

$$\frac{d\hat{r}}{d\omega} = \delta\lambda^2 F_{\hat{s}}(1 + \delta F) = \delta\lambda^2 F_{\hat{s}} + O\left(\delta^2\right),$$

and so our condition becomes,

$$\delta\lambda^2 F_{\hat{s}} = 0 \Rightarrow F_{\hat{s}}(0) = F_{\hat{s}}(1) = 0.$$

The curvature, $\hat{\kappa}$ is the change of the tangential angle as the parameter $\hat{s}$ changes, i.e.

$$\hat{\kappa} = \frac{d\theta}{d\hat{s}}.$$

From Figure 5.4 we can see that as we travel across the elastic surface from each end where it is connected to the horizontal, we turn through an angle of $\pi$ and so,

$$\int_{\hat{s}=0}^{\hat{s}=1} \hat{\kappa}\, d\hat{s} = \pi.$$

We should be able to check this algebraically. So using (5.14) and (5.15) we have,

$$\int_0^1 \hat{\kappa}\, d\hat{s} = \int_0^\pi \hat{\kappa}\,\frac{d\hat{s}}{d\omega}\, d\omega = \int_0^\pi 1 - \delta f_{\omega\omega}\, d\omega + O(\delta^2)$$

$$= \pi - \delta \left[ f_\omega \right]_0^\pi + O(\delta^2). \tag{5.19}$$

But given our boundary conditions, $f_\omega(0) = f_\omega(\pi) = 0$, (5.19) becomes $\pi$ to leading order (of $\delta$) as required.

As well as the four boundary conditions to solve our fourth order equation, (5.18) also include the constant $c_1$. This means that we will require a fifth condition to evaluate this. This condition comes from the non-dimensional form of (5.7), the relation between the arc length and the polar angle,

$$\omega = \frac{\hat{s}}{\lambda} - \frac{\delta}{\lambda} \int_0^{\hat{s}} F d\hat{s}.$$

But $\frac{1}{\lambda} = \pi$ and so,

$$\omega = \pi\hat{s} - \pi\delta \int_0^{\hat{s}} F d\hat{s}.$$

We require $\omega$ to travel from 0 to $\pi$ whilst $\hat{s}$ travels from 0 to 1. So when $\omega = \pi$ we have $\hat{s} = 1$ and so it follows,

$$\pi = \pi - \pi\delta \int_0^1 F d\hat{s},$$

$$\Rightarrow \int_0^1 F d\hat{s} = 0.$$

## 5.3 Checking the Equations

We can check that our work is correct so far by comparing it to when we have a flow of $U = 0$. This means (5.18) reduces to,

$$F_{\hat{s}\hat{s}\hat{s}\hat{s}} + \left( \frac{5}{2\lambda^2} - c_0 \right) F_{\hat{s}\hat{s}} + \left( \frac{3}{2\lambda^4} - \frac{c_0}{\lambda^2} \right) F = -\frac{c_1}{\lambda^2}. \tag{5.20}$$

To find the particular solution we can substitute in an expression of the form,

$$F(\hat{s}) = \alpha.$$

Substituting this in we find,

$$\alpha = \frac{2c_1\lambda^2}{2c_0\lambda^2 - 3}.$$

This gives us a solution that solves the right hand side of (5.20), and so to solve the left hand side we can find our complementary function by making the right hand side of (5.20) equal

to zero and substitute in $F(\hat{s}) = e^{m\hat{s}}$. The resulting quartic equation has roots,

$$\tfrac{1}{\lambda}i \quad , \quad -\tfrac{1}{\lambda}i \quad , \quad \tfrac{\sqrt{6-4c_0\lambda^2}}{2\lambda}i \quad , \quad -\tfrac{\sqrt{6-4c_0\lambda^2}}{2\lambda}i \ .$$

We previously defined $E = \frac{p_\infty L^3}{\epsilon_B}$. Taking $\epsilon_B = 1$ and $a = 1$ with $\lambda = \frac{a}{L}$, this gives $E = \frac{p_\infty}{\lambda^3}$. This means we can simplify our expressions above since $c_0 = \frac{1}{2\lambda^2} - \lambda E$ to obtain,

$$\pi i \quad , \quad -\pi i \quad , \quad (\pi\sqrt{1+p_\infty})i \quad , \quad -(\pi\sqrt{1+p_\infty})i \ .$$

Also,

$$\alpha = -\frac{c_1}{\pi(1+p_\infty)}.$$

Putting the particular and complementary functions together we have a solution,

$$F(\hat{s}) = A\cos\left((\pi\sqrt{1+p_\infty})\hat{s}\right) + B\sin\left((\pi\sqrt{1+p_\infty})\hat{s}\right) + C\cos(\pi\hat{s}) + D\sin(\pi\hat{s}) - \frac{c_1}{\pi(1+p_\infty)}.$$

Notice that when $p_\infty = 0$ we have a repeated solution and hence we will have to consider this as a special case. For now we will continue and remember that the following few pages are only valid when $p_\infty \neq 0$. Substituting in for the conditions,

$$F(0) = F(1) = F_{\hat{s}}(0) = F_{\hat{s}}(1) = 0, \quad \int_0^1 F(\hat{s})d\hat{s} = 0 \ ,$$

we can create the matrix system for finding $A, B, C, D$ and $c_1$.

$$\mathbf{M}\begin{bmatrix} A \\ B \\ C \\ D \\ c_1 \end{bmatrix} = \begin{bmatrix} 0 \\ 0 \\ 0 \\ 0 \\ 0 \end{bmatrix}. \tag{5.21}$$

Where,

$$\mathbf{M} = \begin{bmatrix} 1 & 0 & 1 & 0 & -\frac{1}{\pi^2(1+p_\infty)} \\ \cos\left(\pi\sqrt{1+p_\infty}\right) & \sin\left(\pi\sqrt{1+p_\infty}\right) & -1 & 0 & -\frac{1}{\pi^2(1+p_\infty)} \\ 0 & \pi\sqrt{1+p_\infty} & 0 & \pi & 0 \\ -\pi\sqrt{1+p_\infty}\sin\left(\pi\sqrt{1+p_\infty}\right) & \pi\sqrt{1+p_\infty}\cos\left(\pi\sqrt{1+p_\infty}\right) & 0 & -\pi & 0 \\ \frac{1}{\pi\sqrt{1+p_\infty}}\sin\left(\pi\sqrt{1+p_\infty}\right) & \frac{1}{\pi\sqrt{1+p_\infty}}\left(1-\cos\left(\pi\sqrt{1+p_\infty}\right)\right) & 0 & \frac{2}{\pi} & -\frac{1}{\pi^2(1+p_\infty)} \end{bmatrix}.$$

There will be (multiple) non-trivial solutions to the system if $det(\mathbf{M}) = 0$. We should find the same values of $det(\mathbf{M}) = 0$ at the same values of $p_\infty$ with (4.26), which are shown in Figure 4.2 and Table 4.1. Performing the calculation to find $det(\mathbf{M})$ and substituting in $m^2 = (1 + p_\infty)$ does yield the same expressions as (4.26).

## 5.4 Solving With Flow

When solving (5.18) in its full state (i.e. with flow), the complementary function is identical to when solving (5.20) and is so given by,

$$F_C(\hat{s}) = A\cos\left(\pi\sqrt{1+p_\infty}\,\hat{s}\right) + B\sin\left(\pi\sqrt{1+p_\infty}\,\hat{s}\right) + C\cos(\pi\hat{s}) + D\sin(\pi\hat{s}),$$

where the solution to (5.18) is given by $F(\hat{s}) = F_C(\hat{s}) + F_P(\hat{s})$. This time our particular solution will be of the form,

$$F_P(\hat{s}) = \Omega\cos\left(\frac{2\hat{s}}{\lambda}\right) + \beta\sin\left(\frac{2\hat{s}}{\lambda}\right) + \alpha.$$

Substituting this into (5.18) and equating cos, sin and constant terms on both the left hand side and the right hand side of the equations we find,

$$\alpha = \frac{2(\lambda - c_1)\lambda^2}{3 - 2c_0\lambda^2},$$

$$\beta = 0,$$

$$\Omega = -\frac{4\lambda^3}{3\,(5 + 2c_0\lambda^2)}.$$

After simplifying by substituting in $c_0 = \frac{1}{2\lambda^2} - \lambda E$, $E = \frac{p_\infty}{\lambda^3}$ and $\lambda = \frac{1}{\pi}$ as before, and then putting the particular and complementary functions together we have a solution,

$$F(\hat{s}) = A\cos\left(\pi\sqrt{1+p_\infty}\,\hat{s}\right) + B\sin\left(\pi\sqrt{1+p_\infty}\,\hat{s}\right) + C\cos(\pi\hat{s}) + D\sin(\pi\hat{s}) - \frac{2}{3\pi^3(3-p_\infty)}\cos(2\pi\hat{s}) + \frac{1-\pi c_1}{\pi^3(1+p_\infty)}, \quad (5.22)$$

when $p_\infty \neq 0$. Substituting in for the conditions,

$$F(0) = F(1) = F_{\hat{s}}(0) = F_{\hat{s}}(1) = 0, \quad \int_0^1 F(\hat{s})d\hat{s} = 0\ , \quad (5.23)$$

we can create the matrix system for finding $A, B, C, D$ and $c_1$.

$$\begin{bmatrix} 1 & 0 & 1 & 0 & -\frac{1}{\pi^2(1+p_\infty)} \\ \cos\left(\pi\sqrt{1+p_\infty}\right) & \sin\left(\pi\sqrt{1+p_\infty}\right) & -1 & 0 & -\frac{1}{\pi^2(1+p_\infty)} \\ 0 & \pi\sqrt{1+p_\infty} & 0 & \pi & 0 \\ -\pi\sqrt{1+p_\infty}\sin\left(\pi\sqrt{1+p_\infty}\right) & \pi\sqrt{1+p_\infty}\cos\left(\pi\sqrt{1+p_\infty}\right) & 0 & -\pi & 0 \\ \frac{1}{\pi\sqrt{1+p_\infty}}\sin\left(\pi\sqrt{1+p_\infty}\right) & \frac{1}{\pi\sqrt{1+p_\infty}}\left(1-\cos\left(\pi\sqrt{1+p_\infty}\right)\right) & 0 & \frac{2}{\pi} & -\frac{1}{\pi^2(1+p_\infty)} \end{bmatrix} \begin{bmatrix} A \\ B \\ C \\ D \\ c_1 \end{bmatrix}$$

$$= \begin{bmatrix} \frac{5p_\infty-7}{3\pi^3(3-p_\infty)(1+p_\infty)} \\ \frac{5p_\infty-7}{3\pi^3(3-p_\infty)(1+p_\infty)} \\ 0 \\ 0 \\ -\frac{1}{\pi^3(1+p_\infty)} \end{bmatrix},$$

when $p_\infty \neq 0$. The solution of this system is given by,

$$\begin{bmatrix} A \\ B \\ C \\ D \\ c_1 \end{bmatrix} = \begin{bmatrix} -\frac{2\left(\cos(\pi m)+p_\infty\cos(\pi m)+m^2\right)}{3\pi^2(\pi p_\infty\cos(\pi m)+\pi p_\infty+2mp_\infty\sin(\pi m)+\pi+\pi\cos(\pi m))(p_\infty-3)} \\ -\frac{2m^2\sin(\pi m)}{3\pi^2(\pi p_\infty\cos(\pi m)+\pi p_\infty+2mp_\infty\sin(\pi m)+\pi+\pi\cos(\pi m))(p_\infty-3)} \\ 0 \\ \frac{2m^{\frac{3}{2}}\sin(\pi m)}{3\pi^2(\pi p_\infty\cos(\pi m)+\pi p_\infty+2mp_\infty\sin(\pi m)+\pi+\pi\cos(\pi m))(p_\infty-3)} \\ \frac{10mp_\infty^2\sin(\pi m)-14mp_\infty\sin(\pi m)-9\pi-6\pi p_\infty+3\pi p_\infty^2-9\pi\cos(\pi m)-6\pi p_\infty\cos(\pi m)+3\pi p_\infty^2\cos(\pi m)}{3\pi^2(\pi p_\infty\cos(\pi m)+\pi p_\infty+2mp_\infty\sin(\pi m)+\pi+\pi\cos(\pi m))(p_\infty-3)} \end{bmatrix}, \tag{5.24}$$

where $m^2 = 1 + p_\infty$. These values can then be substituted into (5.22) to give us a solution for $F(\hat{s})$. As well as looking at the special case of when $p_\infty = 0$, it appears from (5.24) that we also have to take special consideration when $p_\infty = 3$.

After a little careful manipulation we can express (5.24) equivalently as,

$$\begin{bmatrix} A \\ B \\ C \\ D \\ c_1 \end{bmatrix} = \begin{bmatrix} -\frac{2m(1+\cos(\pi m))}{3\pi^2G(m)(p_\infty-3)} \\ -\frac{2m\sin(\pi m)}{3\pi^2G(m)(p_\infty-3)} \\ 0 \\ \frac{2m^2\sin(\pi m)}{3\pi^2G(m)(p_\infty-3)} \\ \frac{10m^4\sin(\pi m)+3\pi m^3(1+\cos(\pi m))-34m^2\sin(\pi m)-12\pi m(1+\cos(\pi m))+24\sin(\pi m)}{3\pi G(m)(p_\infty-3)} \end{bmatrix},$$

where $G(m)$ was defined by (4.26) in the situation with no flow. Now that we have an explicit function, $F(\hat{s})$ we should be able to to make use of this to find the shape of the curved elastic

boundary as a flow is passed over the top, as shown in Figure 5.1. We shall consider the general solution to the problem when $p_\infty \neq 0$ and $p_\infty \neq 3$, and then these two special cases independently. We also need to look in more detail at the bifurcation points given when (4.26) is equal to zero. Also, we have our original perturbation as $\hat{r} = \lambda + \delta\lambda f(\omega)$, where the functions $f(\omega)$ and $F(\hat{s})$ were equivalent functions, but with a different parameter. We therefore need to be consistent with $\omega$ and $\hat{s}$.

### 5.4.1 General Solution

We will convert all of our equations so that we can evaluate points numerically as $(x, y)$ coordinates which can then be plotted onto Cartesian axes. Firstly, using standard polar results in our problem,

$$x = \tfrac{1}{\pi}\left(1 + \delta F(\hat{s})\right)\cos\omega \quad \text{and} \quad y = \tfrac{1}{\pi}\left(1 + \delta F(\hat{s})\right)\sin\omega \ .$$

From (5.6) we have,

$$\frac{d\hat{s}}{d\omega} = \lambda\left(1 + \delta f(\omega)\right) = \lambda\left(1 + \delta F(\hat{s})\right) \Rightarrow \frac{d\omega}{d\hat{s}} = \frac{1}{\lambda\left(1 + \delta F(\hat{s})\right)} = \frac{\pi}{1 + \delta F(\hat{s})},$$

which we can integrate with respect to $\hat{s}$ to obtain,

$$\omega = \pi \int_0^{\hat{s}} \frac{1}{1 + \delta F(u)} du,$$

where $0 \leq \hat{s} \leq 1$, and $u$ is the dummy variable of $\hat{s}$ to avoid confusion.

The plotting procedure is then as follows:

- Divide the domain $0 \leq \hat{s} \leq 1$ in to $N$ sections and let $i = 1, 2, 3, ..., N$ for the 1st, 2nd, 3rd etc numerically calculated points where $N \in \mathbb{Z}$. And so, for example, $x_1$ is the first numerically calculated $x$-value. We can also define a step-length $h$ such that $h = \frac{s_N}{N} = \frac{1}{N}$;
- Fix $\delta$ (to be a small value) and set a $p_\infty$ value;
- Set the initial values with $x_0 = 1$, $y_0 = 0$, $s_0 = 0$, $\omega_0 = 0$;
- Calculate each step for $i = 1$, then $i = 2$ etc with,
  - $\hat{s}_i = \hat{s}_{i-1} + h$

- $\omega_i = \pi \int_0^{\hat{s}_i} \frac{1}{1+\delta F(u)} du$
- $x_i = \frac{1}{\pi}\left(1 + \delta F(\hat{s}_i)\right) \cos \omega_i$
- $y_i = \frac{1}{\pi}\left(1 + \delta F(\hat{s}_i)\right) \sin \omega_i$;

where $F(\hat{s})$ can be directly calculated from (5.22) and (5.24), and the integral can be calculated numerical using the trapezium rule. An example result of this procedure is presented in Figure 5.5.

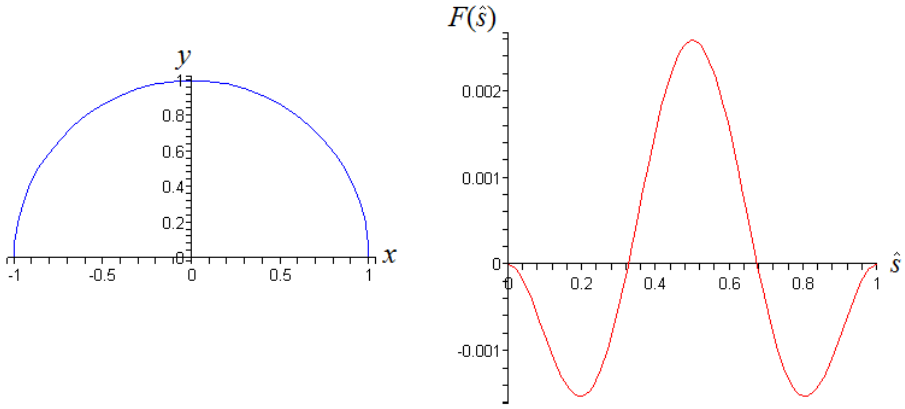


Figure 5.5: Example result of the plotting procedure for (5.22) and (5.24). Here we have $p_\infty = 10$, and $\delta = 0.1$. On the left we have the actual shape of the elastic boundary and on the right we have the perturbation of the shape of the elastic boundary from that of a semi-circular solution.

### 5.4.2 Special Case Solution: $p_\infty = 0$

From the fourth order equation (5.18), when $p_\infty = 0$ we have,

$$F^{IV} + \left(\frac{5}{2\lambda^2} - c_0\right) F^{II} + \left(\frac{3}{2\lambda^4} - \frac{c_0}{\lambda^2}\right) F = -\frac{c_1}{\lambda}.$$

But since

$$c_0 = \pi^2 \left(\frac{1}{2} - p_\infty\right) = \frac{1}{2}\pi^2,$$

and $\frac{1}{\lambda} = \pi$ we have

$$F^{IV} + 2\pi^2 F^{II} + \pi^4 F = -\pi c_1,$$

and so

$$F(\hat{s}) = A\cos(\pi\hat{s}) + B\sin(\pi\hat{s}) + C\hat{s}\cos(\pi\hat{s}) + D\hat{s}\sin(\pi\hat{s}) - c_1\pi.$$

After substitution of the first four boundary conditions (5.23) we find $A = c_1\pi$, $B = 2c_1$, $C = -2c_1\pi$, and $D = 0$, and so,

$$F(\hat{s}) = c_1\pi\cos(\pi\hat{s}) + 2c_1\sin(\pi\hat{s}) - 2c_1\pi\hat{s}\cos(\pi\hat{s}) - c_1\pi.$$

When applying the integral condition from (5.23) we have,

$$c_1\int_0^1 \pi\cos(\pi\hat{s}) + 2\sin(\pi\hat{s}) - 2\pi\hat{s}\cos(\pi\hat{s}) - \pi\, ds = 0 \Rightarrow c_1(-\pi) = 0 \Rightarrow c_1 = 0.$$

The fact we do not find any special solution at $p_\infty = 0$ is not hugely unexpected and somewhat consistent with the earlier work and Table 4.1. Physically speaking this interprets as the only solution possible for a very weak flow with no pressure difference across the elastic cell is a semi-circular solution.

### 5.4.3 Special Case Solution: $p_\infty = 3$

To solve the system for the special case when $p_\infty = 3$ we need to go back to (5.18), using that $\frac{1}{\lambda} = \pi$ and $c_0 = \pi^2\left(\frac{1}{2} - p_\infty\right) = -\frac{5}{2}\pi^2$. This gives,

$$F_{\hat{s}\hat{s}\hat{s}\hat{s}} + 5\pi^2 F_{\hat{s}\hat{s}} + 4\pi^4 F = -2\pi\cos(2\pi\hat{s}) + \pi - c_1\pi^2, \tag{5.25}$$

subject to the same initial conditions,

$$F(0) = F(1) = F_{\hat{s}}(0) = F_{\hat{s}}(1) = \int_0^1 F(\hat{s})d\hat{s} = 0.$$

Substituting $F(\hat{s}) = e^{m\hat{s}}$ into the left hand side of (5.25) equal to zero and solving the corresponding quartic equation gives, $m = \pm 2\pi i, \pi i$ and so the complementary function for (5.25) as,

$$F_C(\hat{s}) = A\cos(\pi\hat{s}) + B\sin(\pi\hat{s}) + C\cos(2\pi\hat{s}) + D\sin(2\pi\hat{s}).$$

We can see here how mathematically we would have an issue with the previous solutions. At $p_\infty = 3$ we have a resonance between the complimentary function and what will be the particular solution due to the $\cos(2\pi\hat{s})$ terms having the same frequency. A more appropriate particular solution will be sought of the form,

$$F_P(\hat{s}) = \Omega\hat{s}\cos(2\pi\hat{s}) + \beta\hat{s}\sin(2\pi\hat{s}) + \alpha.$$

Substituting $F_P(\hat{s})$ into (5.25) and equating terms gives,

$$\alpha = \tfrac{1-\pi c_1}{4\pi^3} \qquad \beta = \tfrac{1}{6\pi^2} \qquad \Omega = 0\ .$$

And so $F(\hat{s}) = F_C(\hat{s}) + F_P(\hat{s})$ which gives, after substituting in the boundary conditions,

$$F(\hat{s}) = \frac{1}{6\pi^2}\sin(\pi\hat{s}) + \frac{1}{4\pi^3}\cos(2\pi\hat{s}) + -\frac{1}{12\pi^2}\sin(2\pi\hat{s}) + \frac{\hat{s}}{6\pi^2}\sin(2\pi\hat{s}) + \frac{1}{4\pi^3} - \frac{2c_1}{4\pi^3}. \quad (5.26)$$

In the real world application of the problem it would be possible to increase or decrease the flow in a smooth fashion and so it would not seem unreasonable to assume that the function we have above for the case when $p_\infty = 3$ yields the same solution as when (5.22) is taken towards the limit of $p_\infty \to 3$ from above and below. This does happen with these equations. Figure 5.6 shows the general shapes of the solution for $F(\hat{s})$ for when $p_\infty = 3$ using (5.26) and a value above and below this using (5.22). The values of $p_\infty$ above and below have been taken for illustrative purposes, as these get closer to $p_\infty$ the lines appear on top of each other. When the values are $p_\infty = 2.999$ and $p_\infty = 3.001$ we have agreement up to an error of order $10^{-8}$ for all values of $\hat{s}$ when $0 \leq \hat{s} \leq 1$.

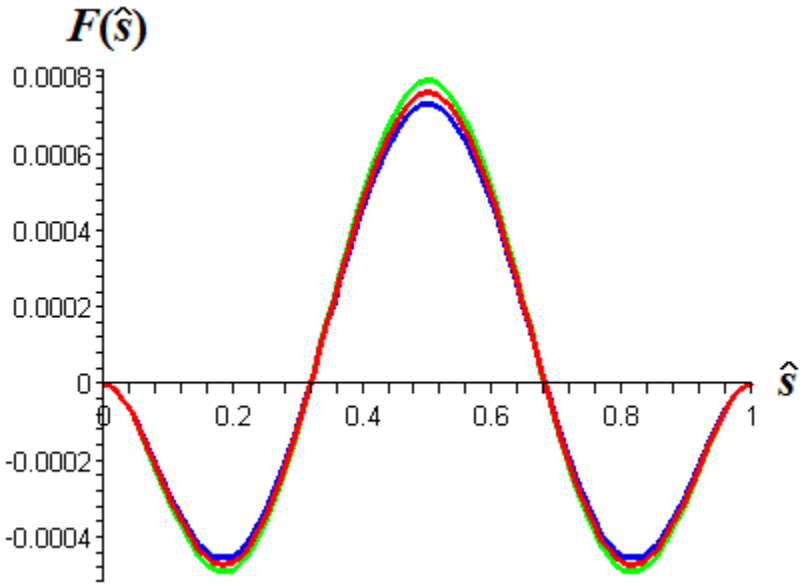


Figure 5.6: The function $F(\hat{s})$ as a solution of the fourth order differential equation (5.18). The green line is using (5.22) with $p_\infty = 3.4$ and the blue line using $p_\infty = 2.6$. These lines converge onto the red curve as $p_\infty \to 3$. The red line is from (5.26) at the particular value of $p_\infty = 3$.

### 5.4.4 Solutions at bifurcation values of $p_\infty$

During the earlier work in Section 3, we could classify the bifurcation values of $p_\infty$ (shown in Table 4.1) into two groups. Those that were odd integers for $m$ (where $m^2 = 1 + p_\infty$), and those that were non-integer values of $m$. We shall first take the case of the odd integer

values for $m$. (5.24), the expression for the constants in the solution for given values of $m$, gives us an indication as to the when the solution breaks down. If we take the expression for the constant $A$ we can see that substituting one of the odd integer values for $m$, for example $m = 3$, we obtain $A = \frac{0}{0}$. However we can still find a value for this constant. We can calculate a Taylor expansion for both the numerator and denominator for each constant in (5.24), then taking the limit of these fractions as we approach the specific odd integer gives a numerical value for the constant. As an example the values we obtain for (5.24) when $m = 3$ (which is when $p_\infty = 8$) are,

$$A = 0 \quad B = -\tfrac{1}{40\pi^2} \quad C = 0 \quad D = \tfrac{3}{40\pi^2} \quad c_1 = \tfrac{11}{5\pi}$$

We can then use (5.22) to plot out the perturbation of the shape of the elastic boundary from the semi-circular solution, Figure 5.7 is an example.

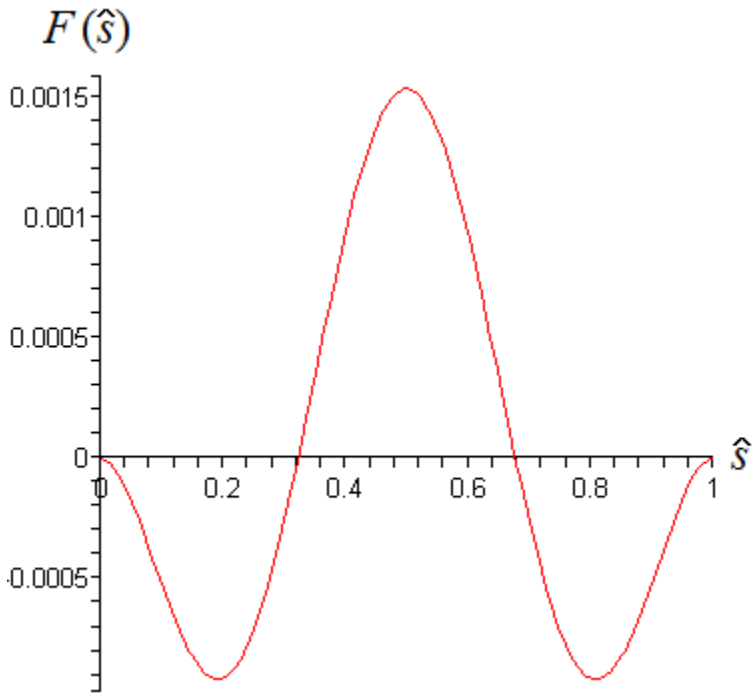


Figure 5.7: The perturbation of the shape of an elastic boundary from the semi-circular solution for the problem shown in Figure 5.4 The function $F(\hat{s})$ is a solution of the fourth order differential equation (5.18). We have $p_\infty = 8$ and the constants from (5.24) were calculated using Taylor expansions centred at $p_\infty = 8$.

Unfortunately the process of expanding the coefficients from (5.24) fails at the non-odd-integer bifurcation values shown in Table 4.1. The constants $A$, $B$, $D$ and $c_1$ all grow rapidly as $p_\infty$

approaches the bifurcation values and all tend to infinity. The problem as presented in Figure 5.1 will have a real solution and in a sense it would be possible to adjust the pressure in a real world example to pass over these bifurcation values. Therefore we can assume that rather than there not being a solution to the problem presented, we have a mathematical model that is breaking down at these particular values, and so we require a different approach to solving the problem from Figure 5.1. In Chapter 6 we look at a more general approach to solving this problem. Also, up until now we have restricted ourselves to a weak flow, which is a restriction we would like to remove. However the work contained in Chapter 5 will form an appropriate comparison for future work so we can validate future models.

# 6

# Profiles for an Elastic Arch Under a General Flow

The shape of a bubble emerging from a corner and exposed to flow has been studied by Ozugurlu and Vanden-Broeck [17]. The motivation for looking at this work is that a numerical technique is used which we can adapt to the problem for this thesis. We will recreate some of the work from [17] as a check that our numerical coding is correct and explain the technique. The numerical procedure makes use of a conformal mapping procedure using complex variables. The general theory behind conformal mapping is provided by Gross [11] and we will present the application in the following pages. Once we have established a working numerical scheme we take a look at the work of Blyth and Parau [4], which modifies the bubble theory to that of a curved elastic cell, before proceeding on with the problem this thesis is concerned with.

## 6.1 The Profile of a Bubble in Corner Flow

We begin by setting up the problem in a similar fashion to Ozugurlu and Vanden-Broeck [17]. Figure 6.1 is a sketch of the physical problem we are representing. The picture represents two infinitely long walls, $OE$ and $OD$, centered at the origin with the lower wall running along the $x$-axis. The two walls create a fixed angle $\alpha$. There is a bubble created between the walls at $A$ and $B$ which creates an angle with the lower wall of $\beta$. There is a pressure difference between the area contained within the bubble and the fluid on the outside which is subject to flow. $B$ is the middle point of the bubble profile. The pressure inside the bubble is assumed to be constant.

The potential function, $\phi$, and the stream function, $\psi$, (see [3] for example) are defined within the outside flow such that $\psi = 0$ along the walls and the bubble, and $\phi = 0$ at $B$. Due to the fact we are more interested in the solving procedure, rather than the derivation of the

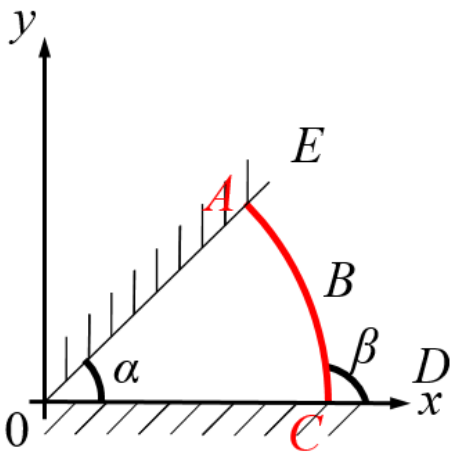


Figure 6.1: Sketch of the corner bubble flow.

problem, we can spare the details which can be readily found in [17] (note we will do the details relating to our specific problem in due course) and begin by quoting the equation to be solved,

$$\frac{1}{2}\left(u^2+v^2\right)-K=\xi, \tag{6.1}$$

on the bubble profile. This comes from Bernoulli's equation (see [1] for example), where $u$ and $v$ are the velocity components of fluid flow in the $x$ and $y$ directions, $K$ dimensionless curvature of the profile of the bubble and $\xi$ is a dimensionaless parameter that is essentially the pressure difference across the bubble boundary. Equation (6.1) is subject to the conditions that $v=0$ on $CD$ and $\frac{v}{u}=\tan\alpha$ on $AE$. We also specify that at $C$ we have $\phi=\pm1$, i.e.

$$\begin{aligned} v &= u\tan\beta \qquad \text{at} \quad \phi=1 \\ v &= -u\tan(\beta-\alpha) \quad \text{at} \quad \phi=-1. \end{aligned}$$

The system is then solved by introducing the complex velocity $\zeta=u-iv$ by then seeking a solution of the form $f=\phi+i\psi$. The flow is then mapped into the complex t-plane (see [11]) using the transformation,

$$f=-\frac{1+t^2}{2t}.$$

The result of this transformation is shown in Figure 6.2. The purpose of this transformation is that now we have a problem that has been transformed onto a semi-circle and as we have fixed geometry we can then discretise and create a numerical scheme. Ozugurlu and Vanden-Broeck

[17] suggest writing the complex potential in the form of,

$$\zeta = \left(1 - t^2\right)^{2-\frac{2\beta}{\pi}} \left(-\frac{1}{t}\right)^{1-\frac{\alpha}{\pi}} \sum_{n=1}^{\infty} a_n t^{n-1}, \tag{6.2}$$

where $a_n$ are real coefficients to be found numerically. Note the first bracketed terms on the right-hand side are to do with singularities specific to the corner problem, and again to go into these details detracts from the purpose of this section.We will have similar singularities when we come to the problem of this thesis.

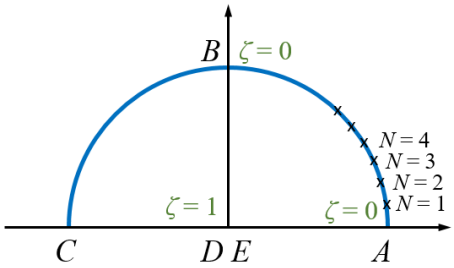


Figure 6.2: Sketch of complex $t$-plane. Includes an illustrative example of points for $N = 1, 2, 3$ etc

The idea behind the numerical procedure is to discretise the semi-circle in Figure 6.2 as shown, and on a finite number of points. We can then substitute into (6.1) at each point on the semi-circle. Each point defines $t$, but the $a_n$ coefficients will be unknown, so we take an initial estimate, substitute in at each point to create a system of equations which can then be solved numerically using Newton's method. From a programming perspective it is more convenient to use the notation $t = |t|e^{i\omega}$, where $\omega$ is the parameter to define the specific point on the semi-circle (i.e. the polar angle). It is worth also noting that $\xi$ is also to be determined during the numerical process. Some results of this process are shown in Figure 6.3. Whilst it is pleasing to be able to recreate the pictures from [17], we can be a little more qualitative and compare the numerical scheme developed to that as used in a similar paper [13]. In this paper the authors are concerned with the deformation of a bubble subject to flow but importantly numerical values are quoted. After running the scheme we are able to achieve the same numerical values.

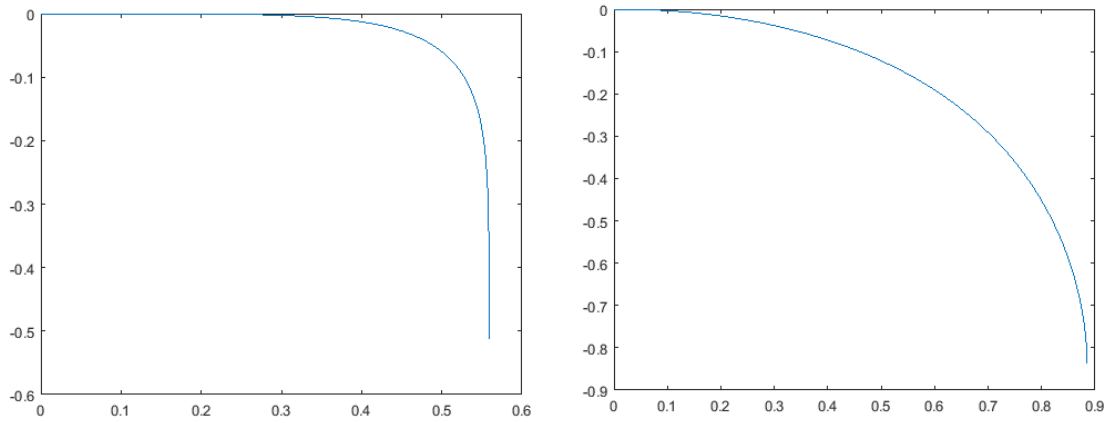


Figure 6.3: Recreation of bubble profiles from Ozugurlu and Vanden-Broeck [17]. For each of the profiles above we have $\alpha = \frac{\pi}{2}$, $\beta = \frac{\pi}{2}$.

## 6.2 Deformation of Elastic Cell in Uniform Flow

After the successful recreation of the work in Section 6.1 we move on to creating a similar numerical procedure for the curved elastic cell in this thesis. In Section 5 we discussed the situation of the flow across a curved elastic boundary when fixed at each end to a horizontal base. Figure 5.1 was a diagrammatic representation of this. The setup of the problem is also shown in Figure 6.4, where we additionally labelled extra points and have colour coded the boundaries to make the coming explanation easier.

We will firstly consider the fluid flow above the boundaries in Figure 6.4. Using the standard

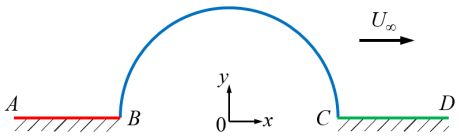


Figure 6.4: Setup of the flow over an elastic cell. The colours are for easy figure recognisation shortly. The green and the red lines are fixed solid walls and the blue line is the elastic membrane connect over the gap. There is a flow across the system with a steady speed of $U_\infty$. Using Cartesian geometry we will have $x$ and $y$ as distances measured in the horizontal and vertical directions respectively.

definitions (see [1] for example) of velocity potential, $\phi$, and stream functions, $\psi$, inside the flow we have,

$$\mathbf{u} = \nabla\phi = \left(\frac{\partial\phi}{\partial x}, \frac{\partial\phi}{\partial y}\right)$$

$$\mathbf{u} = \left( \frac{\partial \psi}{\partial y}, -\frac{\partial \psi}{\partial x} \right)$$

and we can define the complex velocity potential as $w = \phi + i\psi$ where $\phi$ and $\psi$ are both functions of $x$ and $y$. If we also have $z = x + iy$ then, we have that $w$ is a function of $z$. We can choose to have $\psi = 0$ along the fixed walls and the elastic boundary. The $w$-plane is then shown in Figure 6.5

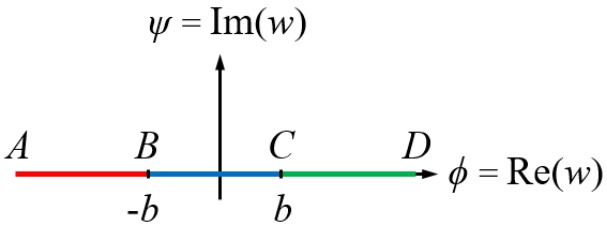


Figure 6.5: $w$-plane.

Where we come to solve our problem of finding the shape created in the (blue) elastic cell in Figure 6.4, we are concerned with only the streamline where $\psi = 0$. Using the transformation,

$$w = -\frac{1 + t^2}{2t}, \tag{6.3}$$

we can transform this into the complex $t$-plane onto a unit semi-circle. This is useful because we then, in a sense, fix the geometry of the problem and solve the problem on a shape which is predetermined. After a little manipulation (6.3) becomes,

$$t = -w \pm \sqrt{w^2 - 1},$$

and so when $\psi = 0$ we have,

$$t = -\phi \pm \sqrt{\phi^2 - 1}. \tag{6.4}$$

If when we come to non-dimensionalise we do this with $\phi = b\tilde{\phi}$ where $b = |OC| = |OB|$ in Figure 6.5 then at $B$ and $C$ we will have $\tilde{\phi} = -1$ and $\tilde{\phi} = 1$ respectively. So from (6.4) we find $B$ at $t = 1$ and $C$ at $t = -1$. At the point where $\tilde{\phi} = 0$ we have $t = i$. When $\tilde{\phi} \to \pm\infty$ we have (6.4) giving us that $t \to 0$. The result of this transformation is represented in Figure 6.6

Recall that the elastic boundary equations are derived from the set of equations from (5.8). These were,

$$q' = p + \kappa\tau \quad , \quad \tau' = -\kappa q \quad , \quad m' = \epsilon_B \kappa' = q \quad , \quad m = \epsilon_B \kappa,$$

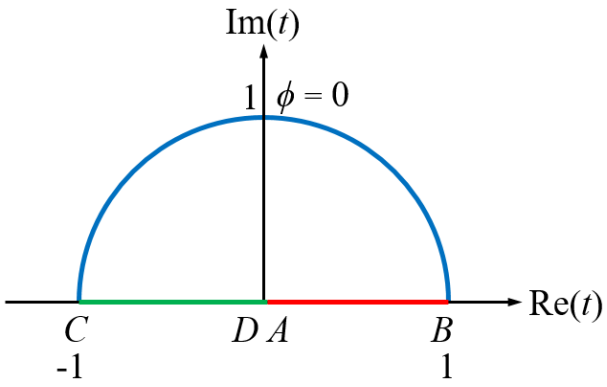


Figure 6.6: $t$-plane.

and combined to give,

$$\epsilon_B \kappa'' + \frac{\epsilon_B}{2}\kappa^3 - c\kappa = p. \tag{6.5}$$

Working from Bernoulli's equation (see Acheson [1] for example) with (6.5) we have,

$$\frac{1}{2}|\mathbf{u}|^2 + \frac{p}{\rho} = B \Rightarrow \frac{1}{2}\rho|\mathbf{u}|^2 + \epsilon_B\left(\kappa'' + \frac{1}{2}\kappa^3 - \frac{c}{\epsilon_B}\kappa\right) = B\rho$$

on the elastic boundary where $B$ is a Bernoulli constant. Also using the Bernoulli equation in the fluid at an infinite distance from the elastic arch where $|\mathbf{u}| \to U_\infty$ and $p \to p_\infty$ we find,

$$\frac{1}{2}\rho|\mathbf{u}|^2 + \epsilon_B\left(\kappa'' + \frac{1}{2}\kappa^3 - \frac{c}{\epsilon_B}\kappa\right) = \frac{1}{2}\rho U_\infty^2 + p_\infty.$$

We will non-dimensionalise using $l$ as a length scale that we will discuss and define shortly. For now we will define $s = l\tilde{s}$ and so $\kappa = \frac{1}{l}\tilde{\kappa}$. We will also define $\mathbf{u} = U_\infty\tilde{\mathbf{u}} = \begin{pmatrix} u \\ v \end{pmatrix} = U_\infty \begin{pmatrix} \tilde{u} \\ \tilde{v} \end{pmatrix}$, then,

$$\frac{1}{2}\frac{\rho l^3 U_\infty^2}{\epsilon_B}|\tilde{\mathbf{u}}|^2 + \left(\tilde{\kappa}'' + \frac{1}{2}\tilde{\kappa}^3 - \frac{l^2 c}{\epsilon_B}\tilde{\kappa}\right) = \frac{1}{2}\frac{\rho l^3 U_\infty^2}{\epsilon_B} + \frac{l^3 p_\infty}{\epsilon_B}.$$

Introducing simplifying substitutions,

$$\tilde{\alpha} = \tfrac{l^3\rho U_\infty^2}{\epsilon_B} \quad \text{and} \quad \tilde{\sigma} = \tfrac{l^2 c}{\epsilon_B} \quad \text{and} \quad \tilde{p} = \tfrac{l^3 p_\infty}{\epsilon_B}\ , \tag{6.6}$$

we arrive at,

$$\frac{1}{2}\tilde{\alpha}|\tilde{\mathbf{u}}|^2 + \left(\tilde{\kappa}'' + \frac{1}{2}\tilde{\kappa}^3 - \tilde{\sigma}\tilde{\kappa}\right) = \frac{1}{2}\tilde{\alpha} + \tilde{p}. \tag{6.7}$$

To set the appropriate length scale, $l$, we need to consider that we have stated we would like to have $\phi = b\tilde{\phi}$. Since $\nabla\phi = \left(\frac{\partial\phi}{\partial x}, \frac{\partial\phi}{\partial y}\right) = \mathbf{u}$ has units of speed, this implies that $\phi$ has units of speed $\times$ distance, therefore the value of $b$ has units of speed $\times$ distance. Since we wish to include $U_\infty$ as part of the non-dimensionalising process, we can then say, $\frac{b}{U_\infty}$ has the units of distance and is an appropriate length scale for the non-dimensionaling process, hence $l = \frac{b}{U_\infty}$.

Equation 6.7 holds on the (blue) elastic boundary shown in Figure 6.6. Since along this line we are a fixed radius (of length 1) from the origin it is convenient to use the form $t = e^{i\omega}$, where $\omega$ is the polar angle with $0 < \omega < \pi$. We will solve the problem numerically using a complex velocity $\zeta = \tilde{u} - i\tilde{v}$. From Figure 6.6 we have $\zeta \sim O\left(t^2 - 1\right)$ as $t \to \pm 1$. We will then seek a solution in the form,

$$\zeta = \left(1 - t^2\right) \sum_{n=1}^{\infty} c_n t^{n-1}, \tag{6.8}$$

where $c_n$ are real coefficients to be found. We will expand on the detail of the above paragraph in the next few pages.

Since we have $\zeta = \tilde{u} - i\tilde{v}$ the (non-dimensional) far field velocity potential gives $\zeta \to 1$ as $t \to 0$. This in turn leads to $c_1 = 1$ from (6.8). In order to numerically solve the problem we will truncate (6.8) after $n = N$ terms. We can then use this to find $\tilde{u}$ and $\tilde{v}$, which can be substituted into (6.7) at $N$ equally spaced points from $B$ to $C$ along the blue curve in Figure 6.6, whilst fixing $\alpha$ and $\tilde{p}$. We will have $N - 1$, $c_n$ coefficients (since $c_1 = 1$) and $\sigma$ will be another unknown ensuring we have $N$ unknowns for $N$ equations. We will solve this numerically using Newton iteration. For our numerical procedure we will use $N$ equally spaced points for $\omega$ with $0 < \omega < \pi$. Since we exclude $\omega = 0$ and $\omega = \pi$, we can create $N + 1$ equally spaced points for $0 \leq \omega \leq \pi$ (we shall call these our "master grid") and then the $N$ collocation points can be at the mid-points between these $N + 1$ master grid points. This will give us the formula for $\omega$ at our $N$ collocation points as,

$$\omega = \pi \frac{n - \frac{1}{2}}{N}, \tag{6.9}$$

where $1 \leq n \leq N$. In order to proceed with the numerical calculations, (6.7) shows us we need to find $\tilde{\kappa}$ in terms of $\tilde{u}$ and $\tilde{v}$.

Working from the definition of the non-dimensional potential flow with,

$$x_\phi = \frac{\tilde{u}}{\tilde{u}^2+\tilde{v}^2} \quad \text{and} \quad y_\phi = \frac{\tilde{v}}{\tilde{u}^2+\tilde{v}^2} \ , \tag{6.10}$$

and the definition of curvature in cartesian coordinates given by,

$$\kappa = \frac{x_\phi y_{\phi\phi} - y_\phi x_{\phi\phi}}{(x_\phi^2 + y_\phi^2)^{3/2}},$$

and apply the chain rule with $\phi = -\cos\omega$ (which we will justify later), we can show that the curvature is given by

$$\tilde{\kappa} = \frac{1}{\sin\omega}\frac{\tilde{u}\tilde{v}_\omega - \tilde{v}\tilde{u}_\omega}{(\tilde{u}^2+\tilde{v}^2)^{1/2}}. \tag{6.11}$$

When substituting into (6.7) we also need to differentiate (6.11) with respect to the arc length, $\tilde{s}$. Working from the same geometrical property from Figure 2.4 which was,

$$ds^2 = dx^2 + dy^2,$$

we can show[1]

$$\frac{d\tilde{s}}{d\tilde{\phi}} = \left(x_{\tilde{\phi}}^2 + y_{\tilde{\phi}}^2\right)^{1/2}. \tag{6.12}$$

Also, note that from (6.3)

$$\tilde{\phi} + i\tilde{\psi} = -\frac{1+t^2}{2t},$$

where $\omega = b\tilde{\omega}$ and $\psi = b\tilde{\psi}$ to be consistent with the earlier definition of $\phi = b\tilde{\phi}$. Since along the boundary we have $t = e^{i\omega}$, see Figure 6.6, we then find,

$$\tilde{\phi} + i\tilde{\psi} = -\frac{1+e^{2i\omega}}{2e^{i\omega}} = -\frac{1}{2}\left(e^{-i\omega} + e^{i\omega}\right) = -\cos\omega. \tag{6.13}$$

We know $\tilde{\psi} = 0$ from the setup of the problem shown in Figure 6.5, but we now have $\tilde{\phi} = -\cos\omega$ along the boundary. This can then be used along with (6.12),

$$\frac{d\tilde{s}}{d\tilde{\phi}} = \frac{d\tilde{s}}{d\omega}\frac{d\omega}{d\tilde{\phi}} = \frac{d\tilde{s}}{d\omega}\left(\frac{1}{\sin\omega}\right) = \left(x_{\tilde{\phi}}^2 + y_{\tilde{\phi}}^2\right)^{1/2}, \tag{6.14}$$

$$\Rightarrow \frac{d\tilde{s}}{d\omega} = \sin\omega\left(x_{\tilde{\phi}}^2 + y_{\tilde{\phi}}^2\right)^{1/2}. \tag{6.15}$$

And since from (6.10),

$$x_\phi^2 + y_\phi^2 = \frac{1}{\tilde{u}^2+\tilde{v}^2}, \tag{6.16}$$

[1]The details of this manipulation are geometrical and do not add/gain anything to the current text here and so are shown only in Appendix F.

we then have,

$$\frac{d\tilde{s}}{d\omega} = \sin\omega\left(\frac{1}{\tilde{u}^2+\tilde{v}^2}\right)^{1/2} \Rightarrow \frac{d\omega}{ds} = \frac{\left(\tilde{u}^2+\tilde{v}^2\right)^{1/2}}{\sin\omega}, \tag{6.17}$$

$$\Rightarrow \frac{d}{d\omega}\left(\frac{d\omega}{d\tilde{s}}\right) = \left(\frac{(\tilde{u}\tilde{u}_\omega+\tilde{v}\tilde{v}_\omega)\sin\omega}{(\tilde{u}^2+\tilde{v}^2)^{1/2}} - \left(\tilde{u}^2+\tilde{v}^2\right)^{1/2}\cos\omega\right) \div \sin^2\omega,$$

$$\Rightarrow \frac{d^2\omega}{d\tilde{s}^2} = \frac{d\omega}{d\tilde{s}}\frac{d}{d\omega}\left(\frac{d\omega}{d\tilde{s}}\right) = \frac{\left(\tilde{u}^2+\tilde{v}^2\right)^{1/2}}{\sin\omega}\left(\frac{(\tilde{u}\tilde{u}_\omega+\tilde{v}\tilde{v}_\omega)\sin\omega}{(\tilde{u}^2+\tilde{v}^2)^{1/2}\sin^2\omega} - \frac{\left(\tilde{u}^2+\tilde{v}^2\right)^{1/2}\cos\omega}{\sin^2\omega}\right),$$

$$\Rightarrow \frac{d^2\omega}{d\tilde{s}^2} = \frac{(\tilde{u}\tilde{u}_\omega+\tilde{v}\tilde{v}_\omega)\sin\omega - \left(\tilde{u}^2+\tilde{v}^2\right)\cos\omega}{\sin^3\omega}. \tag{6.18}$$

Using the chain rule, we can then substitute (6.11) along with (6.17) and (6.18) into (6.7) since,

$$\tilde{\kappa}'' = \frac{d^2\tilde{\kappa}}{d\tilde{s}^2} = \frac{d^2\tilde{\kappa}}{d\omega^2}\left(\frac{d\omega}{d\tilde{s}}\right)^2 + \frac{d\tilde{\kappa}}{d\omega}\frac{d^2\omega}{d\tilde{s}^2},$$

to obtain an equation to be solved where $\omega$ is the independent variable, remembering $\tilde{u}$ and $\tilde{v}$ are functions of $\omega$ from (6.8), and $\frac{d^2\tilde{\kappa}}{d\omega^2}$ can be directly obtained from (6.11)[2].

To evaluate (6.11) we need to know $\tilde{u}_\omega$ and $\tilde{v}_\omega$. Therefore we need to differentiate (6.8) with respect to $\omega$ so we can then take real and imaginary parts. Since we have $t = e^{i\omega}$ we then have,

$$\zeta_\omega = ie^{i\omega}\frac{d\zeta}{dt} = it\frac{d\zeta}{dt}, \tag{6.19}$$

and from (6.8) we have,

$$\frac{d\zeta}{dt} = \left(1-t^2\right)\sum_{n=1}^{\infty}(n-1)c_n t^{n-2} - 2t\sum_{n=1}^{\infty}c_n t^{n-1}. \tag{6.20}$$

From (6.8) and (6.19) we can then evaluate everything we need at each of the $N$ collocation points for (6.11) and (6.18), which means (6.7) can be calculated at each of these $N$ collocation points since,

$$\begin{array}{ll} \tilde{u} = Re(\zeta) & \tilde{v} = -Im(\zeta) \\ \tilde{u}_\omega = Re(\zeta_\omega) & \tilde{v}_\omega = -Im(\zeta_\omega) \end{array}.$$

After numerically satisfying the boundary equations, we then need to consider how to find $(x, y)$ coordinates to be able to plot the shape of the elastic cell. Recall, we have $N$ equally

[2]In practice this is very lengthy to do by hand due to the composite function nature of (6.11), and so could either done numerically as part of the numerical procedure, or more explicitly using algebraic manipulation software such as Maple.

spaced collocation points along the curved semi-circle between $B$ and $C$ in Figure 6.6 excluding the end points, and so if we include the end points we have $N+1$ equally spaced master grid points. This is shown in Figure 6.7. If we let $\bar{\omega}$ be a slightly adjusted value for $\omega$ so that $\bar{\omega}_n$ gives the polar angle at $(x_n, y_n)$ (and so $\omega_n$ would be the mid-point of $\bar{\omega}_{n+1}$ and $\bar{\omega}_n$), we can then use a mid-point finite difference (see [16] for example) to numerically calculate values for $(x_n, y_n)$ as we move around the semi-circle, where $1 \leq n \leq N+1$. It is worth making explicitly clear here that $(x_n, y_n)$ are not points on the semi-circle in Figure 6.7, more that it is at these points where we are able to compute values for $(x_n, y_n)$.


Figure 6.7: The location of numerically calculated variables around the unit-semi-circle from the complex $t$-plane as shown in Figure 6.6. The circular points correspond to the $N$ collocation points that satisfy the boundary conditions. The cross points correspond to where we will calculate the shape of the elastic cell using a mid-point finite difference method. At each circular point we will have numerically calculated $\tilde{u}$ and $\tilde{v}$ whilst $\omega$ was predefined. At each cross point we have defined $\bar{\omega}$ and can computer the physical $(x, y)$ coordinates of the deformed elastic cell.

From (6.10) with $\phi = -\cos\omega$ we have,

$$\frac{dx}{d\omega} = \frac{dx}{d\tilde{\phi}}\frac{d\tilde{\phi}}{d\omega} = \frac{\tilde{u}}{\tilde{u}^2 + \tilde{v}^2}\sin\omega,$$

and so our mid-point finite difference becomes,

$$x_{n+1} = x_n + (\bar{\omega}_{n+1} - \bar{\omega}_n)\frac{\tilde{u}_n}{\tilde{u}_n^2 + \tilde{v}_n^2}\sin\omega_n, \tag{6.21}$$

where here we have $1 \leq n \leq N$. Similarly we also have,

$$y_{n+1} = y_n + (\bar{\omega}_{n+1} - \bar{\omega}_n)\frac{\tilde{v}_n}{\tilde{u}_n^2 + \tilde{v}_n^2}\sin\omega_n, \tag{6.22}$$

and we are free to choose $(x_1, y_1)$ to be any initial point in physical space.

The length scale we have chosen to use, $l = \frac{b}{U_\infty}$, is convenient for solving the problem, but not so convenient for presenting results since the length of the elastic arch changes with the solution due to the fact it is dependent on the velocity potential in $b$ and the flow speed in

$U_\infty$ for each situation. Therefore it is helpful to rescale. We can evaluate the dimensionless cell perimeter, $\lambda l = \lambda \frac{b}{U_\infty}$, of the elastic from $B$ to $C$ in Figure 6.4 using,

$$\lambda = \int_{-b}^{b} \left(\tilde{u}^2 + \tilde{v}^2\right)^{-\frac{1}{2}} d\phi,$$

which comes from integrating (6.14) along the boundary and using (6.16). For numerical calculation purposes it is useful to note that $\tilde{\phi} = -\cos\omega$ along the elastic cell from (6.13), and use the relation (6.15) to calculate $\lambda$ with,

$$\lambda = \frac{1}{b} \int_{-1}^{1} \sin(\omega) \left(\tilde{u}^2 + \tilde{v}^2\right)^{-\frac{1}{2}} d\omega.$$

We then have $0 \leq \tilde{s} \leq \lambda$ around the cell perimeter and so $0 \leq \frac{L}{\lambda}\tilde{s} \leq L$ where $L$ is the physical length of the cell perimeter (in Figure 5.1 for example). Because $s = l\tilde{s}$, this gives $l = \frac{L}{\lambda}$ and $s = \frac{L}{\lambda}\tilde{s}$ since $0 \leq s \leq L$, and then also $\kappa = \frac{\lambda}{L}\tilde{\kappa}$. If we substitute the re-scaling for $\tilde{s}$ (and $\tilde{\kappa}$) back into (6.7) and multiply by $\left(\frac{\lambda}{L}\right)^3$ then we have,

$$\frac{1}{2}\left(\frac{\lambda}{L}\right)^3 \tilde{\alpha}|\tilde{\mathbf{u}}|^2 + \left(\kappa'' + \frac{1}{2}\kappa^3 - \left(\frac{\lambda}{L}\right)^2 \tilde{\sigma}\kappa\right) = \frac{1}{2}\left(\frac{\lambda}{L}\right)^3 \tilde{\alpha} + \left(\frac{\lambda}{L}\right)^3 \tilde{p},$$

which we can simplify with the substitutions,

$$\alpha = \left(\tfrac{\lambda}{L}\right)^3 \tilde{\alpha} \quad \text{and} \quad \sigma = \left(\tfrac{\lambda}{L}\right)^2 \tilde{\sigma} \quad \text{and} \quad P = \left(\tfrac{\lambda}{L}\right)^3 \tilde{p},$$

to have,

$$\frac{1}{2}\alpha|\tilde{\mathbf{u}}|^2 + \left(\kappa'' + \frac{1}{2}\kappa^3 - \sigma\kappa\right) = \frac{1}{2}\alpha + P, \tag{6.23}$$

as an equivalent equation to (6.7) but where we more practically define the length scale within the problem shown in Figure 6.4, i.e. fix $L$ which is the length of the elastic arch.

We still need to impose a condition to fix the gap between $B$ and $C$ in Figure 6.4, i.e. attach the elastic at the end points, but if we relax that condition temporarily then at this point we can look at the work of Blyth and Parau [4] and try to validate the work in this section so far by recreating some results from this paper. The work presented in [4] is actually more concerned with an elastic ring in no fixed space similar to Figure 2.3, and the solution is created in the first quadrant of Cartesian axes and then presented after reflections to create an enclosed loop. Additionally, in order to present results the cell needs to be rescaled so that the cell itself has the correct perimeter with $L = \pi$. The reason for only computing in

the first quadrant is an assumption of both horizontal and vertical symmetry in the solution. Due to the nature of the imposed symmetry the solutions presented in [4] are obtained by solving numerically over only the quarter circle shown in the first quadrant of Figure 6.6. Since $0 < \omega < \frac{\pi}{2}$, (6.9) is replaced with,

$$\omega = \left(\frac{\pi}{2}\right) \frac{n - \frac{1}{2}}{N},$$

at each of the $n$ collocation points for $1 \leq n \leq N$. Additionally, the assumption of symmetry allows a change in power[3] to $2n-2$ instead of $n-1$ in the summation parts of the $\zeta$ functions. And so (6.8) and (6.20) are replaced with,

$$\zeta = \left(1 - t^2\right) \sum_{n=1}^{N} c_n t^{2n-2},$$

$$\frac{d\zeta}{dt} = \left(1 - t^2\right) \sum_{n=1}^{N} (2n-2) c_n t^{2n-3} - 2t \sum_{n=1}^{N} c_n t^{2n-2}.$$

The rest of the procedure is then the same for solving the system described in Figure 6.4, we simply need to reflect the solution vertically. The main equation to solve in [4] is similar to (6.7), however there is a sign difference that comes from the fact when deriving the equations in this thesis we defined $p = p_s - p_i$ where as the authors in [4] define $p = p_i - p_s$, however this is still the same equation since the authors have also defined $\kappa$ to be the negative version as we have defined $\kappa$. Comparison between the results obtained from the numerical procedure above and [4] proved successful and Figure 6.8 is an example of a recreation of some of the solutions found in [4]. Also, in line with [4] we will define a measure of the bending energy as,

$$E = \frac{1}{L} \int_0^L \kappa^2 ds.$$

## 6.3 Compare to Weak Flow Perturbation Method

We can compare the fully non-linear solution from this section of the report to the solution found in Section 5 where we were concerned with a linear method solution of weak flow. In Section 5 we looked at the the situation where the elastic's natural shape, when not subjected

[3]The proof of the different power is in Appendix E.

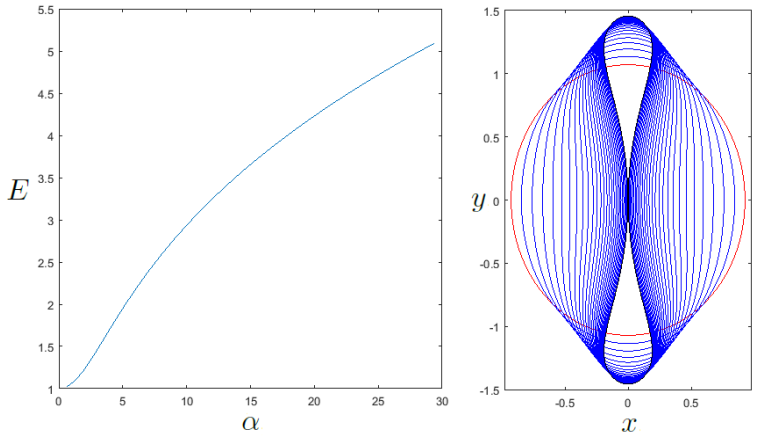


Figure 6.8: Solution to the problem of an elastic cell subjected to a uniform external flow. Here we have a the background pressure of $P = 0$. The left graph is a solution branch showing the energy, $E$, as the flow speed around the cell, $\alpha$, is increased. The right picture shows the cell profiles starting from a circle when there is no flow at $\alpha = 0$, up to when we have "pinching" at $\alpha = 29.3$.

to a pressure difference or flow over the boundary, was a perfect semi-circle with an elastic length $L$ and radius $a$ (see Figure 5.4 for example). Keeping in the symmetry of the problem we can first fix the gap between $B$ and $C$ in Figure 6.4. We can do this by fixing,

$$\frac{L}{\lambda}\left(x_1 - x_{N+1}\right) = a,$$

if we are still solving the problem on the first quarter-circle. In the particular case where we have $a = 1$, and hence $L = \pi$ and the condition becomes,

$$x_1 - x_{N+1} = \frac{\lambda}{\pi}.$$

In order to make sure we have the right number of unknowns for the right number of equations we can sacrifice one of the collocation points in the numerical scheme, where we evaluate the elastic boundary condition (6.7) , and replace it with the new condition.We can introduce a weak flow and then compare the result of this to the work from Section 5.

From (6.21) and (6.22) we have numerically computed $(x, y)$ coordinates for the curved elastic at each of the numerical computed collocations points as we move around the elastic. In the work in Section 5 we looked at a weak flow as a perturbation from a perfect semi-circle. This gave us the function $F(\hat{s})$ where $F$ was the perturbation and $\hat{s}$ was the distance traveled around the elastic. This gives us a good opportunity to compare with our numerical solution. To do this we will need to be able to work out the shape of our elastic boundary after our

numerical streamline solution and subtract a semi-circle, this should then be comparable to $F(\hat{s})$. With a formulation where the origin is at the centre of the base of the semi-circular solutuon, since we have non-dimensionalised such that the semi-circular solution would yield a unit radius, we can work out $F$ at each numerical $(x_i, y_i)$ point by using Pythagoras with,

$$F(\tilde{s}_i) = \sqrt{x_i^2 + y_i^2} - 1,$$

where $\tilde{s}_i$ is the distance traveled around the boundary.

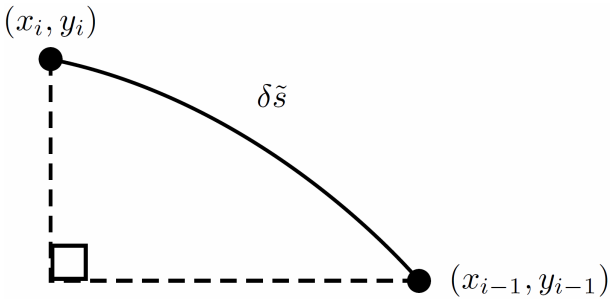


Figure 6.9: Finding the link between $\tilde{s}$, the distance traveled around the elastic cell, and the coordinates at each collocation point $(x_i, y_i)$. Here $\delta\tilde{s}$ is the change in $\tilde{s}$ from $\tilde{s}_i$ and $\tilde{s}_{i-1}$.

In Figure 6.9 we have $\delta\tilde{s}$ as the change in distance between $\tilde{s}_i$ and $\tilde{s}_{i-1}$, where these are computed at $(x_i, y_i)$ and $(x_{i-1}, y_{i-1})$ respectively. Hence,

$$\delta\tilde{s} = \sqrt{(x_i - x_{i-1})^2 + (y_i - y_{i-1})^2},$$

and so,

$$\begin{aligned} \tilde{s}_1 &= \sqrt{(x_1 - x_0)^2 + (y_1 - y_0)^2} \\ \tilde{s}_2 &= \sqrt{(x_2 - x_1)^2 + (y_2 - y_1)^2} + \tilde{s}_1 \\ \tilde{s}_3 &= \sqrt{(x_3 - x_2)^2 + (y_3 - y_2)^2} + \tilde{s}_2 \\ &etc. \end{aligned},$$

and then in general we have,

$$\tilde{s}_i = \sum_{i=1}^{N+1} \sqrt{(x_i - x_{i-1})^2 + (y_i - y_{i-1})^2} + \tilde{s}_{i-1}.$$

Then we have $\tilde{s}_0 = 0$, and after taking into account the length of the cell in the streamline solution (i.e. $\pi$) since the work to create Figure 5.5 had $0 \leq \tilde{s} \leq 1$,

$$\frac{1}{\pi}\left(\sum_{i=1}^{N+1} \sqrt{(x_i - x_{i-1})^2 + (y_i - y_{i-1})^2} + \tilde{s}_{i-1}, \sqrt{x_i^2 + y_i^2} - 1\right),$$

plots $F(\tilde{s})$ at each of the collocation points $(x_i, y_i)$.

In order to make sure we compare the fully non-linear problem in the section to the weak flow linear problem in the earlier work, it will be useful to express the equations from each method in similar ways so we can match up each of the parameters of the problem. The weak flow linear problem was defined by (5.10) which was given by,

$$\hat{\kappa}_{\hat{s}\hat{s}} + \frac{1}{2}\hat{\kappa}^3 - \hat{c}\hat{\kappa} = E + \delta P(\hat{s})$$

where,

$$E = \tfrac{p_\infty L^3}{\epsilon_B} \quad , \quad \delta = \tfrac{1}{2}\tfrac{\rho U^2 L^3}{\epsilon_B} \quad , \quad P(\hat{s}) = 1 - 4\sin^2(\pi\hat{s}) + \delta P_1(\hat{s}) + ... \ ,$$

and so, looking up to terms involving $\delta$ only since $\delta << 0$, we have,

$$\hat{\kappa}_{\hat{s}\hat{s}} + \frac{1}{2}\hat{\kappa}^3 - \hat{c}\hat{\kappa} - \delta\left(1 - 4\sin^2(\pi\hat{s})\right) = \frac{p_\infty L^3}{\epsilon_B}.$$

In the case of $L = \pi$ and taking $\epsilon_B = 1$ the equation above becomes,

$$\frac{4\delta}{\pi^3}\sin^2(\pi\hat{s}) + \frac{1}{\pi^3}\left(\hat{\kappa}_{\hat{s}\hat{s}} + \frac{1}{2}\hat{\kappa}^3 - \hat{c}\hat{\kappa}\right) = \frac{\delta}{\pi^3} + p_\infty.$$

We can also reverse the non-dimensionlising process where,

$$s = L\hat{s} = \pi\hat{s} \quad , \quad \kappa = \tfrac{1}{L}\hat{\kappa} = \tfrac{1}{\pi}\hat{\kappa} \quad , \quad \hat{c} = \tfrac{L^2 c}{\epsilon_B} = \pi^2 c \ ,$$

to obtain,

$$\frac{4\delta}{\pi^3}\sin^2(s) + \left(\kappa_{ss} + \frac{1}{2}\kappa^3 - c\kappa\right) = \frac{\delta}{\pi^3} + p_\infty, \tag{6.24}$$

for the weak flow problem using linear theory.

The full non-linear problem was given by (6.23) which was,

$$\frac{1}{2}\alpha|\tilde{\mathbf{u}}|^2 + \left(\kappa'' + \frac{1}{2}\kappa^3 - \sigma\kappa\right) = \frac{1}{2}\alpha + P, \tag{6.25}$$

and from how we arrived at this equation we have, in the case when $L = \pi$,

$$\alpha = \left(\tfrac{\lambda}{\pi}\right)^3\tilde{\alpha} \quad \text{and} \quad P = \left(\tfrac{\lambda}{\pi}\right)^3\tilde{p} \ .$$

Solving the fully non-linear problem has $\tilde{\alpha}$ and $\tilde{p}$ as predefined parameters to set the flow speed and background pressure, and weak flow linear theory has $\delta$ and $p_\infty$ as predefined parameters to set the flow speed and background. Comparing (6.24) and (6.25) we can see,

$$\delta = \tfrac{\pi^3}{2}\alpha = \tfrac{\lambda^3}{2}\tilde{\alpha} \quad \text{and} \quad p_\infty = P = \left(\tfrac{\lambda}{\pi}\right)^3\tilde{p} \ .$$

Figure 6.10 shows the streamline numerical procedures deviation from the semi-circle on the right and the corresponding linear analysis solution from Chapter 5. Whilst the numerical procedure is converging and gives us a similar profile in shape, there seems to be a slight discrepancy. Upon closer inspection it appears that the integral condition from Chapter 5 is not being satisfied in the numerical process. This appears to be related to the numerical calculation of the length of the cell (and therefore $\lambda$) in the later scheme. This will be referred to the chapter for future investigation.

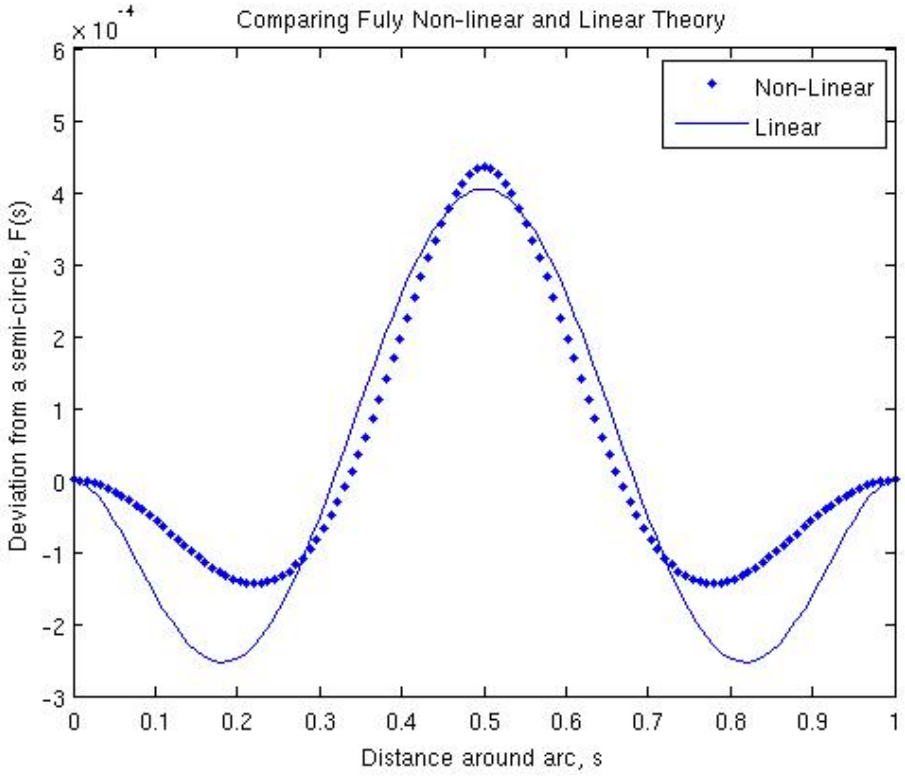


Figure 6.10: Comparing the general numerical solution to the pertubabtion analysis.

# 7

# Future Work

We will briefly outline some ideas for extending and continuing the research presented in each of the previous chapters of this thesis. In chapter 2 we discussed the profiles of an elastic ring under pressure. In particular, during section 2.5 we discussed the contact points where sides of the elastic are deformed to the point where they come into constant with other sides. In Flaherty et al.[10] the problem formulation continues after these contact points using a different method to analyse the profiles where sides become squashed other and the contact point becomes a section of the elastic rather than only point. This type of analysis could be extended into the rest of the problems in this thesis, for example in the fluid annulus situation from chapter 3. For the elastic arch problem presented in chapter 4, Figure 4.1 shows how the elastic arch is fixed at each end, it would be interesting to look at the contact if the area under the arch in Figure 4.1 was a solid base.

The development of the general numerical procedure that was presented in chapter 6 does not have as many restrictions as the analysis methods used in the preceding chapters. For example, in chapter 4 and chapter 5 the analyses are based on perturbing a semi-circle shape and having a weak flow solution respectively. The general numerical procedure does not have small parameter expansions as used in the other two methods and so we can seek a greater range of solutions.

There are three main areas to focus on for continuing work from this thesis. Firstly, from chapter 3 where we look at the fluid annulus problem. This chapter explained and demonstrated the solution for an anulus held by surface tension, and so the next stage was to develop the method when we have elastic boundaries instead of surface tension. The solution would be to continue with the same numerical process from section 3.1, except our Bernoulli equation would become,

$$\frac{1}{2}\rho U_A^2 - \left(\epsilon_A \kappa_A'' + \epsilon_A \frac{\kappa_A^3}{2} - c_A \kappa_A\right) = C_1,$$

$$\frac{1}{2}\rho U_B^2 + \left(\epsilon_B \kappa_B'' + \epsilon_B \frac{\kappa_B^3}{2} - c_B \kappa_B\right) = C_2,$$

where $A$ and $B$ subscripts relate to the outer and inner rings respectively (and where $U$, $\kappa$, $\rho$ and $\epsilon$ are the flow speed, curvature, fluid density and bending modulus respectively, and consisted with the notation in the previous chapter, and the other letter are constants to be found).

In chapters 4 and 5 we looked at the elastic arch problem. In both of these situations we neglected other forces, such as gravity, which would have an impact on the solutions available to find. The force of gravity would not have to act in the downward direction in all the setup diagrams, but could be at different angles. The effect of changing the direction of gravity would be the same problem as studying the arches on slopes. Also, considering the weak flow situation in chapter 5, if gravity was directed upward in Figure 5.4 then it would be the same as turning the problem upside down and having an object with an elastic cushion bottom floating on a water surface. Then we could be looking at the stability of waves on this system, which has obvious applications to floating structures in the real world.

In chapter 6, there is still more work to do. When comparing the fully numerical solution developed in the early part of the chapter to that the perturbation solutions form the earlier chapters it appeared there was a slight discrepancy. It appears that the integral condition from chapter 4 was not being adhered to in the fully numerical procedure. Upon further exploration it appears that the length of the elastic cell was not being maintained correctly in the numerical procedure, and this is where the issue was. Unfortunately this did not prove to be an easy issue to resolve, and due to the ending of research time, this will have to be left as a point to pick up on at a later date. The length of the cell perimeter was the equation,

$$\lambda = \frac{1}{b}\int_{-1}^{1} \sin(\omega)\left(\tilde{u}^2 + \tilde{v}^2\right)^{-\frac{1}{2}} d\omega.$$

Preserving the length of the elastic is the last issue to resolve to then have solved this as a general problem.

# A

# A General Numerical Scheme

We will develop a numerical scheme to solve the equations of an elastic loop that we will use in this report. We will find that we will know some initial conditions and have some additional boundary conditions. We develop a scheme whereby we assume sensible estimates for unknown initial conditions and compare results to the other known boundary conditions to refine our estimate. Assuming that we do not know our initial conditions such that $\tau(0) = \alpha$ and $k(0) = \beta$ (where $\tau$ and $k$ are functions related to whatever problem we attempt to solve, and $\alpha$ and $\beta$ are constants). The idea being to then run the system to include Newton's method (see Jacques and Judd [12] for example) and deduce actual values for $\alpha$ and $\beta$, and then using these values create a plot showing $y$ against $x$ (assuming that $x$ and $y$ are position coordinates).

We will start by expressing the system as a first order system. We then run the Runge Kutta loop on the computer and define some function,

$$\mathbf{F}(\alpha, \beta) = \begin{bmatrix} F_1 \\ F_2 \end{bmatrix} \tag{A.1}$$

defining the function so that $\mathbf{F} = 0$ if we had somehow guessed the correct values for $\alpha$ and $\beta$. We will run through solving the system with a suitable guess for $\alpha$ and $\beta$. We can then perturb our values of $\alpha$ and $\beta$ by a small value $\mathbf{h}$.

If we look at a Taylor expansion of $\mathbf{F}(x_0 + h)$, where $\mathbf{x_0} = (\alpha, \beta)$ we find,

$$\mathbf{F}(\mathbf{x_0} + \mathbf{h}) = \mathbf{F}(\mathbf{x_0}) + \quad \mathbf{J} \Big|_{\mathbf{x_0}} \cdot \mathbf{h} + ... \tag{A.2}$$

where,

$$J_{ij} = \quad \frac{\partial F_i}{\partial x_j} \Big|_{x_0}$$

From the way we have defined $\mathbf{F}$ we require $\mathbf{F} = \mathbf{0}$ and so when we know $\alpha$ and $\beta$ we then have $\mathbf{F}(\mathbf{x_o} + \mathbf{h}) = \mathbf{0}$, i.e. our guess without slight adjustment of $\mathbf{h}$ is closer to zero than when we include the adjustment, and hence (A.2) approximately becomes,

$$0 = \mathbf{F}(\mathbf{x_0}) + \mathbf{J} \cdot \mathbf{h}$$

$$\mathbf{h} = -\mathbf{J}^{-1} \cdot \mathbf{F}(x_0) \tag{A.3}$$

and with this value of $\mathbf{h}$ we can then have a closer approximation to $\mathbf{x} = (\alpha, \beta)$ as $\mathbf{x_1} = \mathbf{x_0} + \mathbf{h}$.

Now, we know our function $\mathbf{F}$, initial values, and we can choose our perturbation so it is suitably small (e.g. $10^{-1}$ ). The question is how do we find $J_{ij}$. Writing $\mathbf{J}$ out as a matrix we see,

$$\mathbf{J} = \begin{bmatrix} \dfrac{\partial F_1}{\partial \alpha} & \dfrac{\partial F_1}{\partial \beta} \\ \dfrac{\partial F_2}{\partial \alpha} & \dfrac{\partial F_2}{\partial \beta} \end{bmatrix} \tag{A.4}$$

If we allow our perturbation $\epsilon = (\epsilon_\alpha, \epsilon_\beta)$ then,

$$\frac{\partial F_1}{\partial \alpha} \simeq \frac{F_1(\alpha + \epsilon_\alpha, \beta) - F_1(\alpha, \beta)}{\epsilon_\alpha}$$

$$\frac{\partial F_1}{\partial \beta} \simeq \frac{F_1(\alpha, \beta + \epsilon_\beta) - F_1(\alpha, \beta)}{\epsilon_\beta}$$

$$\frac{\partial F_2}{\partial \alpha} \simeq \frac{F_2(\alpha + \epsilon_\alpha, \beta) - F_2(\alpha, \beta)}{\epsilon_\alpha}$$

$$\frac{\partial F_2}{\partial \beta} \simeq \frac{F_2(\alpha, \beta + \epsilon_\beta) - F_2(\alpha, \beta)}{\epsilon_\beta}$$

using finite difference approximations.

So, to summarize how we shall numerically solve this problem on the computer.

- Estimate values for $\alpha$ and $\beta$
- Run the Runge Kutta scheme for solving our first order system
- Evaluate $\mathbf{F}$
- Adjust our values of $\alpha$ and $\beta$ by $\epsilon_\alpha$ and $\epsilon_\beta$ respectively
- Run the Runge Kutta scheme again

- Evaluate $\mathbf{F}$ again
- Calculate the matrix (A.4) and then use this to calculate (A.3)

This will then give use a closer approximation for $\alpha$ and $\beta$ as $\mathbf{x_1} = \mathbf{x_0} + \mathbf{h}$. We can then run the whole thing until a suitable degree of accuracy is obtained.

# B

# Approximating the Location of Solutions

To help find the location of the additional bifurcation points, I begin looking at the first graph in Figure 4.7. These bifurcations occur at the tip of the 'peaks' for $\hat{q}(0)$. These appear to be linear so using only those three I tried to fit a linear regression line to see if was good fit to fist find a link between $\hat{q}$ and $\hat{p}$. (Note also if we have $\hat{p}$ than we also have $\hat{\tau}(0) = -\hat{p}$, and $\hat{k}(0) = 1$ from the other graph on Figure 4.7). The linear regression equation for these first three bifurcations came out to be,

$$\hat{q}(0) = 2.8436\hat{p} + 0.1073$$

with an $R^2 = 1$ (not exactly but when rounded to 4 significant figures. If I then number the bifurcations such that $n = 1$ for the first one (smallest $\hat{p}$-value), $n = 2$ for the second, $n = 3$ for the third and so on... I can then attempt to fit a regression model with $\hat{p}(n)$. This came out to be,

$$\hat{p} = 1.6172n^2 + 1.621n + 0.0876$$

again with a $R^2 = 1$.

Using these equations I attempted to predict the point for $n = 4$, which gave $\hat{p} = 32.4468$ and $\hat{q}(0) = 92.3730$. Using these as initial estimations for the numerical scheme I then found the solutions to be, $\hat{p} = 32.45$ and $\hat{q} = 92.41$ correct to two decimal places. Using the additional values I was then able to fit an even more accurate line. Using this process I created Table B.1, with the assumption that the greater the values of $n$ included would give a more accurate prediction equation. Table B.1 is a representation of the fitted prediction lines.
Due to the way we have been working we do have to appreciate rounding errors in numerical and statistical work, however Table B.1 does seem to suggest our equations correct to 2 decimal places are,

$$\hat{p} = 1.62n^2 + 1.64n + 0.06$$

| $n$'s Included | $\hat{p}$ | $\hat{q}(0)$ |
|---|---|---|
| 1,2,3,4 | $1.6174n^2 + 1.6203n + 0.0882$ | $2.8437\hat{p} + 0.1067$ |
| 1,2,3,4,5 | $1.6181n^2 + 1.6171n + 0.0911$ | $2.8441\hat{p} + 0.1019$ |
| 1,2,3,4,5,6 | $1.6281n^2 + 1.5630n + 0.1473$ | $2.8467\hat{p} + 0.0566$ |
| 1,2,3,4,5,6,7 | $1.6155n^2 + 1.6411n + 0.0566$ | $2.8458\hat{p} + 0.0780$ |
| 1,2,3,4,5,6,7,8 | $1.6152n^2 + 1.6432n + 0.0538$ | $2.8447\hat{p} + 0.1072$ |
| 1,2,3,4,5,6,7,8,9 | $1.6156n^2 + 1.6398n + 0.0585$ | $2.8444\hat{p} + 0.1192$ |

Table B.1: Prediction lines for bifurcation points. These are fitted regression lines with $R^2 = 1$ for each line to 4 decimal places.

$$\hat{q}(0) = 2.8\hat{p} + 0.12$$

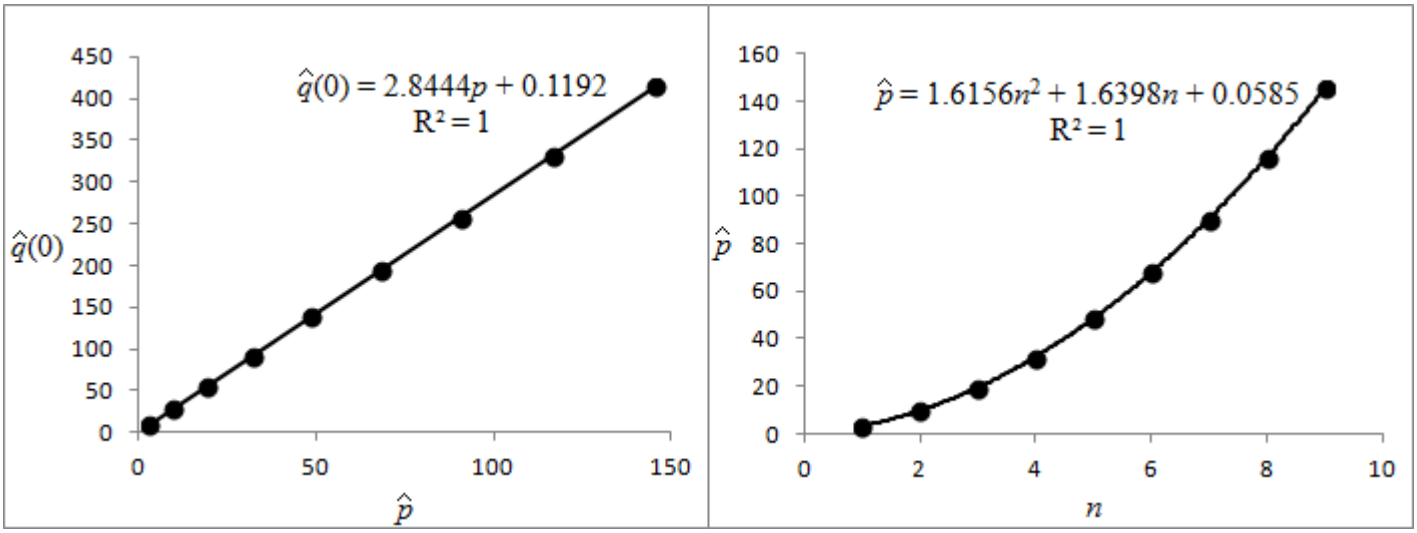


Figure B.1: Regression models to predict bifurcation points. $n$ refers to $n$-th bifurcation along the line of increasing pressure. Here we have a graphical illustration of Table B.1.

Unlike previous bifurcation points, which were all semi-circular solutions, these bifurcations all look somewhat different. These are shown in Figure 4.10.

# C

# General Shape Solution - Fourier series

As we introduce a flow to our situation the shape to the elastic will deform and so not be a perfect (semi) circle. However, it would seem reasonable for a very small flow that we could seek a solution as a perturbation of the flow around a the semi-circle.If we have a shape that is a very slightly deformed circle (as shown in Figure C.1) then we can model the boundary as $r = a + a\delta f(\omega)$ where $\delta << 1$. Note that we have $a\delta f(\omega)$ as opposed to $\delta f(\omega)$ to be consistent with the dimensions for $r$ because $\delta$ and $f(\omega)$ are dimensionless. We can also define $\phi = \phi_0 + \delta\phi_1$ where $\phi_0$ is given by (5.2) and $\phi_1$ is from the perturbed flow.

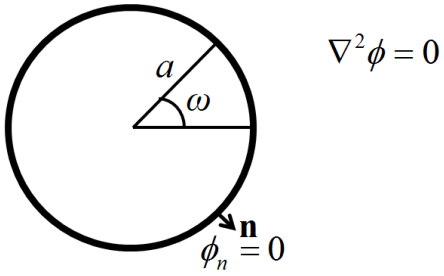


Figure C.1: Flow around a circle. The radius of the circle is $a$, and $\omega$ is the polar angle. The flow around the outside of the circle satisfies Laplace's equation. $\mathbf{n}$ is the vector normal to the surface, and there is now flow through this.

From Laplace's equation, since we already have $\phi_0$ as a satisfying solution, we have,

$$\nabla^2\phi = \nabla^2\phi_0 + \nabla^2\phi_1 = \nabla^2\phi_1 = 0$$

For our infinity solution we have $\nabla\phi_1 = 0$ as $r \to \infty$ because we require $\nabla\phi \to U\mathbf{i}$ and we already have $\nabla\phi_0 \to U\mathbf{i}$. The condition of no normal flow ($\mathbf{n} \cdot \mathbf{u}$) through the boundary is a little harder when we do not have a perfect circle. We require,

$$\mathbf{n} \cdot \nabla\phi = 0 \tag{C.1}$$

The normal to a curve can be found (see [20] page 16) from,

$$\mathbf{n} = \frac{\nabla\left(r - (a + a\delta f)\right)}{\left|\nabla\left(r - (a + a\delta f)\right)\right|}$$

and so in polar coordinates where $\nabla = \left(\frac{\partial}{\partial r}, \frac{1}{r}\frac{\partial}{\partial \omega}\right)$ we have,

$$\mathbf{n} = \frac{\left(1, \frac{1}{r}\left(-a\delta f'\right)\right)}{1 + O\left(\delta^2\right)} = \left(1, -a\delta\frac{f'}{r}\right)$$

since $\delta << 1$. Then (C.1) becomes,

$$\left(1, -a\delta\frac{f'}{r}\right) \cdot \left(\frac{\partial}{\partial r}, \frac{1}{r}\frac{\partial}{\partial \omega}\right)\phi = \frac{\partial \phi}{\partial r} - \frac{a\delta f'}{r^2}\frac{\partial \phi}{\partial \omega} = 0$$

Substituting in $r = a + a\delta f$ we then have,

$$\frac{\partial \phi}{\partial r} - a\delta f'\frac{\partial \phi}{\partial \omega}\left(a + a\delta f\right)^{-2} = 0 \tag{C.2}$$

Now,

$$\left(a + a\delta f\right)^{-2} = a^{-2}\left(1 + 1\delta f\right)^{-2} = a^{-2}\left(1 - 2\delta f + O(\delta^2)\right)$$

and so (C.2) becomes,

$$\begin{aligned} \frac{\partial \phi}{\partial r} - \frac{\delta f'}{a}\frac{\partial \phi}{\partial \omega}\left(1 - 2\delta f + O(\delta^2)\right) &= 0 \\ \frac{\partial \phi}{\partial r} - \frac{\delta f'}{a}\frac{\partial \phi}{\partial \omega} + O(\delta^2) &= 0 \end{aligned} \tag{C.3}$$

On the curved boundary we have,

$$\phi_r(a + a\delta f) = \phi_r(a) + a\delta f\phi_{rr}(a) + ...$$

$$\phi_\omega(a + a\delta f) = \phi_\omega(a) + a\delta f\phi_{\omega r}(a) + ...$$

and so (C.3) becomes,

$$\phi_r(a) + \delta\left(af\phi_{rr}(a) - \frac{f'}{a}\phi_\omega(a)\right) + O(\delta^2) = 0$$

into which we can substitute $\phi = \phi_0 + \delta\phi_1$ to obtain,

$$\left.\frac{\partial \phi_0}{\partial r}\right|_{r=a} + \delta\left(\left.\frac{\partial \phi_1}{\partial r}\right|_{r=a} + af\left.\frac{\partial^2 \phi_0}{\partial r^2}\right|_{r=a} - \frac{f'}{a}\left.\frac{\partial \phi_0}{\partial \omega}\right|_{r=a}\right) + O(\delta^2) = 0$$

But we already have that the first term is zero from our circle solution. Also taking $\delta << 1$ we then end up with a condition on $r = a$ of,

$$\frac{\partial \phi_1}{\partial r} + af\frac{\partial^2 \phi_0}{\partial r^2} - \frac{f'}{a}\frac{\partial \phi_0}{\partial \omega} = 0$$

$$\frac{\partial \phi_1}{\partial r} = -af\frac{\partial^2 \phi_0}{\partial r^2} + \frac{f'}{a}\frac{\partial \phi_0}{\partial \omega} \tag{C.4}$$

Recall that $\phi_0$ is given by (5.2) and so,

$$\frac{\partial \phi_0}{\partial \omega} = -U\left(r + \frac{a^2}{r}\right)\sin\omega$$

$$\frac{\partial^2 \phi_0}{\partial r^2} = \frac{2Ua^2}{r^3}\cos\omega$$

and so when $r = a$ we obtain,

$$\frac{\partial \phi_0}{\partial \omega} = -2Ua\sin\omega$$

$$\frac{\partial^2 \phi_0}{\partial r^2} = \frac{2U}{a}\cos\omega$$

and so (C.4) becomes,

$$\frac{\partial \phi_1}{\partial r} = -2Uf\cos\omega - 2Uf'\sin\omega \tag{C.5}$$

In summary, we are seeking a solution for $\nabla^2\phi_1 = 0$ subject to the conditions that $\nabla\phi_1 \to 0$ as $r \to \infty$, and (C.5) holds when $r = a$. If we seek a solution in the form of $r = a + ag(\omega)$ where $g(\omega)$ can be written as a Fourier series,

$$g(\omega) = \sum_{-\infty}^{\infty} g_n e^{in\omega}$$

then we could then define any shape of our perturbed circle simply by increasing the number of terms in the Fourier series. I.e. we can choose $f(\omega) = b_m\cos(m\omega)$ (where $m \in Z$) as one of our Fourier terms where we are free to choose $m$ to define our shape, and we can include any number of terms for the general solution. Here, $b_m$ is a Fourier coefficient. Understanding the values for these will be the ultimate problem to solve for our fluid flow problem as it is the shape we are looking to find.

An interesting question to pose at this stage is what are the shapes of the deformations as we change values of $m$. There are some example sketches shown in Figure C.2. It is worth noting that these shapes are explored in more detail in [10] and in Section 3 of this report.

The case where $m = 0$ is an enlargement to the size of the circle. We can see this as $r = a + a\delta b_0\cos(0)$ becomes $r = a(1 + \delta b_0)$. Whilst it is interesting in a general sense this will not be relevant for our elastic problem as we are fixing the length of the surface. However,

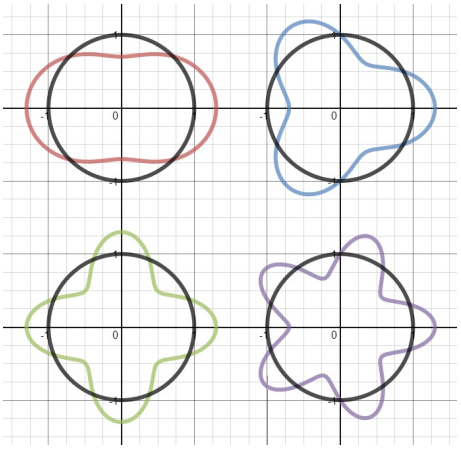

Figure C.2: Example shapes of the elastic curve as we choose various values of $m$. The pictures show $m = 2$, $m = 3$, $m = 4$, and $m = 5$. Purely to construct the pictures we have a unit circle (i.e. $a = 1$) and the deformation (i.e. $\delta b_m$) has been exaggerated.

it does tell us that for that case we must have $b_0 = 0$. The situation for $m = 1$ refers to a translation of the circle along the $x$-axis. Again, whilst interesting in the general sense, for our particular flow problem when the elastic membrane is fixed we will have no $m = 1$ solutions.

Substituting $f(\omega) = b_m \cos(m\omega)$ into (C.5) we obtain,

$$\left.\frac{\partial \phi_1}{\partial r}\right|_{r=a} = -2Ub_m \cos(m\omega)\cos\omega + 2Ub_m m \sin(m\omega)\sin\omega$$

$$\Leftrightarrow \left.\frac{\partial \phi_1}{\partial r}\right|_{r=a} = -2Ub_m\Big(\cos(m\omega)\cos\omega - m\sin(m\omega)\sin\omega\Big) \tag{C.6}$$

This boundary condition now presents us with an opportunity to seek a solution in stages. If we are able to find two solutions, one that solves the problem for the right hand side of (C.6) equal to $-2Ub_m \cos(m\omega)\cos\omega$ and the other that solves for the right hand side equal to $2Ub_m m \sin(m\omega)\sin\omega$, we should be able to find an overall solution by summing them together.

The problem we now turn to is $\nabla^2\phi_1 = 0$ subject to the conditions that $\nabla\phi_1 \to 0$ as $r \to \infty$, and $\left.\frac{\partial \phi_1}{\partial r}\right|_{r=a} = -2Ub_m \cos(m\omega)\cos\omega$ .

It is worth noting the identity $2\cos(m\omega)\cos\omega = \cos(m-1)\omega + \cos(m+1)\omega$ at this stage. We can then transform the problem again into two separate problems to be solves and then summed together in the form of,

$\nabla^2\phi_1 = 0$ subject to the conditions that $\nabla\phi_1 \to 0$ as $r \to \infty$, and $\frac{\partial\phi_1}{\partial r}\Big|_{r=a} = -Ub_m \cos n\omega$,

where $n = m - 1$ for one part of the solution, and $n = m + 1$ for the other part.

We begin by seking a solution of the form $\phi_1 = h(r)\cos n\omega$. Substituting this into $\nabla^2\phi_1 = 0$ we have,

$$\nabla^2\phi_1 = \phi_{1rr} + \frac{\phi_{1r}}{r} + \frac{\phi_{1\omega\omega}}{r^2}$$

$$= h''\cos n\omega + \cos n\omega\frac{h'}{r} - \cos n\omega\frac{n^2 h}{r^2}$$

$$= h'' + \frac{h'}{r} - \frac{n^2 h}{r^2} = 0$$

This form seems to suggest that we could seek a solution of the form $h = r^\beta$. Substituting this into the above gives,

$$\beta(\beta-1)r^{\beta-2} + \beta\frac{r^{\beta-1}}{r} - n^2\frac{r^\beta}{r^2} = 0$$

$$\Leftrightarrow \beta(\beta-1)r^{\beta-2} + \beta r^{\beta-2} - n^2 r^{\beta-2} = 0$$

$$\Rightarrow \beta(\beta-1) + \beta - n^2 = 0$$

$$\Rightarrow \beta^2 = n^2 \Rightarrow \beta = \pm n$$

Hence $h = Ar^n + Br^{-n}$ and therefore $\phi_1 = \left(Ar^n + Br^{-n}\right)\cos n\omega$. From this solution we find,

$$\nabla\phi_1 = \left(\left(nAr^{n-1} - nBr^{-n-1}\right)\cos n\omega, -n\left(Ar^{n-1} + Br^{-n-1}\right)\sin n\omega\right)$$

As $r \to \infty$ we have,

$$\nabla\phi_1 \to \left(nAr^{n-1}\cos n\omega, -nAr^{n-1}\sin n\omega\right)$$

Because we require $\nabla\phi_1 \to 0$ we must have $A = 0$. So $\phi_1 = Br^{-n}\cos n\omega$. This then gives $\phi_{1r} = -Bnr^{-n-1}\cos n\omega$. When $r = a$ we require $\phi_{1r} = -Ub_m\cos n\omega$ and so,

$$\frac{-Bn}{a^{n+1}}\cos n\omega = -Ub_m\cos n\omega$$

$$\Rightarrow \frac{-Bn}{a^{n+1}} = -Ub_m \Rightarrow B = \frac{Ub_m a^{n+1}}{n}$$

Therefore,

$$\phi_1 = \frac{Ub_m a^{n+1}}{nr^n}\cos n\omega$$

Recall that this was half a solution, we must have a two part solution (that when $n = m - 1$ and when $n = m + 1$) and so,

$$\phi_1 = \frac{Ub_m a^m}{(m-1)r^{m-1}} \cos(m-1)\omega + \frac{Ub_m a^{m+2}}{(m+1)r^{m+1}} \cos(m+1)\omega \tag{C.7}$$

Turing ourselves back to how we solved the problem by splitting (C.6) into two parts we now solve the similar problem of... $\nabla^2\phi_1 = 0$ subject to the conditions that $\nabla\phi_1 \to 0$ as $r \to \infty$, and $\left.\frac{\partial\phi_1}{\partial r}\right|_{r=a} = 2Ub_m m \sin(m\omega)\sin\omega$ .

Again it is worth noting an identity $2m\sin(m\omega)\sin\omega = m\cos(m-1)\omega - m\cos(m+1)\omega$ at this stage. Then again we can solve in two parts the problem $\nabla^2\phi_1 = 0$ subject to the conditions that $\nabla\phi_1 \to 0$ as $r \to \infty$, and $\left.\frac{\partial\phi_1}{\partial r}\right|_{r=a} = Ub_m m\cos n\omega$,

where $n = m - 1$ for one part of the solution, and $n = m + 1$ for the other part.

We begin by seeking a solution of the form $\phi_1 = h(r)m\cos n\omega$. Substituting this into $\nabla^2\phi_1 = 0$ as before and applying the infinity condition we have,

$$\phi_1 = \frac{Bm}{r^n}\cos n\omega$$

which gives,

$$\phi_{1r} = -\frac{Bnm}{r^{n+1}}\cos n\omega$$

And so, applying the condition when $r = a$ we have,

$$\phi_{1r} = -\frac{Bnm}{a^{n+1}}\cos n\omega = Ub_m m\cos n\omega$$

$$\Rightarrow -\frac{Bn}{a^{n+1}} = Ub_m$$

$$\Rightarrow B = -\frac{Ub_m a^{n+1}}{n}$$

And so we have,

$$\phi_1 = -\frac{Ub_m a^{n+1} m}{nr^n}\cos n\omega$$

Substituting in the two values for $n$ and summing we obtain the solution,

$$\phi_1 = -\frac{Ub_m a^m m}{(m-1)r^{m-1}}\cos(m-1)\omega + \frac{Ub_m a^{m+2} m}{(m+1)r^{m+1}}\cos(m+1)\omega$$

This can then be put together with (C.7) to give an overall solution,

$$\phi_1 = \frac{Ub_m a^m}{(m-1)r^{m-1}}\cos(m-1)\omega + \frac{Ub_m a^{m+2}}{(m+1)r^{m+1}}\cos(m+1)\omega$$
$$- \frac{Ub_m a^m m}{(m-1)r^{m-1}}\cos(m-1)\omega + \frac{Ub_m a^{m+2} m}{(m+1)r^{m+1}}\cos(m+1)\omega \quad \text{(C.8)}$$

$$\Rightarrow \phi_1 = \frac{Ub_m a^m(1-m)}{(m-1)r^{m-1}}\cos(m-1)\omega + \frac{Ub_m a^{m+2}(1+m)}{(m+1)r^{m+1}}\cos(m+1)\omega$$

$$\Rightarrow \phi_1 = -\frac{Ub_m a^m}{r^{m-1}}\cos(m-1)\omega + \frac{Ub_m a^{m+2}}{r^{m+1}}\cos(m+1)\omega$$

$$\Rightarrow \phi_1 = Ub_m\left(-\frac{a^m}{r^{m-1}}\cos(m-1)\omega + \frac{a^{m+2}}{r^{m+1}}\cos(m+1)\omega\right) \quad \text{(C.9)}$$

Taking (5.2) as $\phi_0$ and (C.9) as $\phi_1$ with $\phi = \phi_0 + \delta\phi_1$. We are looking to substitute this into (5.4) to find an equation for the pressure on the boundary. However, $\phi$ is a function of $r$ and $\omega$. Our perturbation still has the quantity of $\omega$, but now $r = a + a\delta f(\omega)$, where $\delta << 1$. A Taylor expansion is useful here to enable us to calculate the derivatives,

$$\phi(a + a\delta f) = \phi(a) + a\delta f\phi_r(a) + ...$$

and so the derivatives become,

$$\phi_r(a + a\delta f) = \phi_r(a) + a\delta f\phi_{rr}(a) + ...$$

$$\phi_\omega(a + a\delta f) = \phi_\omega(a) + a\delta f\phi_{\omega r}(a) + ...$$

Using all of this information and substituting and evaluating when $r = a + a\delta f$, we can find pressure in ascending powers of $\delta$. As we are looking at small values of $\delta$ for a weak flow we can approximate this. The $\delta^0$ coefficient is,

$$\frac{1}{2}U^2\rho + p_\infty - 2\rho U^2\sin^2\omega \quad \text{(C.10)}$$

which is consistent with when we did not have a flow (i.e. $\delta = 0$). The $\delta^1$ coefficient is,

$$\frac{2\rho U^2 b_m \sin\omega}{a}\left(\frac{a^m(m-1)\sin\Big((m-1)\omega\Big)}{a^{m-1}} - \frac{a^{m+2}(m+1)\sin\Big((m+1)\omega\Big)}{a^{m+1}}\right)$$

which simplifies to,

$$2\rho U^2 b_m \sin\omega\Big((m-1)\sin\Big((m-1)\omega\Big) - (m+1)\sin\Big((m+1)\omega\Big)\Big) \quad \text{(C.11)}$$

We will define $p = p_0(\omega) + \delta p_1(\omega)$, where $p_0$ is equivalent to (C.10) and $p_1$ is equivalent to (C.11).

# D

# Bending Moments

Bending moments are produced by forces acing on a beam/rod/elastic section. The moment is given by the product of the force and the distance from the section, and has SI units Newton metres. Within a section this is balanced by an internal moment that comes from the internal stresses. This is given by the summation of all the internal forces acting on each element within the section. So, from Figure 2.2, we can define the moment by,

$$m = \int qds \Rightarrow q = \frac{dm}{ds}.$$

Forces from $\tau$ are not included since the force acts along the line through $s$ and so the moment is $\tau$ multiplied by a distance of zero.

To calculate bending moments, we can total up all the internal stresses over a cross section to give the total force of $\sigma dA$, (where $\sigma$ is the stress and $dA$ is a small section of area), the moment of this small area is then given by the distance from a neutral axis within the elastic section (say $y$) multiplied by $\sigma dA$. The total moment, $m$, will then be given by summing up all of these small area moments, hence,

$$m = -\int_A y\sigma dA.$$

The negative sign is included by convention so that a sagging beam has a positive moment. For elastic equations Hooke's Law gives,

$$\sigma = -\frac{Ey}{R}$$

where $R$ is the radius of curvature and $E$ is the modulus of elasticity. This gives the sum of moments as,

$$m = \int_A \frac{Ey^2}{R} dA \Rightarrow m = \frac{E}{R}\int_A y^2 dA$$

But $\int_A y^2 dA$ is the moment of inertia ($I$) and so,

$$m = \frac{E}{R}I$$

The radius of curvature is the inverse of curvature ($k$) and $EI$ is combined to become $\epsilon_B$ in the derivation used in this report and in [6], and so,

$$m = \epsilon_B k \Leftrightarrow q = \epsilon_B \frac{dk}{ds}$$

# E

# Symmetry effecting the power in series expansion

The solution we seek to Figure 6.6 is of the form

$$\zeta = \left(1 - t^2\right) \sum_{n=1}^{\infty} c_n t^{n-1} \tag{E.1}$$

Taking $t = e^{i\omega}$ and letting $m = n - 1$ then (E.1) becomes,

$$\zeta(e^{i\omega}) = \left(1 - e^{2i\omega}\right) \sum_{m=0}^{\infty} c_n e^{mi\omega} \tag{E.2}$$

If we were taking a symmetric solution to Figure 6.6 then we would have $\zeta(e^{i\omega}) = \overline{\zeta(e^{i(\pi-\omega)})}$ and so we also have,

$$\begin{aligned}
\overline{\zeta(e^{i(\pi-\omega)})} &= \left(1 - e^{-2i(\pi-\omega)}\right) \sum_{m=0}^{\infty} c_n e^{-mi(\pi-\omega)} \\
&= \left(1 - e^{2i\omega}\right) \sum_{m=0}^{\infty} c_n e^{-mi\pi} e^{mi\omega} \\
&= \left(1 - e^{2i\omega}\right) \sum_{m=0}^{\infty} c_n (-1)^m e^{mi\omega}
\end{aligned} \tag{E.3}$$

Performing series expansions on both (E.2) and (E.3) we obtain,

$$\left(1 - e^{2i\omega}\right)\left(c_0 + c_1 e^{i\omega} + c_2 e^{2i\omega} + c_3 e^{3i\omega} + c_4 e^{4i\omega} + ...\right)$$

$$\left(1 - e^{2i\omega}\right)\left(c_0 - c_1 e^{i\omega} + c_2 e^{2i\omega} - c_3 e^{3i\omega} + c_4 e^{4i\omega} + ...\right)$$

respectively. For a symmetric solution we must have both of these series expansions to be equal and so $c_m = 0$ for all odd values of $m$. We could write $2m$ instead of $m$ and not lose any generality using integers for $m$ as opposed to using purely even numbers. Hence, we could also use $2n - 2$ instead of $n - 1$, and so (E.1) becomes,

$$\zeta = \left(1 - t^2\right) \sum_{n=1}^{\infty} c_n t^{2n-2}$$

for symmetric solutions.

# F

## Show $\frac{ds}{d\phi} = \left(x_\phi^2 + y_\phi^2\right)^{1/2}$ from $ds^2 = dx^2 + dy^2$

$$ds^2 = dx^2 + dy^2 \tag{F.1}$$

If we take a general parameterized coordinate on in the $xy$-plane where $\phi$ is our parameter then we have,

$$\mathbf{x} = (x(\phi), y(\phi)) \tag{F.2}$$

and so the tangent, $\mathbf{t}$, to $\mathbf{x}$ can be found by,

$$\mathbf{t} = \frac{d\mathbf{x}}{d\phi} = (x_\phi, y_\phi) \tag{F.3}$$

From the chain rule we have,

$$\frac{d\mathbf{x}}{ds} = \frac{d\mathbf{x}}{d\phi}\frac{d\phi}{ds}$$
$$\Rightarrow \left|\frac{d\mathbf{x}}{ds}\right| = \left|\frac{d\mathbf{x}}{d\phi}\right|\frac{d\phi}{ds}$$

Using (F.2) and (F.3), we then have,

$$\left(\frac{dx^2 + dy^2}{ds^2}\right)^{1/2} = \left(x_\phi^2 + y_\phi^2\right)^{1/2}\frac{d\phi}{ds}$$

and so from (F.1),

$$\left(\frac{ds^2}{ds^2}\right)^{1/2} = 1 = \left(x_\phi^2 + y_\phi^2\right)^{1/2}\frac{d\phi}{ds}$$
$$\Rightarrow \frac{ds}{d\phi} = \left(x_\phi^2 + y_\phi^2\right)^{1/2}$$

# G

# Alternative Plotting Method

Instead of thinking about the matrix transformations as describedin chapter 2, there is an easier way to plot the entire shape. Once the numerical scheme has found values for $\alpha$ and $\beta$, the program can be run again with the calculated values but this time run the whole numerical scheme for $0 \leq \hat{s} \leq 2\pi$. Figure G.1 is a demonstration of this alternative calculation for the central picture of Figure 2.10. Notice it looks the same apart from the whole image has been shifted as we have excluded not only the reflection and rotation transformations but also the initial translation.

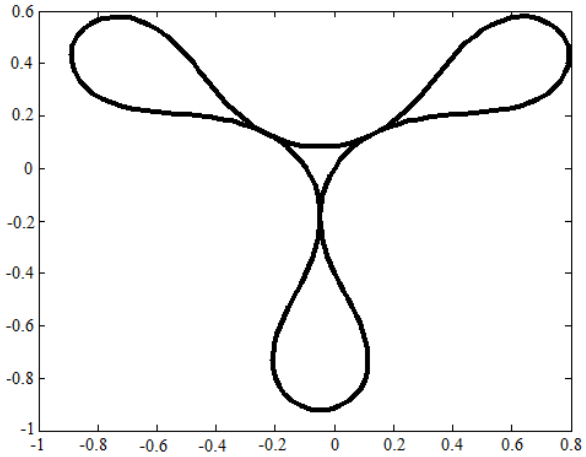


Figure G.1: Alternative plotting method at contact pressure point for Mode 3. Plot obtained by solving (4.1) numerically with $n = 3$ and $\hat{p} = 21.65$.

# Bibliography


[1] D. J. Acheson, *Elementary fluid dynamics*, Oxford University Press, Oxford, 1990.

[2] H. Anton, *Elementary linear algebra*, John Wiley and Sons, Inc, New York, 2000.

[3] G. K. Batchelor, *An introduction to fluid dynamics*, Cambridge Mathematical Library, New York, 2005.

[4] M. G. Blyth and E. I. Parau, *Deformation of an elastic cell in a uniform stream and in a circulatory flow.*, J. Appl Math. **78** (2013), 665–684.

[5] M. G. Blyth, E. I. Parau, and J. M. Vanden-Broeck, *Hydroelastic waves on fluid sheets.*, J. Appl Math. **689** (2011), 541–551.

[6] M. G. Blyth and C. Pozrikidis, *Buckling and collapse of heavy tubes resting on a horizontal or inclined plane.*, European Journal of Mechanics A/Solids **21** (2002), 831–843.

[7] M. G. Blyth and J. M. Vanden-Broeck, *New solutions for capillary waves on curved sheets of fluid.*, J. Appl Math. **70** (2005), 588–601.

[8] J. Casey, *Exploring curvature*, Springer Vieweg Verlag, Berlin, 1996.

[9] D. G. Crowdy, *Exact solutions for steady capillary waves on a fluid annulus.*, J. Nonlinear Sci. **9** (1999), 615–640.

[10] J. E. Flaherty, J. B. Keller, and S. I. Rubinow, *Post buckling behavior of elastic tubes and rings with opposite sides in contact*, J. Appl Math. **23** (1972), no. 4, 446–455.

[11] H. Gross, *Calculus of complex variables, differential equations, and linear algebra. part i: Complex variables. lecture 3: Conformal mappings, 1971.*, Massachusetts Institute of Technology: MIT OpenCourseWare, http://ocw.mit.edu, November 21, 2015.

[12] I. Jacques and C. Judd, *Numerical analysis*, Chapman and Hall, London, 1987.

[13] J. B. Keller and J. M. Vanden-Broeck, *Deformation of a bubble or drop in a uniform flow*, J. Appl Math. **Vol. 101, part 4** (1980), 673–686.

[14] A. Korobkin, E. I. Parau, and J-M. Vanden-Broeck, *The mathematical challenges and modelling of hydroelasticity.*, Phil. Trans. R. Soc. A **369**, 2803–2812.

[15] P. S. MacIlwaine, *Coordinate geometry and complex numbers*, Palgrave, New York, 1984.

[16] K. W. Morton and D. F. Mayers, *Numerical solutions of partial differential equations*, Cambridge University Press, Cambridge, 1994.

[17] E. Ozugurlu and J. M. Vanden-Broeck, *The distortion of a bubble in a corner flow*, J. Appl Math. **11** (2000), 171–179.

[18] C. Pozrikidis, *Buckling and collapse of open and closed cylindrical shells*, J. Eng. Math. **Vol. 42** (2002), 157–180.

[19] C. Pozrikidis and M. G. Blyth, *Solution space of axisymmetric capsules enclosed by elastic membranes.*, European Journal of Mechanics A/Solids **23** (2004), 877–892.

[20] H. M. Schey, *Div, grad, curl, all that: an infomal text on vector calculus. 3rd edition*, Norton and Company.

[21] J. F. Toland, *Steady periodic hydroelastic waves.*, Nucl. Engng Des. **189** (2008), 325–362.